HELMHOLTZ ZENTRUM MÜNCHEN
SELBSTSTÄNDIGE ABTEILUNG FÜR APOPTOSE IN HÄMATOPOIETISCHEN STAMMZELLEN
LEITUNG: IRMELA JEREMIAS

Single Stem Cell Clones of an Acute Myeloid Leukaemia Patient Display Functional Heterogeneity In Vivo

---

Dissertation der Fakultät für Biologie
der Ludwig-Maximilians-Universität München

vorgelegt von
Christina Maria Zeller
aus Weilheim in O.B.

München, August 2020

Diese Dissertation wurde angefertigt
unter der Leitung von Prof. Dr. Wolfgang Enard
im Bereich für Anthropologie und Humangenetik
an der Ludwig-Maximilians-Universität München

Erstgutachter/in:	Prof. Dr. Wolfgang Enard
Zweitgutachter/in:	Prof. Dr. Irmela Jeremias
Tag der Abgabe:	20.08.2020
Tag der mündlichen Prüfung:	22.12.2020

Eidesstattliche Versicherung und Erklärung

Ich versichere hiermit an Eides statt, dass die vorgelegte Dissertation mit dem Titel

"Single Stem Cell Clones of an Acute Myeloid Leukaemia Patient Display Functional Heterogeneity In Vivo"

von mir selbstständig und ohne unerlaubte Hilfsmittel angefertigt ist.

Hiermit erkläre ich, dass die Dissertation nicht ganz oder in wesentlichen Teilen einer anderen Prüfungskommission vorgelegt worden ist.

Ich erkläre weiter, dass ich mich anderweitig einer Doktorprüfung ohne Erfolg nicht unterzogen habe.

München, den 01. Februar 2021

_____

Christina Maria Zeller

Zusammenfassung

Die akute myeloische Leukämie (AML) ist ein bösartiger Tumor des hämatopoietischen Systems. Als klinische Herausforderung gilt die große genetische und funktionelle Heterogenität zwischen Patienten, aber auch innerhalb eines Patienten; der Subklon mit den ungünstigsten Eigenschaften entscheidet über das Überleben des Patienten. Ein besseres Verständnis der Tumorheterogenität ist erforderlich, um Behandlungsstrategien gegen besonders herausfordernde Subklone zu lenken.

In der vorliegenden Arbeit sollte die genetische, epigenetische, transkriptomische und funktionelle Heterogenität innerhalb des Tumors eines einzelnen Patienten mit AML charakterisiert werden. Um funktionelle *in vivo* Studien zu ermöglichen, wurde aus der AML-Probe ein Xenograft-Mausmodell (*engl. patient-derived xenograft*, PDX) etabliert. Durch Re-Transplantation einer geringen Anzahl von AML-Zellen in immunsupprimierte Mäuse generierte ich zwölf AML-Populationen, die jeweils von einer einzelnen Stammzelle abstammten, ersichtlich durch molekulare Barcodes, die unter Verwendung von Lentiviren übertragen wurden. Die resultierenden Einzelzellklone (*engl. single cell clones*, SCCs) wurden mit einer individuellen Kombination von Fluorochromen lentiviral markiert, was eine separate Analyse mittels Durchflusszytometrie in kompetitiven *in vivo* Untersuchungen ermöglichte.

In epigenetischen und transkriptomischen Analysen bildeten die SCCs deutliche Gruppen entsprechend ihres Ursprungs des ersten oder zweiten Rezidivs. Genetische Analysen zeigten zudem die Existenz von mindestens vier genetisch unterschiedlichen Subklonen auf. Funktionelle *in vivo* Untersuchungen offenbarten Heterogenität zwischen verschiedenen SCCs bezüglich Stammzellkapazität, Wachstum, Dormanz und Therapieansprechen. Der widrigste SCC zeichnete sich durch schnelles Wachstum in kompetitiven *in vivo* Untersuchungen in Kombination mit einer partiellen Resistenz gegen die Behandlung mit herkömmlicher Chemotherapie aus. Dieses aggressive funktionelle Verhalten war mit einer einzigartigen Deletion von Chromosom 17q assoziiert, die u.a. mit HOX-Signalisierung korrelierte. Obwohl dieser SCC resistent gegenüber verschiedenen Behandlungsoptionen war, sprach er auf eine systemische Behandlung mit der hypomethylierenden Substanz 5-Azacitidin an.

Zusammenfassend zeigen die Daten, dass die bekannte Heterogenität innerhalb der Tumorzellen eines einzelnen AML-Patienten zu erheblicher funktioneller Heterogenität *in vivo* führt. Die klonale Evolution genetischer Veränderungen kann funktionell aggressive Klone erzeugen, die durch eine gut gewählte Zweitlinienbehandlung dennoch angreifbar sein könnten und somit kann die klinische Situation verbessert werden.

Abstract

Acute myeloid leukaemia (AML) is a haematopoietic malignancy characterised by major genetic and functional heterogeneity. As clinical challenge, the most adverse subclone determines a patient's outcome. A better understanding of tumour heterogeneity is required to direct treatment strategies against adverse subclones.

In the present work, I aimed at characterising the genetic, epigenetic, transcriptomic and functional heterogeneity within the tumour sample of a single patient with AML. To enable functional *in vivo* studies, a patient-derived xenograft (PDX) mouse model was established from the AML sample. Upon re-transplanting minor numbers of PDX AML cells into immunocompromised mice, I generated twelve PDX AML populations that derived from a single stem cell, as proven by molecular barcoding using lentiviruses. The resulting PDX AML single cell clones (SCCs) were lentivirally marked with an individual combination of fluorochromes, enabling their separate analysis via flow cytometry in competitive *in vivo* assays.

Epigenetic and transcriptomic analyses showed that PDX AML SCCs clustered according to their origin from first or second relapse. Genetic analyses revealed the existence of at least four genetically distinct subclones. Functional *in vivo* assays uncovered heterogeneity between the different PDX AML SCCs concerning stem cell capacity, growth, dormancy and treatment response. The most adverse PDX AML SCC displayed rapid growth in competitive *in vivo* assays combined with a partial resistance towards treatment with conventional chemotherapy. The aggressive functional behaviour was associated with a unique deletion of chromosome 17q correlating to i.a. an enrichment in HOX signalling. Of clinical importance and while resistant towards several treatment options, the clone responded to systemic treatment with the hypomethylating agent 5-azacitidine.

Taken together, the data revealed that the known heterogeneity within tumor cells of a single patient with AML results in major functional heterogeneity *in vivo*. Clonal evolution of genetic changes can generate functionally aggressive clones, which might still respond to well-chosen second-line treatment, improving the clinical situation.

Contents

Abbreviations

#	Number
A	Adenine
AL	Acute leukaemia
ALL	Acute lymphoblastic leukaemia
AML	Acute myeloid leukaemia
ANOVA	Analysis of variance
Ara-C	Cytarabine
Aza	5-Azacitidine
BC	Barcode
Bcl-2	B cell lymphoma 2
BCOR	BCL-6 corepressor
BLI	Bioluminescence *in vivo* imaging
BM	Bone marrow
BSA	Bovine serum albumine
C	Cytosine
CEBPA	CCAAT enhancer binding protein α
CFSE	Carboxyfluorescein succinimidyl ester
CI	Confidence interval
CN	Dytogenetically normal
CNV	Copy number variation
CRISPR	Clustered regularly interspaced short palindromic repeats
CSC	Cancer stem cell
DAPI	4',6-Diamidino-2-phenylindole
del	Deletion
DMSO	Dimethyl sulfoxide
DNA	Desoxyribonucleic acid

DNMT3A	DANN methyltransferase 3A
dNTP	Desoxyribonukleosidtriphosphate
E.coli	Escherichia coli
EDTA	Ethylenediaminetetraacetic acid
eFFly	Enhanced firefly
eGFP	Enhanced green fluorescent protein
ETV6	ETS variant transcription factor 6
EZH2	Enhancer of zeste homolog 2
f	Female
FACS	Fluorescence-activated cell sorting
FCS	Fetal calf serum
FLT3	Fms like tyrosine kinase 3
FLT3L	Recombinant human FMS-like tyrosine kinase 3 ligand
FSC	Forward scatter
G	Guanine
G-CSF	Granulocyte-colony stimulating factor
GEPDX	Genetically engineered patient-derived xenograft
GSEA	Gene set enrichment analysis
HEK	Human embryonal kidney
HMA	Histone modifying agent
HRV	Hypervariable region
HSC	Haematopoietic stem cell
ID	Initial Diagnosis
IDH1/2	Isocitrate dehydrogenase (NADP(+)) 1/2
IL3	Recombinant human iterleukin 3
iRFP720	Infrared fluorescent protein 720
JAK1	Janus kinase 1
KDM6A	Lysine demethylase 6A
KRAS	Kirsten RAS
LDTA	Limiting dilution transplantation assay
LIC	Lekaemia initiating cell
LOH	Loss of heterozygosity
LRC	Label-retaining cells

LSC	Leukaemia stem cell
m	Male
MACS	Magnetic-activated cell sorting
mCherry	Monomeric cherry fluorescent protein
MDS	Myelodysplastic syndrome
MFI	Mean fluorescence intensity
MLL	Mixed-lineage leukaemia
MRD	Minimal residual disease
mtagBFP	Monomeric blue fluorescent protein
N	Nucleotide
n.d.	Not determined
NGFR	Nerve growth factor receptor
NGS	Next generation sequencing
NOD	Non-obese diabetic
NPM1	Nucleophosmin 1
NRAS	Neuroblastoma RAS
ns	Not significant
NSG	NOD.Cg-Prkdc^{scid} Il2rg^{tm1Wjl}/SzJ
pB	Peripheral blood
PBS	Phosphate buffered saline
PCR	Polymerase chain reaction
PDX	Patient-derived xenograft
Pen/Strep	Penicillin/Streptavidin
PTPN11	Tyrosine-protein phosphatase non-receptor type 11
RAS	Rat sarcoma viral oncogene
Rel	Relapse
RGB	Red/green/blue
RNA	Ribonucleic acid
RT	Room temperature
RUNX1	Runt-related family transcription factor 1
S	Strong nucleotide
SCC	Single cell clone
SCF	Recombinant human stem cell factor

SCID	Severe combined immunodeficiency
SCRB-seq	Single cell RNA barcoding and sequencing
shRNA	short hairpin RNA
SNP	Single nucleotide polymorphism
SNV	Single nucleotide variant
SSC	Side scatter
T	Thymine
TET2	Tet methylcytosine dioxygenase 2
TP53	Tumour suppressor protein 53
TPO	Recombinant human thrombopoietin
VAF	Variant allele frequency
W	Weak nucleotide

List of Figures

List of Tables

List of Publications

Publications

Christina Zeller[*], Daniel Richter[*], Binje Vick, Vindi Jurinovic, Ilse Valtierra, Johannes W. Bagnoli, Maja Rothenberg-Thurley, Klaus H. Metzeler, Ines Hellmann, Tobias Herold, Wolfgang Enard[#], Irmela Jeremias[#]. "Characterization of Genetically Distinct Single Stem Cell Clones Derived from a Patient's Acute Myeloid Leukemia Xenograft Reveals A Cytarabine Resistant Subclone."

[*] co-first author; [#] co-last author.

Manuscript in preparation

Sarah Ebinger, **Christina Zeller**, Michela Carlet, Daniela Senft, Johannes W. Bagnoli, Wen-Hsin Liu, Maja Rothenberg-Thurley, Wolfgang Enard, Klaus H. Metzeler, Tobias Herold, Karsten Spiekermann, Binje Vick, Irmela Jeremias. "Plasticity in growth behavior of patients' acute myeloid leukemia stem cells growing in mice." *Haematologica* (2020) haematol.2019.226282; doi: 10.3324/haematol.2019.226282.

Abstracts

Christina Zeller, Daniel Richter, Binje Vick, Tobias Herold, Johannes Bagnoli, Maja Rothenberg-Thurley, Klaus H. Metzeler, Karsten Spiekermann, Wolfgang Enard, Irmela Jeremias. "Single Cell Clones Derived from a Patient's AML Xenograft Display Genetic and Functional Heterogeneity." *Blood* (2019) 134 (Supplement_1): 1450; doi: 10.1182/blood-2019-127867

1. Introduction

1.1. Acute Myeloid Leukaemia

Leukaemia, a cancer of the haematopoietic system, belongs to the ten or twelve most common cancers in the U.S. or U.K., respectively (Siegel et al., 2020; American Cancer Society, 2020; Cancer Research UK, 2020). Even though leukaemia is the most common childhood cancer, incidence increases with age and, thus, it is mostly a disease of the elderly (Siegel et al., 2020; American Cancer Society, 2020; Cancer Research UK, 2020). Whereas acute lymphoblastic leukaemia (ALL) predominates in children and adolescent, acute myeloid leukaemia (AML) preponderates in adults (Siegel et al., 2020). Overall, AML constitutes one third of new leukaemia cases and almost 50% of leukaemia related deaths making it the most challenging leukaemia subtype (Siegel et al., 2020; American Cancer Society, 2020).

1.1.1. Biology of the Disease

AML is a haematopoietic malignancy involving abnormal proliferation and block in differentiation of myeloid stem or progenitor cells. In healthy humans, haematopoietic stem cells give rise to myeloid as well as lymphoid progenitors, which in turn differentiate to healthy blood cells such as erythrocytes, platelets, granulocytes and monocytes as well as T and B lymphocytes, respectively (Murphy and Weaver, 2016). In AML, immature, non-functional myeloblasts accumulate, which interfere with normal haematopoiesis (figure 1.1). This accumulation of blasts leads to unspecific symptoms such as fatigue, bleeding and increased risk for infection and, eventually, bone marrow (BM) failure (De Kouchkovsky and Abdul-Hay, 2016; Estey, 2014).

Although AML is characterised by few mutations compared to other types of cancers (The Cancer Genome Atlas Research Network, 2013), molecular changes leading to the block in differentiation and increased proliferation are variable between patients. While 70-85% of paediatric AML cases display cytogenetic abnormalities including translocations and deletions (Manola, 2009), almost 50% of adult AML patients have a normal cytogenetic profile (The Can-

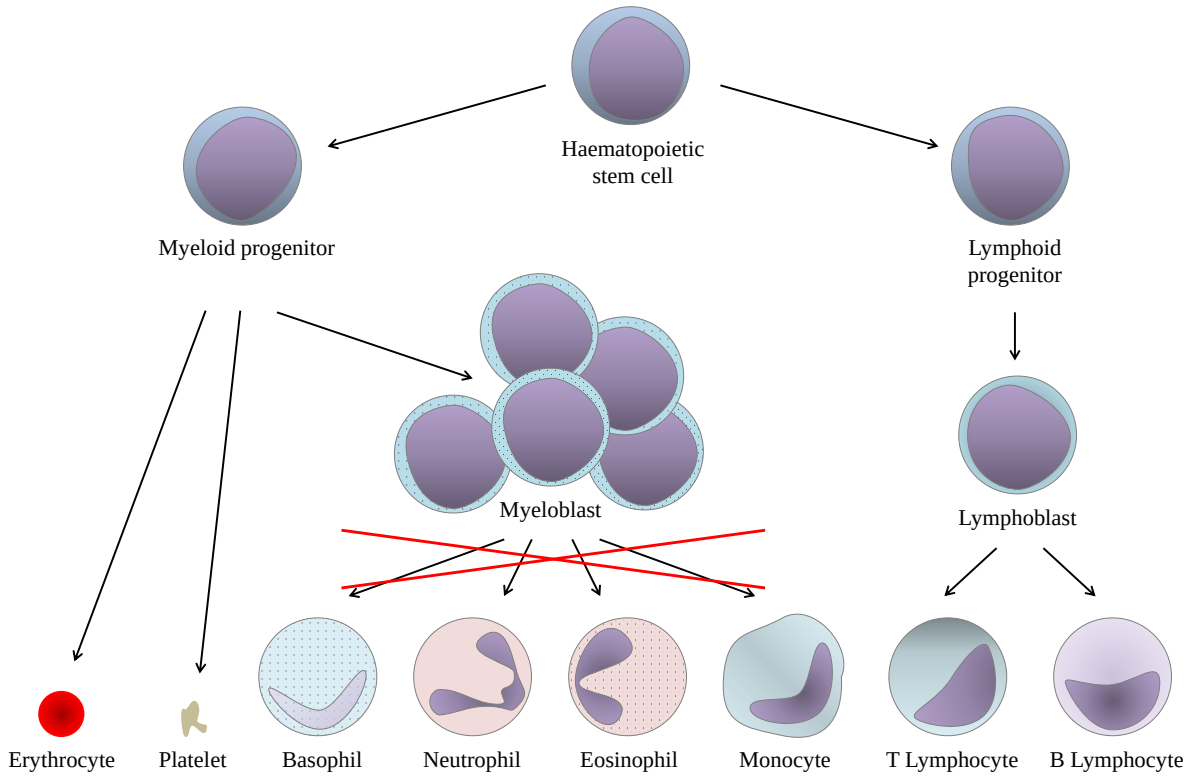

Figure 1.1. Haematopoietic differentiation and development of AML. Haematopoietic stem cells differentiate either to myeloid or lymphoid progenitors, which give rise to fully differentiated blood cells, e.g. erythrocytes, platelets, granulocytes and monocytes, or T and B lymphocytes, respectively. Due to a block in differentiation and increased proliferation myeloblasts accumulate leading to AML (Estey, 2018; Murphy and Weaver, 2016; De Kouchkovsky and Abdul-Hay, 2016; Estey, 2014).

cer Genome Atlas Research Network, 2013). Additionally, genetic alterations and mutations in signalling pathways, transcription factors, epigenetic regulators and tumour suppressor genes, even though present in AML of all ages, are more common in adult cases (Renneville et al., 2008). One reason for this higher frequency of mutations in adult AML is age-related clonal haematopoiesis, meaning the gradual accumulation of premalignant alterations in haematopoietic stem and progenitor cells during aging (Watson et al., 2020; Shlush, 2018; Busque et al., 2018; Jaiswal et al., 2014). Furthermore, patients present with individual combinations of genetic alterations (Renneville et al., 2008). Even though a diverse range of molecular changes may occur in AML, this results in one cellular phenotype, namely a block in differentiation and increased proliferation of blasts. Thus, AML is a heterogeneous disease with major genetic inter-patient variability.

1.1.2. Diagnosis, Prognosis and Treatment of AML Patients

Patients are diagnosed with AML, when blast counts are higher than 20% in BM (Estey, 2018; Arber et al., 2016; De Kouchkovsky and Abdul-Hay, 2016). Morphologic, immunophenotypic, cytogenetic and mutational analyses are used for further classification of AML (National Cancer Institute, 2020).

While the overall 5-year-survival rate is 25% in adults and 66% in children (Siegel et al., 2020; American Cancer Society, 2020), numerous factors lead to an even worse prognosis: age, patient history (e.g. previous chemotherapy treatment), elevated white blood cell count and specific translocations or mutations (National Cancer Institute, 2020; De Kouchkovsky and Abdul-Hay, 2016; Döhner et al., 2015). Certain mutations and cytogenetics can be further used to classify AML cases into favourable, intermediate and adverse prognostic risk groups, e.g. mutations in the tumour suppressor gene *TP53*, a complex karyotype and specific translocations such as the *BCR-ABL1* fusion lead to an adverse prognosis, while mutated *CEBPA* and *RUNX1-RUNX1T1* fusion are favourable (National Cancer Institute, 2020; Ravandi et al., 2018; Döhner et al., 2017; Papaemmanuil et al., 2016).

In spite of recent advances in the molecular characterisation of AML, the standard of care treatment has not changed significantly within decades (Döhner et al., 2017; De Kouchkovsky and Abdul-Hay, 2016; Döhner et al., 2015). First, induction chemotherapy consisting of a ”7 + 3” regimen of cytarabine (Ara-C) and an anthracycline is applied (De Kouchkovsky and Abdul-Hay, 2016; Döhner et al., 2015). Ara-C is a cytosine analogue inhibiting DNA and RNA synthesis, especially in proliferating cells (Galmarini et al., 2001), whereas anthracyclines intercalate into DNA and inhibit topoisomerase II (Hortobagyi, 1997), thus, inhibiting DNA synthesis, promoting growth arrest and initiating apoptosis (Galmarini et al., 2001; Hortobagyi, 1997). This combination induction therapy for one week followed by two to four cycles of cytarabine consolidation treatment leads to a complete response, meaning $<5\%$ of blasts in BM, in $80-90\%$ of favourable and $<50\%$ of adverse AML cases (Döhner et al., 2017, 2015; Estey, 2014). Additional to consolidation therapy haematopoietic stem cell transplantation is employed, if possible (Döhner et al., 2017; De Kouchkovsky and Abdul-Hay, 2016; Döhner et al., 2015). Unfortunately, most patients relapse eventually (35-40% with favourable, 50-80% with intermediate and $>90\%$ with adverse risk classification) (Döhner et al., 2015; Estey, 2014). Furthermore, AML patients may face treatment-related toxicity or are not eligible for intensive chemotherapy or stem cell transplantation, e.g. elderly patients and, therefore, face dismal prognosis (Döhner et al., 2017). Thus, new treatment options are urgently needed.

Recently, new therapeutic approaches have been developed: (i) immunotherapeutics such as (a) adoptive cell therapy with e.g. chimeric antigen receptor T cells, (b) immune checkpoint inhibitors like anti-PD-1 antibodies and (c) antibody drug conjugates like gemtuzumab ozogamicin, an anti-CD33 antibody conjugated to a DNA-targeting cytotoxic agent, are currently in clinical trials or even approved for treatment of AML patients (ClinicalTrials.gov, 2019*a*,*b*; Baron and Wang, 2018; Daver et al., 2016; Wang et al., 2015; Castaigne et al., 2012); (ii) epigenetic active drugs like hypomethylating agents (HMAs) such as azacitidine and decitabine have been approved as AML medication (Estey, 2018; Döhner et al., 2017); (iii) apoptosis inducing drugs, e.g. venetoclax, an inhibitor of B cell lymphoma 2 (Bcl-2) protein, an anti-apoptotic regulator, have been approved for treatment of AML patients (DiNardo et al., 2018; Wei et al., 2018); (iv) targeted therapies like (a) the FLT3 kinase inhibitor midostaurin and (b) the IDH inhibitor ivosidenib have been approved not long ago or are in clinical trials (ClinicalTrials.gov, 2020; Stone et al., 2018, 2017). Due to the major inter-patient heterogeneity observed in AML, treatment has become more and more individualised with an increasing number of specialised and targeted therapeutic approaches. However, even though new treatment options emerge, therapy resistance and relapse remain a major clinical challenge creating the need for further research.

1.1.3. Minimal Residual Disease and Relapse

Even though most AML patients respond to conventional chemotherapy, many patients relapse eventually, especially with AML of adverse classification (Döhner et al., 2015; Estey, 2014).

In the first weeks of treatment, most leukaemic cells are eradicated in the majority of patients leading to partial or complete remission, defined as persistence of 5%-25% or $<$5% of blasts in BM, respectively (figure 1.2) (Döhner et al., 2017). However, therapy resistant leukaemic blasts may persist in the BM as minimal residual disease (MRD) (Ediriwickrema et al., 2020; Ravandi et al., 2018; Buckley et al., 2013). Remaining AML cells may over time re-induce the disease, instigating relapse. Indeed, higher levels of MRD have been associated with a higher risk for relapse (Ravandi et al., 2017; Othus et al., 2016; Buccisano et al., 2006).

The occurrence of chemoresistant MRD cells in contrast to therapy sensitive cells, which are eliminated in the first phase of treatment, demonstrates the functional heterogeneity of cancer cells, even within an individual patient (Ediriwickrema et al., 2020; Selim and Moore, 2018). Therefore, the existence of MRD provides evidence for intra-tumour heterogeneity and represents a major challenge for curative treatment of AML.

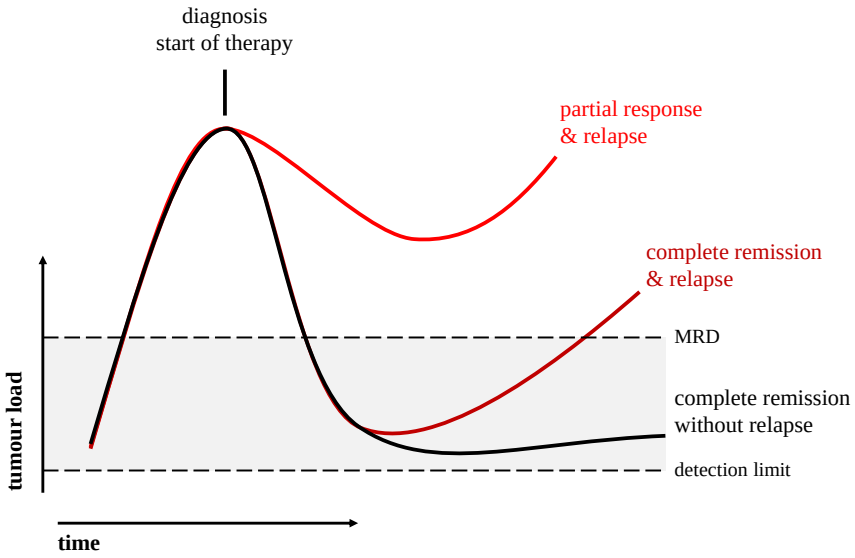

Figure 1.2. Disease progression of AML. Over months or even years, AML progresses undetected. At diagnosis of the disease patients are treated with conventional chemotherapy or novel therapeutics. A subgroup of patients respond only partially to therapy and relapse ultimately (red line), whereas others reach complete remission with a tumour load below 5% of blasts (dark red and black line). The reduced leukaemic disease is called minial residual disease (MRD). However, some of the patients in complete remission may also relapse eventually (dark red line).

1.2. Challenging Characteristics of Cancer Cells

MRD and relapse have been associated with challenging cellular characteristics including drug resistance, quiescence, i.e. inactivity or dormancy of cells, and stemness, i.e. the ability to repopulate the tumour (Thomas and Majeti, 2017; Döhner et al., 2015; Kreso and Dick, 2014). In order to successfully eliminate adverse cells responsible for MRD and relapse, it is essential to better understand the mechanisms behind these processes such as genetic and epigenetic alterations, changes in transcriptome and protein expression.

1.2.1. Drug Resistance

One reason for therapeutic failure may be a population of resistant cells. These cells may either be present already in the initial tumour before therapy start and are selected through the treatment pressure or, alternatively, these cells may develop escape mechanisms during therapy, e.g. through additional mutations gained in a tumour subpopulation in a process of clonal evolution (Greif et al., 2018; Shlush et al., 2017; Li et al., 2016b; Gerlinger et al., 2014b; Ding et al., 2012).

Even though the ability to predict treatment resistance is limited, some genetic mutations commonly found in AML have been associated with poor prognosis and resistance (Döhner

et al., 2015). Mutations in the tumour suppressor gene *TP53* as well as mutation or partial duplication in the tyrosine kinase *FLT3* have been associated with poor chemotherapy response rates (Konig and Levis, 2015; Renneville et al., 2008; Wattel et al., 1994). Specific chromosomal translocations resulting in e.g. *KMT2A* rearrangement or *BCR-ABL1* fusion are considered adverse as well (Döhner et al., 2017). Furthermore, loss-of-function of the epigenetic regulators *EZH2* and *KDM6A* has been shown to correlate with lower overall survival and resistance towards cytotoxic drugs and tyrosine kinase inhibitors (Stief et al., 2019; Greif et al., 2018; Göllner et al., 2017).

Besides genetic alterations, there are additional factors that might limit therapy success: (i) the dosage of a chemotherapeutic might be reduced in patients not eligible for high-dose treatment due to toxicity (Döhner et al., 2017); (ii) targeted therapies might eliminate only the cancer subpopulation with the specific alteration, whereas minor subpopulations may not be affected (McMahon et al., 2019; Ojamies et al., 2017); (iii) deregulation of protective pathways may lead to the development of resistance, e.g. enhanced export of drugs through upregulation of plasma membrane transporters has been described as a mechanism of resistance (Shaffer et al., 2012; de Jonge-Peeters et al., 2007) and (iv) the tumour microenvironment might play a role in MRD and resistance due to its function as a protective niche (Ebinger et al., 2016; Tabe and Konopleva, 2015).

Additionally, drug resistance may correlate with dormancy of cancer cell, since conventional chemotherapy targets actively proliferating cells enabling therapy escape of quiescent cells (Ebinger et al., 2020; Pollyea and Jordan, 2017; Ebinger et al., 2016; Saito et al., 2010; Galmarini et al., 2001; Hortobagyi, 1997).

1.2.2. Dormancy

Treatment failure and relapse have been related to the outgrowth of quiescent MRD cells (Thomas and Majeti, 2017; Pollyea and Jordan, 2017). Due to the anti-proliferative nature of standard therapy in acute leukaemias (ALs), it is challenging to eradicate inactive, non- or low-cycling cancer cells (Ebinger et al., 2020; Thomas and Majeti, 2017; Pollyea and Jordan, 2017; Ebinger et al., 2016). These dormant cells may persist over a long period of time, upon reactivation by yet-to-be-defined factors, start proliferating and, subsequently, repopulate the disease leading to relapse (Ravandi et al., 2017; Othus et al., 2016; Buccisano et al., 2006).

It has been described that these quiescent leukaemic cells may be found in the endosteal niche of the BM (Ebinger et al., 2016; Saito et al., 2010; Ishikawa et al., 2007). This osteoblast-rich

area of the BM may protect the inactive cells from chemotherapy-induced apoptosis (Ebinger et al., 2016; Ishikawa et al., 2007; Saito et al., 2010).

Due to the close relationship between dormancy and resistance, the induction of proliferation in these quiescent cells represents a valuable treatment strategy (Saito et al., 2010). Indeed, it has been demonstrated that converting AML cells into an active cell cycle by granulocyte colony-stimulating factor (G-CSF) in combination with anti-proliferative chemotherapy enhances the induction of apoptosis and, therefore, the eradication of AML cells (Saito et al., 2010).

Furthermore, cell cycle quiescence has been strongly linked with leukaemic stem cells (LSCs) capable of inducing the disease (Vetrie et al., 2020; Thomas and Majeti, 2017; Pollyea and Jordan, 2017; Saito et al., 2010).

1.2.3. Stemness

Ultimately, chemotherapy resistant and dormant cells need to have the ability to repopulate the leukaemia in order to cause relapse. Thus, stemness presents a crucial characteristic of adverse tumour cells.

The cancer stem cell (CSC) model states that tumours consist of heterogeneous cell types with the majority of cells actively proliferating (so-called bulk cells) and a minor subpopulation of non-cycling CSCs (Thomas and Majeti, 2017; Kreso and Dick, 2014; Clevers, 2011; Reya et al., 2001; Lapidot et al., 1994). CSCs represent a distinct population functionally characterised by their capacity for self-renewal and repopulation of the disease (Kreso and Dick, 2014; Clevers, 2011; Reya et al., 2001). Since CSCs are genetically and epigenetically diverse, this diversity is also represented in the clonal architecture of the tumour (Thomas and Majeti, 2017; Kreso and Dick, 2014; Clevers, 2011).

Unfortunately, conventional chemotherapy targets mainly the bulk population of the tumour, sparing CSCs (figure 1.3) (Kreso and Dick, 2014; Reya et al., 2001). Thus, CSCs capable of repopulating the tumour induce relapse (Kreso and Dick, 2014). Subsequently, it is crucial for successful cancer treatment to eliminate CSCs (Kreso and Dick, 2014; Reya et al., 2001).

AML is a stem cell disease with LSCs as tumour initiating cells and, therefore, potentially profiting immensely from CSC-directed therapy (Vetrie et al., 2020; Thomas and Majeti, 2017; Kreso and Dick, 2014). These LSCs have been described to reside in the $CD34^{+}$ $C38^{-}$ compartment of the haematopoietic cells (Thomas and Majeti, 2017; Pollyea and Jordan, 2017; Reya et al., 2001). However, there is also evidence that additional compartments harbouring LSCs

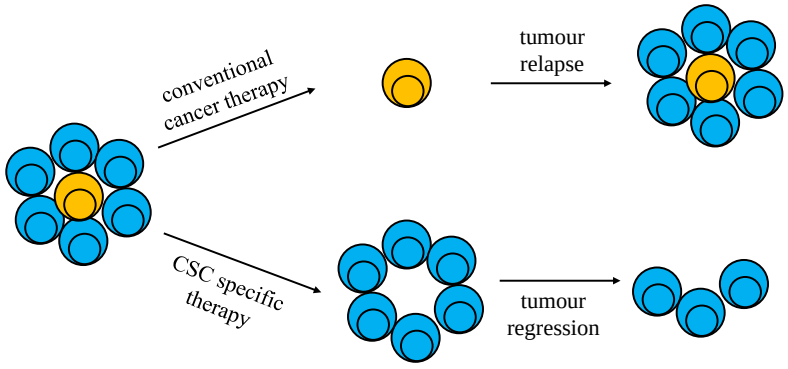

Figure 1.3. Conventional and stem cell specific cancer therapy. Conventional chemotherapy eradicates the bulk, actively proliferating tumour cells (non-CSCs, marked in bluw), whereas the rare subpopulation of quiescent CSCs (yellow) capable of repopulating the disease is spared. However, if the CSCs are eradicated with CSC-targeted therapy, the tumour may shrink and, subsequently, the patient cured (Kreso and Dick, 2014; Reya et al., 2001).

may exist making a clear identification of these LSCs difficult (Vetrie et al., 2020; Thomas and Majeti, 2017; Pollyea and Jordan, 2017). The gold standard to provide evidence for LSCs is xenotransplantation into immunodeficient mice; only CSCs harbour the ability to initiate tumour outgrowth under these conditions (Thomas and Majeti, 2017; Saito et al., 2010; Ishikawa et al., 2007; Hope et al., 2004; Lapidot et al., 1994). With these xenotransplantation assays it is also possible to determine the stem cell, or for haematopoietic cancers, the leukaemia initiating cell (LIC) frequency (Krivtsov et al., 2013; Lapidot et al., 1994).

Commonly, CSCs are characterised by cell cycle quiescence and drug resistance causing the discovery of CSC-targeted therapy as one of the main goals of cancer research today (Thomas and Majeti, 2017; Pollyea and Jordan, 2017; Saito et al., 2010). In fact, CSCs have been associated with therapy resistant MRD cells (Terwijn et al., 2014). It has even been demonstrated that the LSC frequency and heterogeneity is even increased at relapse making it all the more important to target these cells in the first line of treatment (Pollyea and Jordan, 2017).

Taken together, drug resistance, dormancy and stemness present challenging characteristics of leukaemic cells leading to therapy failure and, subsequently, relapse. An additional feature of cancer enabling these hallmarks of adversity is intra-tumour heterogeneity.

1.3. Intra-Tumour Heterogeneity and Evolution

Tumours are heterogeneous cell populations consisting of genetic and epigenetic diverse cells (Waanders et al., 2020; Marusyk et al., 2020; Li et al., 2016b; Burrell and Swanton, 2014; Corces-Zimmerman et al., 2014a; Marusyk et al., 2012; Hanahan and Weinberg, 2011). Ad-

ditionally, functional features such as growth behaviour, drug resistance, stemness, and niche interactions may differ within a single cancer as well (Marusyk et al., 2012; Hanahan and Weinberg, 2011). This represents a major challenge for the treatment of patients since all tumourigenic subclones need to be eliminated to guarantee successful therapy outcomes (Hausser and Alon, 2020; Burrell and Swanton, 2014; Fisher et al., 2013).

Generally, it is assumed that cancer arises from one single altered cell which undertook a stepwise progress from a healthy benign cell to an aberrant malignant tumour cell through acquired genetic mutations or chromosomal translocations and sequential selection (figure 1.4) (Desai et al., 2018; Corces-Zimmerman and Majeti, 2014b; Jan and Majeti, 2013; Fisher et al., 2013; Nowell, 1976). Due to a process of linear or branched evolution cancers consist of diverse cell populations at a time (Turajlic et al., 2019; Gerlinger et al., 2014b; Grove and Vassiliou, 2014; Burrell and Swanton, 2014).

The application of a selection pressure such as chemotherapy in turn may lead to the selection of the most adverse clone (Yilmaz et al., 2019; Gerlinger et al., 2014b; Burrell and Swanton, 2014; Krönke et al., 2013; Jan and Majeti, 2013; Mullighan et al., 2008). However, chemotherapy may not only select the most resistant subpopulation of cancer cells, but also induce further evolution through additional mutations (Burrell and Swanton, 2014; Krönke et al., 2013; Mullighan et al., 2008).

A major factor in intra-tumour heterogeneity, which can be detected with next generation sequencing (NGS) technologies, is genetic diversity (Turajlic et al., 2019; Yilmaz et al., 2019; Desai et al., 2018; Krönke et al., 2013; Fisher et al., 2013).

1.3.1. Genetic Heterogeneity

Various studies have demonstrated the presence of genetically distinct subclones within an individual tumour analysing single nucleotide polymorphisms (SNPs) and copy number variations (CNVs) using SNP arrays, targeted, exome or genome sequencing and even single cell sequencing techniques (Chen et al., 2019; Rothenberg-Thurley et al., 2018; Greif et al., 2018; Martincorena et al., 2018; Shiba et al., 2016; Krönke et al., 2013; The Cancer Genome Atlas Research Network, 2013; Ding et al., 2012; Jan et al., 2012; Welch et al., 2012). These diverse subclones can be related to each other according to ancestry allowing conclusions on the time-dependent occurrence of mutations (Chen et al., 2019; Rothenberg-Thurley et al., 2018; Xie et al., 2014; Krönke et al., 2013; Ding et al., 2012; Jan et al., 2012).

It has been demonstrated that several classes of mutations are common to develop AML (Li

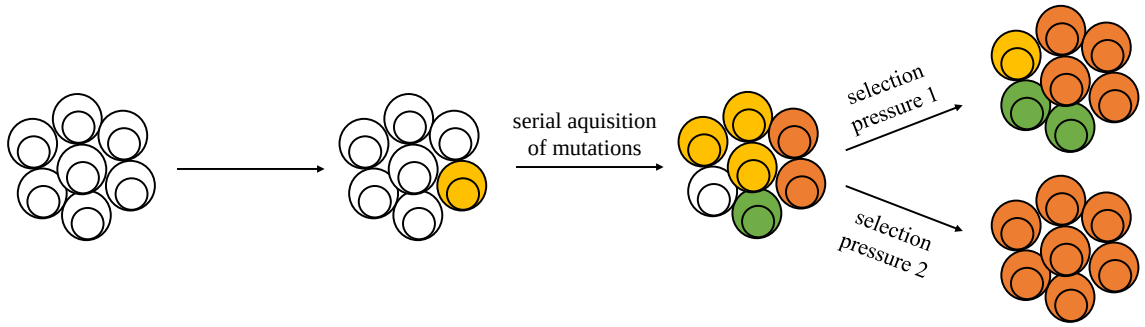

Figure 1.4. Tumour evolution. Healthy cells may be altered through tumourigenic mutations leading to cancer precursor cells. Through serial aquisition of addional alterations a tumour can develop and evolve further into a complex clonal population. Selection pressure such as chemotherapy may alter the clonal cancer composition over time (Burrell and Swanton, 2014; Gerlinger et al., 2014b; Jan and Majeti, 2013).

et al., 2016b): (i) alterations that activate signalling pathways, e.g. in the receptor tyrosine kinase *FLT3* or GTPase *NRAS*, lead to enhanced proliferation and survival; (ii) mutations and translocations in transcription factors, e.g. *RUNX1* or *CEBPA*, hinder cell differentiation and, thus, enable the accumulation of immature progenitors (Li et al., 2016b) and (iii) initiating mutations mostly in epigenetic regulators, e.g. *DNMT3A*, *NPM1*, *IDH1/2* or *TET2*, may enable these mutations through providing a fertile ground and are often associated with age-related clonal haematopoiesis (Watson et al., 2020; Ostrander et al., 2020; Shlush, 2018; Li et al., 2016b; Jaiswal et al., 2014; Krönke et al., 2013; Welch et al., 2012). Additionally, specific genetic alterations are often gained during therapy and induce relapse, e.g. *FLT3-ITD* and mutation *KDM6A* (Greif et al., 2018).

Since this is a stepwise process, diverse precursor cells may still be present at any given time resulting in the genetic heterogeneity observed in most tumours (figure 1.5, linear evolution) (Turajlic et al., 2019; Burrell and Swanton, 2014; Gerlinger et al., 2014b). Furthermore, various co-operating mutations may occur leading to the divergence of several clones (branched evolution) (Turajlic et al., 2019; Burrell and Swanton, 2014; Gerlinger et al., 2014b).

Since in most patients therapy is not able to eradicate all tumour subclones, relapse may occur eventually (Yilmaz et al., 2019; Gerlinger et al., 2014b; Krönke et al., 2013; Jan et al., 2012; Mullighan et al., 2008). These resistant and out-grown cells can originate from one of the following four cell populations: (i) a clone already present at diagnosis, either the main clone or a subclone; (ii) a clone present at diagnosis that underwent evolution; (iii) an ancestral clone that underwent evolution; or (iv) a genetically distinct leukaemic clone (Waanders et al., 2020; Shlush et al., 2017; Krönke et al., 2013; Ding et al., 2012; Mullighan et al., 2008).

However, genetic heterogeneity is only one aspect of intra-tumour heterogeneity. Epige-

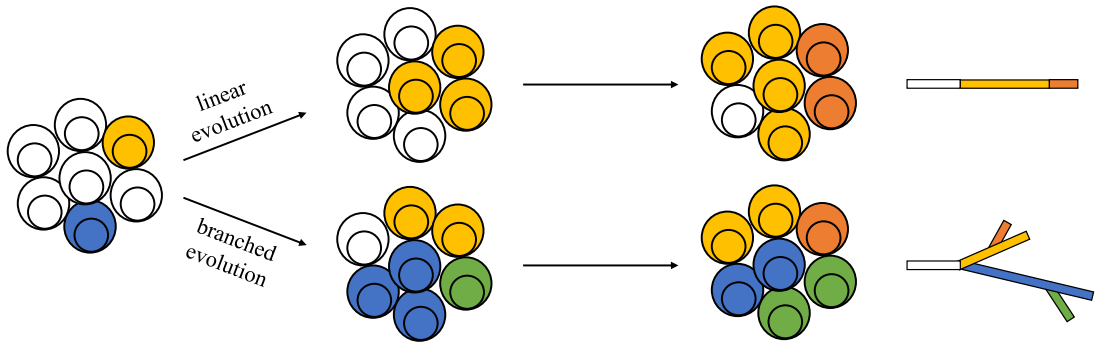

Figure 1.5. Linear and branched tumour evolution. Tumours may evolve either linearly or branched: (i) during linear evolution one lineage survives over time; (ii) in branched evolution divergence occurs due to continuous division and mutations resulting in various tumour lineages (Turajlic et al., 2019; Burrell and Swanton, 2014).

netic heterogeneity may also play an important role in the subclonal architecture of cancer and resistance development (Li et al., 2016b).

1.3.2. Epigenetic Heterogeneity

Epigenetic changes are heritable alterations in gene activation and expression that cannot be explained by variations in the DNA sequence (Caiado et al., 2016; Virani et al., 2012). These changes affect i.a. DNA methylation and histone modifications, and are considered reversible (Caiado et al., 2016; Virani et al., 2012).

Mutations in epigenetic regulators are often initiating DNA alterations that enable genetic instability demonstrating the significant role of epigenetic changes in AML (chapter 1.3.1) (Caiado et al., 2016; Li et al., 2016b; Corces-Zimmerman et al., 2014a) Furthermore, epigenetic variance is linked to inferior outcome in AML (Li et al., 2016a). Additionally, it has been demonstrated for several types of leukaemia that intra-tumour epigenetic diversity increases during disease progression (de Boer et al., 2018; Caiado et al., 2016; Li et al., 2016a,b; Corces et al., 2016; Li et al., 2014; Landau et al., 2014). Thus, the evolutionary fitness of the cancer is enhanced increasing the chance to survive under various selection pressures (Li et al., 2016b; Caiado et al., 2016; Corces et al., 2016). Furthermore, Corces et al. (2016) found variable regulome profiles for single AML cells with the help of single cell sequencing techniques. Moreover, global chromatin changes have been associated with drug resistant subpopulations in otherwise drug sensitive cell lines of multiple cancer types (Caiado et al., 2016; Kreso and Dick, 2014; Sharma et al., 2010).

Due to this significant effect of epigenetic alterations and variability on tumour adversity and the reversibility of these alterations, epigenetic drugs have been applied more and more for the

treatment of cancer (Estey, 2018). In AML, HMAs such as azacitidine and decitabine have shown promising effects so far (Papageorgiou et al., 2020; Estey, 2018; Fenaux et al., 2009).

In addition to heritable traits of a genetic and epigenetic nature, functional diversity plays a major role in determining adverse tumour subpopulations and treatment outcomes (Kreso and Dick, 2014).

1.3.3. Functional Heterogeneity

Functional heterogeneity regarding i.a. growth behaviour, stemness, dormancy, location within the tumour niche, and therapy response represents a major challenge in the successful treatment of AML and other tumour types since the most adverse cells determine patients' outcome (de Boer et al., 2018; Caiado et al., 2016; Kreso and Dick, 2014).

With regard to the CSC model (chapter 1.2.3) it is evident that tumour cells display variability regarding stemness (Caiado et al., 2016; Kreso and Dick, 2014). Thus, subpopulations within an individual AML display differences in their ability to engraft in immunocompromised mice (de Boer et al., 2018; Shlush et al., 2017; Klco et al., 2014; Kreso and Dick, 2014; Kreso et al., 2013). Accompanying this heterogeneity in stemness, variability in the proliferative state of AL cells has been described as well (Ebinger et al., 2020, 2016; Kreso and Dick, 2014; Kreso et al., 2013; Saito et al., 2010). In one of the first studies to link genetic and functional characteristics of AML subclones, de Boer et al. (2018) demonstrated that expression of plasma membrane proteins correlates with subclonal genetic mutations and is associated with engraftment *in vivo*, proliferation *in vitro* and chemotherapy response. Additionally, AL cells may locate and grow in different locations of the BM upon transplantation into mice (Belderbos et al., 2017; Elder et al., 2017; Verovskaya et al., 2014).

On the one hand, this functional heterogeneity is a demanding challenge in the aim to cure cancer. On the other hand, this may be exploited for the treatment of the disease in the future by combination or sequential therapy (Marusyk et al., 2020; Dagogo-Jack and Shaw, 2018).

Taken together, the combination of genetic, epigenetic and functional heterogeneity enables tumour cells to adapt to various selection pressures and, thus, facilitates evolutionary fitness. Accordingly, this heterogeneity represents a reservoir for potentially therapy resistant and relapse-inducing clones. Therefore, in order to treat cancer patients successfully, it is necessary to better understand the intra-patient heterogeneity and to correlate genetic and epigenetic alterations with functional characteristics.

1.4. A Clinic Close Model of AML

To study tumour heterogeneity and the biology of adverse subclones within an individual leukaemia, certain prerequisites for a cellular model have to be fulfilled: (i) the model is representative of the patient's AML; (ii) the model displays genetic heterogeneity; and (iii) the model allows functional studies.

Cell lines are commonly used to investigate the biology of adverse cancers (Ben-David et al., 2019). However, cell lines are usually insufficient to study tumour heterogeneity since their clonality is reduced over time (Belderbos et al., 2017). Additionally, unphysiologic mutations accumulate in cell lines leading to changes in transcriptome and proteome (Liu et al., 2019b; Ben-David et al., 2018; Fasterius and Szigyarto, 2018; Pan et al., 2009).

One option to study the complex biology of AML are patients' primary leukaemic cells. This is as close to the situation in the patient as possible. However, functional studies remain difficult in patient's AML cells, since these cells rarely proliferate *in vitro* (Brenner et al., 2019). Moreover, primary material is limited impeding research further.

An alternative model, which is suitable to study the clonal heterogeneity of AL, is the patient-derived xenograft (PDX) mouse model, where primary patients' tumour cells are engrafted into immunocompromised mice (Griessinger et al., 2018; Vick et al., 2015; Lapidot et al., 1994; Cesano et al., 1992; Kamel-Reid et al., 1989). Here, the genetic diversity of the disease can be mimicked (Richter-Pechańska et al., 2018; Vick et al., 2015), and additionally, functional studies are possible (Liu et al., 2019a; Ebinger et al., 2016; Townsend et al., 2016; Vick et al., 2015).

1.4.1. The Patient-Derived Xenograft Mouse Model of AML

In the 1980s, AL cell lines and primary patients' cells were transplanted into mice homozygous for severe combined immunodeficiency (SCID) (Kamel-Reid et al., 1989). However, engraftment rates were low and, therefore, mice with stronger immunodeficiency were developed and transplanted with tumour cells (Shultz et al., 1995, 2005). Currently, the standard for leukaemic PDX models are non-obese diabetic (NOD)/ SCID/ interleukin-2 receptor γ chain mutated (NSG) mice, which lack mature T, B and natural killer cells and are deficient in cytokine signalling pathways (Shultz et al., 2005). This severely immunocompromised mouse strain allows engraftment of 23 - 58% of patients' AML in the first passage, and up to 60% in later passages (Townsend et al., 2016; Vick et al., 2015).

Primary patients' AL cells obtained from BM aspirates or peripheral blood (pB) are trans-

planted into immunocompromised mice, where the cells home and proliferate in the haematopoietic niche and mimic the disease (Ebinger et al., 2016; Townsend et al., 2016; Vick et al., 2015). At advanced time points, tumour cells can disseminate into peripheral organs such as blood, spleen and liver (Belderbos et al., 2017; Ebinger et al., 2016; Townsend et al., 2016; Vick et al., 2015). Leukaemic cells can then be re-isolated from murine BM and spleen and re-injected into next recipient mice for several rounds of passaging (Ebinger et al., 2016; Vick et al., 2015).

PDX AML lines span a broad range of diagnostic categories, cytogenetic profiles and genotypes (Townsend et al., 2016). Furthermore, they represent the genetic landscape of the primary patients' cells (Townsend et al., 2016; Vick et al., 2015), even though it has been reported that minor subclones may constitute the leukaemia in the xenograft (Townsend et al., 2016; Klco et al., 2014; Clappier et al., 2011).

Because of this, PDX models of AL are the gold standard for performing preclinical treatment trials (Townsend et al., 2016; Ebinger et al., 2016), analysing the leukaemic niche (Habringer et al., 2018; Zong et al., 2016; Ebinger et al., 2016), studying LSCs (Ebinger et al., 2016; Hope et al., 2003; Bhatia et al., 1997) and clonal heterogeneity and evolution (Belderbos et al., 2017; Elder et al., 2017; Clappier et al., 2011).

1.4.2. The Genetically Engineered PDX Mouse Model of AML

To study these biological processes and the underlying molecular mechanisms, the PDX model of AL was developed further into a genetically engineered PDX (GEPDX) model (figure 1.6). Here, serially transplantable PDX AML cells can be genetically manipulated using lentiviruses (Liu et al., 2019a; Ebinger et al., 2016; Vick et al., 2015; Terziyska et al., 2012). Transgenes such as cell surface markers, e.g. the nerve growth factor receptor (NGFR), and fluorochromes, e.g. mCherry, can be introduced into the cellular genome and subsequently expressed (Liu et al., 2019a; Ebinger et al., 2016; Vick et al., 2015). These markers serve for enrichment and monitoring of cells by magnetic (MACS) and/or fluorescence activated cell sorting (FACS). Additionally, the transduction of a luciferase enables reliable and sensitive *in vivo* monitoring of leukaemic burden via bioluminescence imaging (BLI) in order to follow up tumour growth and chemotherapy response (Liu et al., 2019a; Ebinger et al., 2016; Vick et al., 2015). Furthermore, studies on molecular signalling pathways involved in leukaemia maintenance, therapy resistance and relapse are enabled by the GEPDX model using knock-down, knock-out or knock-in approaches (Liu et al., 2019a).

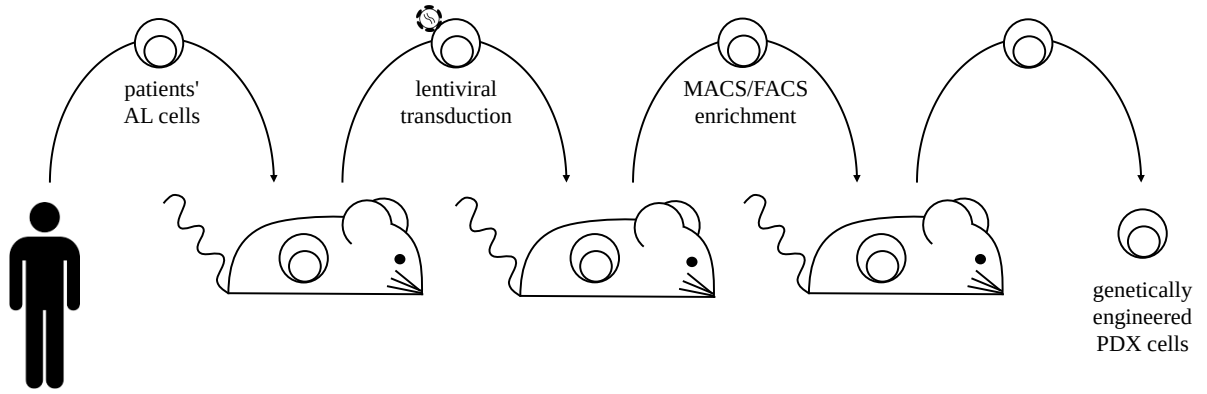

Figure 1.6. The genetically engineered PDX (GEPDX) AL model. Primary patients' AL cells are transplanted into immunocompromised mice, where they home and proliferate in the haematopoietic niche. Tumour cells can be re-isolated from murine bone marrow (BM) and spleen, lentivirally transduced to express transgenes, enriched via magnetic (MACS) or fluorescence acitvated cell sorting (FACS), and serially transplanted (Ebinger et al., 2016; Vick et al., 2015).

1.5. Tools to Investigate Tumour Heterogeneity

In order to better understand cancer heterogeneity and evolution, mostly primary tumour material has been studied (Chen et al., 2019; Labuhn et al., 2019; Desai et al., 2018; Rothenberg-Thurley et al., 2018; Shlush et al., 2014; Corces-Zimmerman et al., 2014a; Gerlinger et al., 2014a; Wang et al., 2014a; Ding et al., 2012). Several groups have applied next generation sequencing, e.g. exome, whole genome and targeted sequencing, to investigate the heterogeneity within an individual patient (Chen et al., 2019; Labuhn et al., 2019; Yilmaz et al., 2019; Greif et al., 2018; Rothenberg-Thurley et al., 2018; Shlush et al., 2014; Corces-Zimmerman et al., 2014a; Gerlinger et al., 2014a, 2012; Ding et al., 2012; Jan et al., 2012). Recent developments have enabled DNA and RNA single cell sequencing and are used to study intra-tumour heterogeneity (van Galen et al., 2019; Pellegrino et al., 2018; Wang et al., 2014a; Patel et al., 2014). Furthermore, fluorescence *in situ* hybridization, proteome and flow cytometric analyses of cell surface proteins are applied to investigate cancer heterogeneity (de Boer et al., 2018; Anderson et al., 2011). However, even though these methods enable a snapshot of the heterogeneity at one point in time, longitudinal studies are not possible, and insights into functional differences still remain elusive with these techniques.

1.5.1. Genetic Barcoding

A recently developed technique to study clonal heterogeneity whithin individual samples, which has been applied especially in the haematopoietic and leukaemic field, is genetic barcoding (figure 1.7) (Jacobs et al., 2019; Roh et al., 2018; Belderbos et al., 2017; Elder et al.,

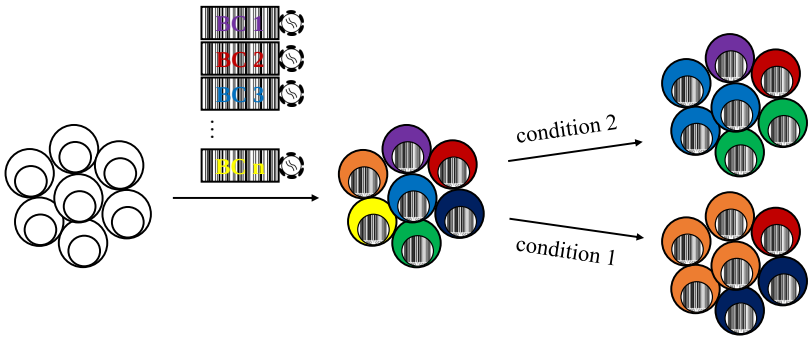

Figure 1.7. Genetic barcoding. Cells of interest are lenti- or retrovirally transduced with a BC pool marking every single cell with an unique BC. This allows distinction as well as space- and time-dependent tracking of individual cells (Bystrykh and Belderbos, 2016; Bystrykh et al., 2014).

2017; Bystrykh and Belderbos, 2016; Levy et al., 2015; Verovskaya et al., 2014; Bystrykh et al., 2014; Cheung et al., 2013). Here, cells are marked retro- or lentivirally with a barcode (BC) pool allowing distinction of single cells and their descendants by their individual BC (Bramlett et al., 2020; Adair et al., 2020; Belderbos et al., 2017; Elder et al., 2017; Bystrykh and Belderbos, 2016; Verovskaya et al., 2014; Bystrykh et al., 2014).

BCs are synthetic DNA sequences of a defined length, which consist of random nucleotides (Bystrykh and Belderbos, 2016; Bystrykh et al., 2014). Three major BC designs have been applied: (i) random BCs (N_x) with a sequence of length x consisting of random nucleotides (N; adenine (A), thymine (T), guanine (G), and cytosine (C)) (Bramlett et al., 2020; Wu et al., 2014; Lu et al., 2011); (ii) restricted-random BCs (SW_x) with a succession of strong (S) and weak (W) nucleotides. This enables a constant GC-ratio (Hyo-eun et al., 2015); and (iii) semi-random BCs (e.g. AANNATCNNGAT), which comprise a succession of fixed and random nucleotides. This recognizable sequence has an advantage in cloning and sequence analysis (Jacobs et al., 2019; Belderbos et al., 2017; Elder et al., 2017; Bystrykh and Belderbos, 2016).

Genetic barcoding represents a novel, reliable and sensitive tool to study processes of clonal proliferation and expansion, to monitor clonal dynamics over time, and to trace stem cell differentiation (Bramlett et al., 2020; Adair et al., 2020; Jacobs et al., 2019; Belderbos et al., 2017; Elder et al., 2017; Bystrykh and Belderbos, 2016; Brugman et al., 2015; Verovskaya et al., 2014; Cheung et al., 2013; Lu et al., 2011; Schepers et al., 2008).

1.5.2. Red/Green/Blue Fluorochrome Marking

An additional technique to track single cells over time and space is red/green/blue (RGB) colour marking (figure 1.8) (van der Heijden et al., 2019; Gambera et al., 2018; Cornils et al., 2014; Weber et al., 2012, 2011). Here, cells are genetically labelled with three lenti- or retroviruses

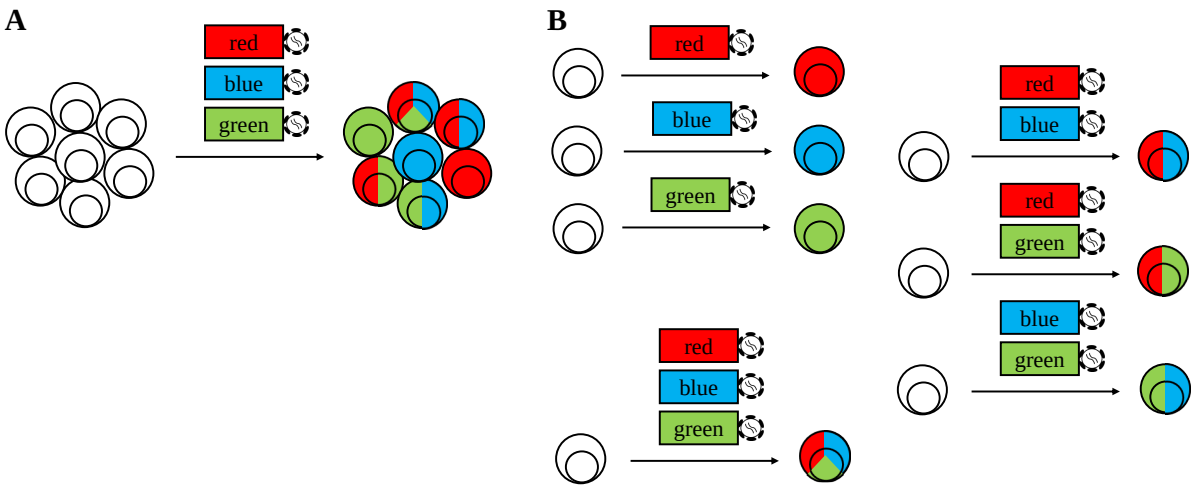

Figure 1.8. RGB marking strategies. A. Cells of interest are transduced with lenti- or retroviruses encoding a red, green or blue fluorochrome resulting in single, double, and triple transduced cells . **B.** Cell clones of interest are marked with a predefined colour combination leading to single, double, and triple transduced clones (Maetzig et al., 2018, 2017; Weber et al., 2011).

encoding a red, green or blue fluorochrome (van der Heijden et al., 2019; Finkenzeller, 2016; Abramowski et al., 2015; Gomez-Nicola et al., 2014; Weber et al., 2012, 2011). Various numbers of integration of each vector in each cell result in specific colour-coding of individual cells (figure 1.8A) (Finkenzeller, 2016; Weber et al., 2012, 2011). Alternatively, cell populations of interest can be marked with predetermined colour combinations (figure 1.8B) (Maetzig et al., 2018, 2017). This has the advantage of defined colours for each clone, but is limited to monoclonal cell populations. RGB marking is a useful tool since it enables isolation and identification of viable cell populations in contrast to genetic barcoding, however, both methods have been applied in combination as well to allow both genetic and functional characterisation of cells (Maetzig et al., 2017; Cornils et al., 2017, 2014).

RGB marking presents an innovative and valuable method to assess tumour heterogeneity and clonal dynamics and dominance, both in solid and liquid tumours (van der Heijden et al., 2019; Gambera et al., 2018; Cornils et al., 2017; Finkenzeller, 2016; Abramowski et al., 2015). Moreover, migration of individual CSCs can be tracked over time (Gomez-Nicola et al., 2014).

1.6. Aim of this Work

Despite good initial response rates of a majority of AML patients to standard chemotherapy, relapse is a common event. Clonal heterogeneity is expected to be one major reason for this phenomenon and the most adverse tumour subpopulation determines patients' outcomes. Thus, novel therapeutic approaches that eliminate also the most challenging leukaemic cells are ur-

gently needed.

To discover putative targets for new treatment options, it is essential to better understand the clonal heterogeneity and to identify the most aggressive subclone(s) within an individual tumour. Therefore, it is not only necessary to characterise the (epi-)genetic heterogeneity of AML, but also to correlate this information to functional traits.

The first aim of the present study was to characterise PDX AML samples to identify a patient's leukaemia model suitable to study clonal heterogeneity. In the second part, PDX AML clones derived from single stem cells (single cell clones, SCCs) of one individual patient were generated and validated. In the third part of this work, the produced SCCs were characterised functionally in order to find the most adverse subclone(s) within this patient's AML. Additionally, SCCs were analysed genetically and phenotypically to correlate functional aggressiveness to genetics and phenotype.

With these objectives the present study enables not only a better understanding of the genetic, epigenetic and functional intra-tumour heterogeneity in AML, but also lays the ground work for the discovery of potential targets for novel therapeutic options.

2. Material

2.1. Laboratory Animals

Table 2.1. Laboratory animals.

Laboratory animals	Provider
NOD.Cg-Prkdc^{scid} Il2rg^{tm1Wjl}/SzJ (NSG)	Jackson Laboratory, Bar Harbor, MA, USA

In this study human acute myeloid leukaemia (AML) cells were engrafted into NSG mice (Shultz et al., 2005). NSG have a interleukin-2 receptor gamma chain knockout on a non-obese diabetic/severe combined immunodeficiency (NOD/SCID) background. These mice are severely immunocompromised animals lacking mature T, B and natural killer cells and deficient in cytokine signalling pathways (Shultz et al., 2005).

2.2. Cell Lines and Bacterial Strains

Table 2.2. Cell lines.

Cell line	Description	Provider
HEK-293T	human embryonal kidney cell line expressing the temperature sensitive mutant of SV-40 large T-antigen	DSMZ, Braunschweig, Germany
MOLM-13	human AML cell line	DSMZ, Braunschweig, Germany
NALM-6	human B cell precursor leukaemia cell line	DSMZ, Braunschweig, Germany

Table 2.3. Bacterial strains.

Bacterial Strain	Description	Provider
Escherichia coli (E.coli) DH5α	F$^-$ Φ80*lac*ZΔM15 Δ(*lac*ZYA-*arg*F) U169 *rec*A1 *end*A1 *hsd*R17(r_k^-, m_k^+) *pho*A *sup*E44 *thi*-1 *gyr*A96 *rel*A1 λ^-	Thermo Fisher Scientific, Waltham, MA, USA
NEB Stable Competent *E.coli*	F' *proA+B+ lacI^q* Δ*(lacZ)M15 zzf::Tn10 (Tet^R)* Δ*(ara-leu) 7697 araD139 fhuA* Δ*lacX74 galK16 galE15 e14-* Φ*80dlacZ*Δ*M15 recA1 relA1 endA1 nupG rpsL (Str^R) rph spoT1* Δ*(mrr-hsdRMS-mcrBC)*	New England Biolabs, Frankfurt am Main, Germany

2.3. Plasmids, Primers and Enzymes

Table 2.4. Plasmids, part 1.

Plasmid	Provider
pCDH-BC-EF1α-H2K^k-T2A-NGFR (w/o NheI, with AvrII)	cloned by Daniel Richter
pCDH-BC-EF1α-H2K^k-T2A-NGFR-eBC (w/o NheI, with AvrII)	cloned by Daniel Richter
pCDH-EF1α-eFFly-T2A-eGFP	cloned by Michela Carlet
pCDH-EF1α-eFFly-T2A-iRFP720	cloned by Christina Zeller for this study
pCDH-EF1α-eFFly-T2A-mCherry	cloned by Michela Carlet
pCDH-EF1α-eFFly-T2A-mtagBFP	cloned by Michela Carlet
pCDH-EF1α-eGFP	cloned by Christina Zeller for this study
pCDH-EF1α-Gluc-T2A-iRFP720	cloned by Wen-Hsin Liu
pCDH-EF1α-H2K^k-T2A-NGFR	cloned by Omar Elakad
pCDH-EF1α-H2K^k-T2A-NGFR (w/o NheI)	cloned by Christina Zeller for this study

Table 2.5. Plasmids, part 2.

Plasmid	Provider
pCDH-EF1α-H2K^k-T2A-NGFR (w/o NheI, with AvrII)	cloned by Christina Zeller for this study
pCDH-EF1α-iRFP720	cloned by Wen-Hsin Liu
pCDH-EF1α-mCherry	cloned by Cornelia Finkenzeller
pCDH-EF1α-mtagBFP	cloned by Cornelia Finkenzeller
pMD2.G	Addgene, Cambridge, MA, USA
pMDLg/pRRE (393)	Addgene, Cambridge, MA, USA
pRSV-Rev (392)	Addgene, Cambridge, MA, USA

All primers were ordered by Integrated DNA Technologies, Skokie, IL, USA.

Table 2.6. Primers, part 1.

Sequence	Application	T_m [°C]
TTTGCCTGACCCTGCTTG	Sanger sequencing	56.0
CATAGCGTAAAAGGAGCAACA	Amplification of eGFP, Sanger sequencing	55.9
TCCACCATTAGCACCCAAAGC	Finger printing of PDX samples	59.8
TCGGATACAGTTCACTTTAGC	Finger printing of PDX samples	55.9
GGGGTACCCCGGATGAATCCTAGGAAA AGAAAAGGGGGGACTGG	Introduction of AvrII restriction site	77.8
TGCTCACATGTTCTTTCCTGCGTTATCC	Introduction of AvrII restriction site	65.1
CCATCGATACTAGTAAGGATCTGCG	Destruction of NheI restriction site, Sanger sequencing	63.0
CCGGAATTCAAGAGCTCTAGAGTAGG	Destruction of NheI restriction site	64.8
CTCAAGTCAGAGGTGGCGAAA	Sanger sequencing	59.8
TTTCGCCACCTCTGACTTGAG	Sanger sequencing	59.8
AAGAAGGGCGGCAAGTGAGGATC	Sanger sequencing	64.2
CGGGATCCATGGTGAGCAAGGGCGAG	Amplification of eGFP	71.1

Table 2.7. Primers, part 2.

Sequence	Application	T_m [°C]
TTGGTCTCTCATGGCACTGT	Amplification of NRAS mutation	57.3
AGCATTGCATTCCCTGTGGT	Amplification of NRAS mutation, Sanger sequencing	57.3
GGCCTGCTGAAAATGACTGA	Amplification of KRAS mutation	57.3
TGTATCAAAGAATGGTCCTGCA	Amplification of KRAS mutation, Sanger sequencing	56.5
GTTCTTGGCCAGCGTTGAC	Amplification of JAK1 mutation, Sanger sequencing	58.8
GAGAACAAGGCTTGGCAGTG	Amplification of JAK1 mutation	59.3
GCCCTTAGAGATCATGCTAG	Amplification of EZH2 mutation, Sanger sequencing	57.3
CCTGGAACAATAGTGTGTTC	Amplification of EZH2 mutation	55.3
GGACACTCTTTCCCTACACGACGCTCTT CCGATCTNNNNNNNNNNNNATGGGAA AGAGTGTCC-CTGGTACCTTTAAGACCA ATGACT	Amplification of BC	82.8
GTGACTGGAGTTCAGACGTGTGCTCTT CCGATCTGCTTAAGCAGTGGGTTCCCT	Amplification of BC	82.2

Table 2.8. Enzymes, part 1.

Enzyme	Application	Manufacturer
Actinase E	Polymerase inactivation	Sigma-Aldrich, St. Louis, MO, USA
AvrII	Restriction digest	New England Biolabs, Frankfurt am Main, Germany
BamHI-HF	Restriction digest	New England Biolabs, Frankfurt am Main, Germany
ClaI	Restriction digest	New England Biolabs, Frankfurt am Main, Germany
EcoRI-HF	Restriction digest	New England Biolabs, Frankfurt am Main, Germany
Exonuclease I	Primer digest	Thermo Fisher Scientific, Waltham, MA, USA

Table 2.9. Enzymes, part 2.

Enzyme	Application	Manufacturer
GoTaq Polymerase	PCR	Promega, Madison, WI, USA
KAPA HiFi HotStart Polymerase	PCR	Roche, Mannheim, Germany
KpnI	Restriction digest	New England Biolabs, Frankfurt am Main, Germany
KpnI-HF	Restriction digest	New England Biolabs, Frankfurt am Main, Germany
NheI-HF	Restriction digest	New England Biolabs, Frankfurt am Main, Germany
NsiI-HF	Restriction digest	New England Biolabs, Frankfurt am Main, Germany
PciI	Restriction digest	New England Biolabs, Frankfurt am Main, Germany
Pfu Polymerase	PCR	Thermo Fisher Scientific, Waltham, MA, USA
Phusion High-Fidelity PCR Master Mix	PCR	New England Biolabs, Frankfurt am Main, Germany
Phusion II HotStart Polymerase	PCR	Thermo Fisher Scientific, Waltham, MA, USA
Proteinase K	Protein digest	Thermo Fisher Scientific, Waltham, MA, USA
Q5 HotStart High Fidelity Polymerase	PCR	New England Biolabs, Frankfurt am Main, Germany
SalI-HF	Restriction digest	New England Biolabs, Frankfurt am Main, Germany
SpeI-HF	Restriction digest	New England Biolabs, Frankfurt am Main, Germany
T4 DNA Ligase	Ligation	Thermo Fisher Scientific, Waltham, MA, USA

2.4. Antibodies

Table 2.10. MACS beads.

MACS beads	Manufacturer
Mouse cell depletion kit	Miltenyi, Bergisch Gladbach, Germany

Table 2.11. Antibodies.

Antibody	Manufacturer
anti-human CD271(NGFR)-FITC, clone ME20.4, # 345104	Biozol, Eching, Germany
anti-human CD271(NGFR)-PerCP-Cy5.5, clone H100-27.R55, # 130-102-346	Biolegend, San Diego, CA, USA
anit-murine $H2K^k$-APC, clone H100-27.R55, # 130-102-346	Miltenyi, Bergisch Gladbach, Germany
anti-human CD33-PE, clone IV M505, # 555450	BD Bioscience, Heidelberg, Germany
anti-human CD45-APC, clone IV N816, # 555485	BD Bioscience, Heidelberg, Germany
mouse IgG1 APC isotype control, clone MOPC-21, # 400119	BD Bioscience, Heidelberg, Germany
mouse IgG1 FITC isotype control, clone MOPC-21, # BLD-400107	Biozol, Eching, Germany
mouse IgG1 PE isotype control, clone MOPC-21, # 400140	BD Bioscience, Heidelberg, Germany
mouse IgG1 PerCP-Cy5.5 isotype control, clone MOPC-21, #BLD-400150	Biozol, Eching, Germany

2.5. Chemotherapeutics

Table 2.12. Chemotherapeutics.

Chemotherapeutic	Manufacturer
5-Azacitidine	Selleck Chemicals Llc, Houston, TX, USA
Cytarabine incl. Sodium-(S)-lactate solution (50%)	Cell Pharma GmbH, Vilbel, Germany
Venetoclax	Selleck Chemicals Llc, Houston, TX, USA

2.6. Commercial Kits

Table 2.13. Commercial kits, part 1.

Commercial Kit	Application	Manufacturer
DNeasy Blood & Tissue Kit	Isolation of genomic DNA	Qiagen, Venlo, Netherlands
DNeasy Micro Kit	Isolation of genomic DNA	Qiagen, Venlo, Netherlands
Haloplex	Sequencing of recurrently mutated genes	Agilent Technologies, Santa Clara, CA, USA
High Sensitivity DNA Kits	Quantification of sequencing libraries	Agilent Technologies, Santa Clara, CA, USA
Infinium Methylation-EPIC BeadChip	DNA methylation analysis	Illumina, San Diego, CA, USA
KAPA HiFi PCR Kit	PCR	Peqlab, Erlangen, Germany
MinElute PCR Purifcation Kit	Purification of PCR product	Qiagen, Venlo, Netherlands
Monarch DNA Gel Extraction Kit	DNA extraction	New England Biolabs, Frankfurt am Main, Germany
Nextera XT Kit	Generation of Nextera libraries	Illumina, San Diego, CA, USA
NucleoBond Extra Midi	Isolation of plasmid DNA (Midi)	Macherey-Nagel, Duren, Germany
NucleoSpin Gel and PCR Clean-Up	Purification of PCR products, extraction of DNA from agarose gels	Macherey-Nagel, Duren, Germany
NuleoSpin Plasmid Easy Pure	Isolation of plasmid DNA (Mini)	Macherey-Nagel, Duren, Germany
PureYield Midi Prep Kit	Isolation of plasmid DNA (Midi)	Promega, Madison, WI, USA
QIAamp DNA Blood Mini Kit	Isolation of genomic DNA	Qiagen, Venlo, Netherlands
QIAamp DNA Mini Kit	Isolation of genomic DNA	Qiagen, Venlo, Netherlands
QuantiT PicoGreen dsDNA Assay	Quantification of genomic DNA	Thermo Fisher Scientific, Waltham, MA, USA

Table 2.14. Commercial kits, part 2.

Commercial Kit	Application	Manufacturer
Qubit dsDNA HS Assay Kit	Quantification of genomic DNA	Invitrogen, Carlsbad, CA, USA
SureSelect Human All Exon V6 Kit	Preparation of exome libraries	Agilent Technologies, Santa Clara, CA, USA

2.7. Reagents and Solutions

Table 2.15. Reagents and solutions, part 1.

Reagent	Manufacturer
β-mercaptoethanol	Sigma-Aldrich, St. Louis, MO, USA
Acetic acid	Carl Roth, Karlsruhe, Germany
Agar-Agar Kobe I	Carl Roth, Karlsruhe, Germany
Agarose	Life Technologies, Carlsbad, CA, USA
Ampicillin	Sigma-Aldrich, St. Louis, MO, USA
ATP	New England Biolabs, Frankfurt am Main, Germany
Baytril (2.5%)	Bayer, Leverkusen, Germany
BSA	Carl Roth, Karlsruhe, Germany
$CaCl_2$	Carl Roth, Karlsruhe, Germany
Carboxymethylcellulose sodium	Sigma-Aldrich, St. Louis, MO, USA
CutSmart buffer	New England Biolabs, Frankfurt am Main, Germany
DAPI (1 mg/ml)	Sigma-Aldrich, St. Louis, MO, USA
D-Luciferin	Biomol GmbH, Hamburg, Germany
DMEM	Gibco, San Diego, CA, USA
DMSO	Sigma-Aldrich, St. Louis, MO, USA
DNA ladder mix	Thermo Fisher Scientific, Waltham, MA, USA
DNA loading dye	Thermo Fisher Scientific, Waltham, MA, USA
DNase I	Roche, Mannheim, Germany
DNase I Buffer	Roche, Mannheim, Germany
dNTPs (10 mM each)	Biozym, Hessisch Oldendorf, Germany

Table 2.16. Reagents and solutions, part 2.

Reagent	Manufacturer
EDTA (0.5 M)	Lonza, Basel, Switzerland
Ethanol	Carl Roth, Karlsruhe, Germany
FACS Lysing solution	BD Bioscience, Heidelberg, Germany
Fetal calf serum (FCS)	Gibco, San Diego, CA, USA
Ficoll	GE Healthcare, Freiburg, Germany
Gentamycin	Lonza, Basel, Switzerland
Glucose (20%)	Braun, Melsungen, Germany
Glycerine 98%	Carl Roth, Karlsruhe, Germany
GoTaq Polymerase reaction buffer	Promega, Madison, WI, USA
Heparin	Ratiopharm, Ulm, Germany
Isoflurane	Sigma-Aldrich, St. Louis, MO, USA
Isopropyl alcohol	Merck Milipore, Darmstadt, Germany
K-Acetate	Sigma-Aldrich, St. Louis, MO, USA
KCl	Merck Milipore, Darmstadt, Germany
KH_2PO_4	Merck Milipore, Darmstadt, Germany
L-Glutamine	Gibco, San Diego, CA, USA
Midori Green	Biozym, Hessisch Oldendorf, Germany
$MnCl_2$	Sigma-Aldrich, St. Louis, MO, USA
MOPS	Sigma-Aldrich, St. Louis, MO, USA
Na_2HPO_4	Sigma-Aldrich, St. Louis, MO, USA
NaCl	Carl Roth, Karlsruhe, Germany
NEBuffer 3.1	New England Biolabs, Frankfurt am Main, Germany
Nitrogen	Linde AG, Pullach, Germany
PBS	Gibco, San Diego, CA, USA
Penicillin/Streptavidin (Pen/Strep, 5,000 U/ml)	Gibco, San Diego, CA, USA
Pfu Polymerase reaction buffer	Life Technologies, Carlsbad, CA, USA
Polybrene	Sigma-Aldrich, St. Louis, MO, USA
Recombinant human FMS-like tyrosine kinase 3 ligand (FLT3L)	R&D Systems, Minneapolis, MN, USA

Table 2.17. Reagents and solutions, part 3.

Reagent	Manufacturer
Recombinant human iterleukin 3 (IL3)	Peprotech, Rocky Hill, NJ, USA
Recombinant human stem cell factor (SCF)	Peprotech, Rocky Hill, NJ, USA
Recombinant human thrombopoietin (TPO)	Peprotech, Rocky Hill, NJ, USA
RLT buffer	Qiagen, Venlo, Netherlands
RPMI-1640	Gibco, San Diego, CA, USA
Selected peptone 140	Gibco, San Diego, CA, USA
StemPro-34 including Nutrient Supplement	Thermo Fisher Scientific, Waltham, MA, USA
T4 Ligation buffer	Thermo Fisher Scientific, Waltham, MA, USA
TE buffer	Thermo Fisher Scientific, Waltham, MA, USA
Trypan blue	Sigma-Aldrich, St. Louis, MO, USA
Trypsine dissociation agent (0.05%)	Gibco, San Diego, CA, USA
Turbofect	Thermo Fisher Scientific, Waltham, MA, USA
Yeast extract	Carl Roth, Karlsruhe, Germany

2.8. Buffers and Media

Table 2.18. Buffers, part 1.

Buffer	Ingredients
Phosphate buffered saline (PBS)	H_2O
	137 mM NaCl
	2.7 mM KCl
	10 mM Na_2HPO_4
	1.8 mM KH_2PO_4
PBS + 2% FCS	
PBS + 0.5% BSA	
PBE	PBS
	0.5% BSA
	5 mM EDTA

Table 2.19. Buffers, part 2.

Buffer	Ingredients
TAE buffer	H_2O
	1.8 g Tris/HCl, pH 8.5
	1.14 ml acetic acid
	0.7 g EDTA
TFB I buffer	H_2O, pH 5.8
	100 mM KCl
	10 mM $CaCl_2$
	30 mM K-Acetate
	50 mM $MnCl_2$
	15% glycerine
TFB II buffer	H_2O, pH 7.0
	10 mM KCl
	75 mM $CaCl_2$
	10 mM MOPS
	15% glycerine

Table 2.20. Media, part 1.

Medium	Ingredients
LB agar	H_2O
	1% Selected peptone 140
	0.5% Yeast extract
	1% NaCl
	1.5% Agar-Agar Kobe I
LB medium	H_2O
	1% Selected peptone
	0.5% Yeast extract
	1% NaCl

Table 2.21. Media, part 2.

Medium	Ingredients
Medium for cultivation of AL cell lines	RPMI-1640
	10% FCS
	1% L-Glutamine
Medium for cultivation of HEK-293T cells	DMEM
	10% FCS
	1% L-Glutamine
Medium for cultivation of PDX AML cells	StemPro-34 including Nutrient Supplement
	2% FCS
	1% L-Glutamine
	1% Pen/Strep
	10 ng/ml FLT3L
	10 ng/ml SCF
	10 ng/ml IL3
	10 ng/ml TPO

2.9. Consumable Supplies

Table 2.22. Consumable supplies, part 1.

Consumable Supplies	Manufacturer
2% E-Gel Agarose EX gel	Life Technologies, Skokie, IL, USA
Amicon-Ultra 15ml centrifugal filter units	Merck Milipore, Darmstadt, Germany
Bacterial tubes (for mini)	Corning, Corning, NY, USA
Cell culture EasyFlask T75	Thermo Fisher Scientific, Waltham, MA, USA
Cell culture flasks (T25, T75, T175)	Greiner bio-one, Frickenhausen, Germany
Cell strainer (45 μm, 70 μm)	Greiner bio-one, Frickenhausen, Germany
Centrifuge tubes (15 ml and 50 ml)	Greiner bio-one, Frickenhausen, Germany
Colony picking sticks	Sarstedt, Nümbrecht, Germany

Table 2.23. Consumable supplies, part 2.

Consumable Supplies	Manufacturer
Cryotubes	Thermo Fisher Scientific, Waltham, MA, USA
Disposable serological pipettes (5 ml, 10 ml, 25 ml and 50 ml)	Greiner bio-one, Frickenhausen, Germany
Eppendorf reagent tubes (0.5 ml, 1.5 ml and 2.0 ml)	Greiner bio-one, Frickenhausen, Germany
FACS tubes (with and without filter)	Corning, Corning, NY, USA
LS columns	Miltenyi, Bergisch Gladbach, Germany
Microcentrifuge tube, DNA LoBind (1.5 ml)	Sigma-Aldrich, St. Louis, MO, USA
Microvette	Sarstedt, Nümbrecht, Germany
Needles RN G32 PST3 51MM	Hamilton, Reno, USA
Nitrile gloves (S)	Starlab, Hamburg, Germany
Petri dishes	Greiner bio-one, Frickenhausen, Germany
Pipette filter tips TipOne	Starlab, Hamburg, Germany
Pipette tips TipOne	Starlab, Hamburg, Germany
Pipettes (5 ml, 10 ml, 25 ml)	Greiner bio-one, Frickenhausen, Germany
Well plates for tissue culture (6-well, 12-well, 24-well, 48-well and 96-well)	Corning, Corning, NY, USA

2.10. Equipment

Table 2.24. Equipment, part 1.

Equipment	Manufacturer
B 6060 microbiological incubator	Heraeus, Hanau, Germany
Bioanalyzer 2100	Agilent Technologies, Santa Clara, CA, USA
Biological safety cabinet Safe 2020	Thermo Fisher Scientific, Waltham, MA, USA
Calibration check pH meter HI 221	Hanna Instruments Deutschland GmbH, Vöhringen, Germany
Cell sorter BD FACS AriaIII	BD Bioscience, Heidelberg, Germany
Centrifuge Rotanta 460R	Andreas Hettich GmbH & Co.KG, Tuttlingen, Germany

Table 2.25. Equipment, part 2.

Equipment	Manufacturer
Cryotube label printer BMP51	Brady, Egelsbach, Germany
Flow cytometer BD Calibur	BD Bioscience, Heidelberg, Germany
Flow cytometer BD LSRFortessa X20	BD Bioscience, Heidelberg, Germany
Fluorescence microscope Axioplan	Zeiss, Jena, Germany
Freezer (−20°C)	Siemens, Berlin, Germany
Freezer (−80°C)	Thermo Fisher Scientific, Waltham, MA, USA
Freezing container Nalgene Mr.Frosty	Sigma-Aldrich, St. Louis, MO, USA
Gel documentation station E-box VX5	Peqlab, Erlangen, Germany
Heating block MixerHC	Starlab, Hamburg, Germany
HiSeq1500 Sequencer	Illumina, San Diego, CA, USA
Incubator Hera Cell 150i	Heraeus, Hanau, Germany
IVIS Lumina II Imaging System	Caliper Life Sciences, Mainz, Germany
Light microscope 550 1317	Zeiss, Jena, Germany
Magnetic stirrer MR3001	Heidolph Instruments, Schwabach, Germany
Micro Scales Artorius 2001 MP2	Sartorius AG, Göttingen, Germany
Microarray Scanner	Illumina, San Diego, CA, USA
Microwave MW 1226CB	Bomann, Kempen, Germany
MiSeq Sequencer	Illumina, San Diego, CA, USA
Nanodrop OneC	Thermo Fisher Scientific, Waltham, MA, USA
PerfectBlue Gelsystem Mini S	Peqlab, Erlangen, Germany
Power supply PowerPac	Bio-Rad, München, Germany
ProFlex PCR system	Life Technologies, Carlsbad, CA, USA
QIACube	Qiagen, Venlo, Netherlands
Quietek CO_2 Induction Systems	Next Advance, Averill Park, NY, USA
Refrigerator	Liebherr, Bulle, Germany
Roller mixer SRT6D	Stuart, Staffordshire, UK
Table Centrifuge mini Spin	Eppendorf, Hamburg, Germany
Water bath	Memmert, Schwabach, Germany

2.11. Software

Table 2.26. Software.

Software	Provider
Geneious 11	Biomatters Ltd, Auckland, New Zealand
MyIMouse	Bioslava, Hagenbach, Germany
GSEA	Broad Institute of MIT and Harvard, Cambridge, MA, USA
FlowJo 10	FlowJo LLC, Ashley, OR, USA
GraphPad Prism 7	Graphpad Prism, La Jolla, CA, USA
Microsoft Office	Microsoft Corporation, Tulsa, OK, USA
Living Image Software 4.4	PerkinElmer, Krakow, Poland
RStudio	Rstudio, Inc., Boston, MA, USA

3. Methods

3.1. Ethical Statements

3.1.1. Patient Material

Fresh bone marrow (BM) or peripheral blood (pB) samples from adult AML patients were collected in the Department of Internal Medicine III, Ludwig-Maximilians-Universiät München for diagnostic purposes before start of treatment and residual material used for this study. Written informed consent was obtained from the patients. The study was performed in accordance with the ethical standards of the responsible committee on human experimentation (written approval by Ethikkommission des Klinikums der Ludwig-Maximilians-Universität, Munich, number 068-08) and with the Helsinki Declaration of 1975, as revised in 2000.

3.1.2. Animal Work

NSG mice were maintained under specific pathogen-free conditions in the research animal facility of the Helmholtz Zentrum München, Munich, Germany. Free access to food and water, a 12-hour light-dark cycle and constant temperature was provided. All animal trials were performed in accordance with the current ethical standards of the official committee on animal experimentation (written approval by Regierung von Oberbayern, number ROB-55.2Vet-2532.Vet_03-16-56 and ROB-55.2Vet-2532.Vet_02-16-7).

3.2. The Patient-Derived Xenograft Mouse Model

Acute leukaemia (AL) cells were amplified in immunocompromised NSG mice using the individualized patient-derived xenograft (PDX) mouse model (Ebinger et al., 2016; Vick et al., 2015; Terziyska et al., 2012; Lee et al., 2007; Shultz et al., 2005; Liem et al., 2004; Kamel-Reid et al., 1989).

3.2.1. Engraftment and Expansion of Primary Patients' and PDX Cells

To engraft leukaemic cells from AML patients, up to 10^7 pB or BM cells in 100 μl sterile filtered PBS were injected intravenously into 6 - 15 weeks old NSG mice. For expansion freshly isolated (chapter 3.2.8 and 3.2.9) or thawed PDX AML cells (chapter 3.3.4) were injected. After transplantation of cells Baytril (2.5%) was added to the drinking water of animals for 7 days to prevent infections.

Engraftment was monitored every 2 - 3 weeks by flow cytometry measurement of human leukaemic cells in murine pB (chapter 3.2.3) or bioluminescence *in vivo* imaging (chapter 3.2.4). Mice were sacrificed (chapter 3.2.7) (i) at defined time points, (ii) at signs of advanced leukaemia (more than 50% leukaemic cells within murine pB), or (iii) at first clinical signs of disease (rough fur, hunchback, and/or reduced motility). If leukaemia became not apparent, mice were killed 52 weeks after transplantation by latest.

3.2.2. Competitive Transplantation Assay

For competitive engraftment, growth and therapy experiments, cells of different PDX AML single cell clones (SCCs) were thawed (chapter 3.3.4), counted (chapter 3.3.3) and sorted for expressed fluorochromes (chapter 3.3.12). Cells were mixed and between $2 * 10^5$ and $6.4 * 10^5$ cells injected into NSG mice (chapter 3.2.1). Animals were either taken down at defined time points or leukaemic burden (chapter 3.2.7) or, alternatively, treated with chemotherapy (chapter 3.2.5) and taken down at end of therapy.

3.2.3. Flow Cytometry Analysis of Human Leukaemic Cells in Murine Peripheral Blood

To monitor disease progression blood samples (around 50 μl) were obtained from the tail vein of mice transplanted with AML cells with heparin coated glass capillaries every 1 - 4 weeks starting 3 - 5 weeks after xenotransplantation. Blood was incubated with 5 μl huCD45-APC antibody and 3 μl huCD33-PE antibody for 30 min in the dark at room temperature (RT). Erythrocytes were lysed by incubation with 1 ml FACS Lysing solution for 15 min in the dark at RT. After washing with FACS buffer (300 g, 4 min, RT) samples were measured in the flow cytometer BD LSRFortessa X20 (chapter 3.3.10) and data analysed using FlowJo software.

3.2.4. Bioluminescence *In Vivo* Imaging

For quantification of leukaemia burden in NSG mice engrafted with PDX AML cells expressing a recombinant codon-optimized form of firefly luciferase (enhanced firefly, eFFly) *in vivo* imaging was performed by bioluminescence *in vivo* imaging (BLI) with the IVIS Lumina II Imaging System as previously described (Vick et al., 2015; Bomken et al., 2013; Terziyska et al., 2012; Barrett et al., 2011; Rabinovich et al., 2008).

In brief, mice were anaesthetised with isoflurane and immobilized in the imaging chaber. D-luciferin, the substrate of eFFly luciferase, was dissolved in sterile PBS (30 mg/ml) and 4.5 mg injected into the tail vein. Pictures were taken immediately for 15 sec to 2 min using a field of view of 12.5 cm with binning 8, f/stop 1 and open filter setting. Depending on imaging signal binning and f/stop were adjusted. Mice were imaged typically every 1 - 2 weeks.

For data acquisition and quantification of light emission the Living Image Software 4.4 was used.

3.2.5. *In Vivo* Treatment of Mice Engrafted with PDX AML Cells

To assess *in vivo* response of PDX AML samples to treatment, NSG mice were transplanted with samples expressing eFFly luciferase, in an individual or competitive approach (chapters 3.2.1 and 3.2.2) and were treated systemically with one of the following three drugs: (i) 100 mg/kg cytarabine (Ara-C), disolved in 50% Sodium-(S)-lactate solution, intraperitoneally 4 days per week (day 2 - 5) for up to 4 consecutive weeks with or without a week of rest between weeks with treatment starting at a leukaemic burden of a total flux of $2.2 * 10^8 - 3.2 * 10^{10}$ photons/sec; (ii) 5 mg/kg 5-azacitidine (Aza), disolved in H_2O, intraperitoneally 3 days per week (day 1, 3 and 5) for up to 4 weeks starting at a leukaemic burden of a total flux of $1.2 * 10^7 - 4.5 * 10^9$ photons/sec; or (iii) 100 mg/kg venetoclax, disolved in 1% Carboxymethylcellulose sodium solution, orally 5 days per week (day 1 - 5) for 3 weeks starting at a leukaemic burden of a total flux of $8.6 * 10^7 - 1.3 * 10^8$ photons/sec. Animal were monitored every one to two weeks using BLI (chapter 3.2.4) and sacrificed 3 days after stop of therapy (chapter 3.2.7).

3.2.6. Limiting Dilution Transplantation Assay

To determine the stem cell, or leukaemia initiating cell (LIC), frequency in PDX AML samples, limiting dilution transplantation assays (LDTAs) were performed. Here fresh or frozen cells were counted with trypan blue (chapter 3.3.3) and suspended in PBS. Cells were diluted and injected into groups of mice as indicated in tables A.1 - A.5. Engraftment and disease

progression was monitored by flow cytometric analysis of murine pB (chapter 3.2.3) or BLI (chapter 3.2.4). Mice were sacrificed (chapter 3.2.7) and PDX AML cells isolated from the BM (chapter 3.2.8) or spleen (chapter 3.2.9) of engrafted animals.

Stem cell frequencies were determined by Poisson distribution using the ELDA software (http://bioinf.wehi.edu.au/software/elda/) (Hu and Smyth, 2009).

3.2.7. Sacrificing Mice by CO_2 Exposure

Mice were sacrificed using CO_2 asphyxiation by the Quietek CO_2 Induction Systems with a flow rate of 150 ml/min for one minute, followed by 2,250 ml/min for four minutes. Death of animals was verified before organ removal.

3.2.8. Isolation of PDX Cells from the Murine Bone Marrow

To isolate PDX AML cells from the murine BM, femur, tibiae, hips, spine and sternum were extracted and crushed using mortar and pestle. Cells were resuspended in PBS, filtered (70 μm cells strainer) and washed in PBS (400 g, 5 min, RT). Cells were re-suspended in PBS or the required buffer and counted (chapter 3.3.3).

3.2.9. Isolation of PDX Cells from the Murine Spleen

For the isolation of PDX AML cells from murine spleen, cells were squashed through a 70 μm cell strainer, resuspended in PBS and filtered (70 μm cells strainer). Ficoll was underlaid and a gradient centrifugation (400 g, 30 min, no brake, RT) performed for separation of mononuclear cells from plasma, erythrocytes and other particles. Mononuclear cells were harvested and washed twice with PBS (400 g, 5 min, RT). Cells were re-suspended in PBS or the required buffer and counted (chapter 3.3.3).

3.3. Cell Culture Methods

3.3.1. *Ex Vivo* Cultivation of PDX AML Cells

PDX AML cells were cultured *in vitro* at $1 - 1.25 * 10^6$ cells/ml in PDX AML cell medium for up to six days at 37°C and 5% CO_2.

3.3.2. Maintainance of Cell Lines

AL cell lines were maintained at $0.5 - 2.0 * 10^6$ cells/ml in AL cell line medium at 37°C and 5% CO_2 and passaged 1:10 every 2 - 3 days.

HEK-293T cells were maintained at $0.5 - 2.0 * 10^6$ cells/ml in HEK-293T cell medium at 37°C and 5% CO_2. For passaging every 2 - 3 days, medium was removed, cells washed with PBS and dissociated with 0.05% trypsin. Cells were then re-suspended in fresh HEK-293T cell medium and passaged 1:10.

3.3.3. Determination of Cell Numbers

PDX AML cells and cell lines were counted using a Neuerbauer counting chamber. For this purpose cells were stained 1:10 with trypan blue and 10 μl counted.

Cell concentration was calculated as follows:

$$cell\ concentration = mean\ of\ counted\ cells * dilution\ factor * 10^4/ml$$

3.3.4. Cryopreservation of PDX AML Cells and Cell Lines

Cells for later usage were frozen as $2 * 10^6$ or $5 * 10^6$ aliquots in 400 μl or 1 ml FCS + 10% DMSO, respectively. Here counted cells (chapter 3.3.3) were centrifuged (400 g, 5 min, RT) and pellets suspended in one part of FCS, then one part of freezing medium (80% FCS, 20% DMSO) was slowly added. Cells were then frozen at rate of 1°C/min to −80°C using a freezing container Nalgene Mr.Frosty. Primary patient's cells, early passage and transduced and sorted PDX AML cells were transferred to −196°C.

For high viability PDX AML cells were thawed rapidly at 37°C. 0.1 mg/ml DNase was added dropwise and the suspension mixed. After an incubation of 1 min the cells were transferred to a 50 ml tube, FCS was added dropwise in equal parts to volume of frozen cells and incubated for 1 min. 10 ml PBS + 2% FCS were added slowly and incubated for 1 min. Up to 30 ml PBS + 2% FCS were added slowly and cells centrifuged (200 g, 5 min, RT) (Bonnet, 2008). Cell lines were thawed rapidly at 37°C, transferred into 10 ml PBS and centrifuged (400 g, 5 min, RT). PDX AML cells or cell lines were then suspended in the appropriate medium and cultured (chapter 3.3.1 and 3.3.2) or sorted (chapter 3.3.12) and/or injected in NSG mice (chapter 3.2.1).

3.3.5. Carboxyfluorescein Succinimidyl Ester Staining of PDX AML Cells

To detect low-cycling label-retaining cells (LRC) freshly isolated PDX AML cells (chapter 3.2.8 and 3.2.9) were stained with Carboxyfluorescein succinimidyl ester (CFSE). For competitive approaches, counted cells (chapter 3.3.3) were mixed and CFSE staining was performed. PDX AML cells were suspended in 37°C prewarmed PBS + 0.5% BSA at a concentration of 10^6 cells/ml. CFSE was dissolved in DMSO and added to the cell suspension at afinal concentration of 10 μM and incubated for 10 min at 37°C. Staining was stopped by addition of four parts cold RPMI + 10% FCS. Cells were incubated for 5 min at 4°C, centrifuged (400 g, 5 min, RT) and resuspended in sterile filtered PBS for injection into NSG mice.

3.3.6. Production of Lentivirus

For production of third generation lentivirus, HEK-293T cells at a confluence of 50% - 80% were transfected with the packaging plasmids pMD2.G (1.25 μg/ml final concentration), pMDLg/pRRE (5 μg/ml final concentration), pRSV-Rev (2.5 μg/ml final concentration) and the transfer vector (250 ng/ml final concentration). Here plasmid DNA was mixed in DMEM without FCS with 2.4% turbofect and incubated for 20 min at RT. After changing of HEK-293T cell medium, the DNA-turbofect mix was added dropwise to the cells. After three days the supernatant was withdrawn, centrifuged (400 g, 5 min, RT) and filtered (0.45 μm). For concentration of virus, the supernatant was ultrafiltrated using an Amicon-Ultra 15 ml centrifugal filter unit and centrifugation (2,000 g, 30 -40 min, RT). Concentrated virus was used directly for determination of virus titer (chapter 3.3.7) or lentiviral transduction (chapter 3.3.8). Alternatively, virus was frozen as aliquots at -80°C.

3.3.7. Determination of Virus Titer

To monitor quality of produced viruses (chapter 3.3.6) a virus titer was determined using the cell line NALM-6. $0.5 * 10^6$ cells in 0.5 ml AL cell line medium were transduced with 0.03 μl, 0.1 μl, 0.3 μl, 1 μl, 3 μl or 10 μl together with 8 μg/ml polybrene. After one day, the cells were washed three times with PBS (400 g, 5 min, RT). On day 4 - 6 after transduction cells were stained with antibody if necessary and analysed using a flow cytometer (chapter 3.3.9). Virus titers were calculated as follows:

$$virus\,titer = (\frac{F*Z}{V})\,TU/ml$$

F = transduced cells [%]; Z = number of cells at infection; V = volume of virus [ml]

3.3.8. Lentiviral Transduction

For genetic engineering of cell lines and PDX AML cells, between $2 * 10^6$ and 10^7 cells in 1 ml of the appropriate medium were incubated with third generation lentivirus(es) (chapter 3.3.6) together with 8 μg/ml polybrene. After one day cells were washed three times with PBS (400 g, 5 min, RT) and either resuspended in PBS for the injection into mice (chapter 3.2.1) or cultured for 4 - 6 days in PDX AML cell medium for subsequent fluorescence-activated cell sorting (FACS) enrichment (chapter 3.3.12).

3.3.9. FACS Staining

To analyse expression of huCD33 or transgenes such as $H2K^k$ or NGFR in FACS, AL cell lines or PDX AML cells, fresh or thawed (chapter 3.3.4), were stained with an appropriate antibody (table 2.11). $5 * 10^5$ cells were pelleted (400 g, 5 min, RT) and resuspended in 40 - 100 μl PBE buffer. 5 μl of huCD33-PE antibody, 2 μl $H2K^k$-APC antibody or 2 μl of CD271(NGFR)-FITC/PerCP-Cy5.5 antibody was added and incubated for 30 min at RT, 10 min at 4°C or 20 min at 4°C, respectively. Cells were washed with PBE (400 g, 5 min, RT) and resuspended in an appropriate amount of PBE or PBS for FACS analysis (chapter 3.3.10) or sorting (chapter 3.3.12).

3.3.10. Flow Cytometric Analysis

Flow cytometric analyses were performed using a BD LSRFortessa X20, BD FACS AriaIII or BD FACSCalibur (BD Bioscience, Heidelberg, Germany). Expressed fluorochromes (mtag-BFP, eGFP, mCherry and/or iRFP720) and fluorophores conjugated to an antibody (FITC, PE, APC, PerCP-Cy5.5) were analysed with the laser settings indicated in tables 3.2 and 3.1.

Table 3.1. Filter settings of flow cytometry, part 1.

FACS Equipment	Laser [nm]	Longpass Filter [nm]	Bandpass Filter [nm]	Parameter
FACSCalibur	488		488/10	SSC
			530/30	FL1 FITC
			585/42	FL2 PE
			>670	FL3 PerCP
	635		661/16	FL4 APC

Table 3.2. Filter settings of flow cytometry, part 2.

FACS Equipment	Laser [nm]	Longpass Filter [nm]	Bandpass Filter [nm]	Parameter
LSRFortessa X20	405	750	780/60	BV785
		685	710/50	BV711
		653	670/30	BV650
		600	610/20	BV605
		505	525/50	tSapphire, AmCyan, BV510
			450/50	mtagBFP, CFP, BV421
	488	685	710/50	PerCP, PerCP-Cy5.5
		505	530/30	GFP, FITC, CFSE, AlexaFluor 488
			488/10	SCC
	561	750	780/60	PE-Cy7
		685	710/50	Pe-Cy5.5
		635	670/30	Pe-Cy5.5
		600	610/20	mCherry, PE-Texas Red
		505	586/15	DsRed, PE
	640	750	780/60	APC-Cy7
		690	730/45	iRFP720, Alexa Fluor 700
			670/30	APC
FACS AriaIII	375/405	735	780/60	Qdot710
		610	616/23	Qdot605
		558	584/42	PacOrange
		502	530/30	Cerulan
			450/40	DAPI, mtagBFP
	488	655	695/40	PerCP-Cy5.5
		502	530/30	FITC, eGFP, CFSE
			488/10	SSC
	561	735	780/60	PE-Cy7
		630	670/14	PE-Cy5
		600	610/20	mCherry
			582/15	PE
	633	735	780/60	APC-Cy7
			660/20	APC

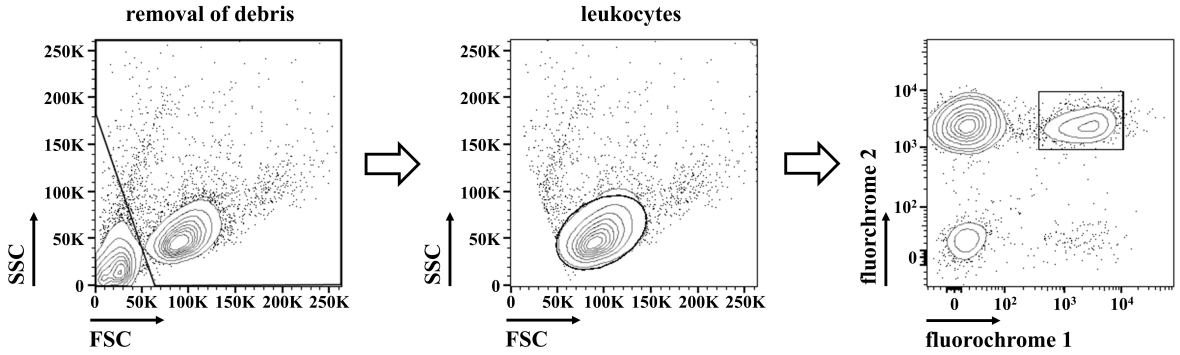

Figure 3.1. Gating strategy for flow cytometric analyses. First, debris was removed with a gating in FSC/SSC. Second, cells were gated for leukocytes in FSC/SSC. Third, cells were gated for the fluorochromes or antibody-conjugated fluorophores of interested. If more than two colours were of interest, a fourth gate was placed on cells positive for these colours.

Cell line and PDX cell samples were gated for living cells in FSC/SSC and then for the respective fluorochromes (e.g. figure 3.1).

3.3.11. Enrichment of PDX Cells by Magnetic Cell Separation

To enrich human PDX AML cells from murine BM cells (chapter 3.2.8) negative selection by magnetic cell separation (MACS) was performed using a cocktail of monoclonal antibodies against murine epitopes bound to magnetic beads.

After isolation from murine BM (chapter 3.2.8) or thawing (chapter 3.3.4), cells were suspended in 3 ml PBS + 0.5% BSA and incubated with 100 μl - 400 μl mouse cell depletion cocktail for 15 min at 4°C. 10 ml PBS + 0.5% BSA was added and the solution loaded to a LS column in a magnet prepared by rinsing with PBS + 0.5% BSA. After washing the column twice with PBS + 0.5% BSA, the flow-through was collected, centrifuged (400 g, 5 min, RT) and re-suspended in a required buffer or medium for further applications.

3.3.12. Enrichment of PDX Cells and Cell Lines by Fluorescence-Activated Cell Sorting

In order to enrich PDX AML cells or AL cell lines carrying one or more transgenes such as $H2K^k$, NGFR or a fluorochrome (mtagBFP, eGFP, mCherry and/or iRFP720), FACS was performed using a cell sorter BD FACS AriaIII (BD Bioscience, Heidelberg, Germany) (chapter 3.3.10). When $H2K^k$ or NGFR was sorted, cells were antibody stained (chapter 3.3.9). PDX AML cells suspended in PBS at a concentration of around 10^7 cells/ml were sorted, gating on leukocytes and subsequently on transgene carrying cells (chapter 3.3.10), into a FACS tube containing appropriate medium.

3.4. Microbiology Methods

3.4.1. Generation of Competent *E.coli* DH5α for Heat Shock Transformation

To generate competent *E.coli* for transformation of plasmid DNA 100 ml of LB medium were inoculated with 1 ml of an overnight culture of *E.coli* DH5α (chapter 3.4.2). When an OD_{600} of 0.4 - 0.5 nm was reached, the culture was cooled on ice. The cells were pelleted (4,000 g, 5 min, 4°C), resuspended in 15 ml TFB I buffer and incubated for 5 min on ice. After centrifugation (4,000 g, 5 min, 4°C) the cell pellet was resuspended in 4 ml TFB II buffer. The cells were stored as 50 μl aliquots at -80°C.

3.4.2. Cultivation of *E.coli* DH5α

E.coli DH5α cells were culture in LB medium at 37°C. After heat shock transformation (chapter 3.4.3), bacteria were cultured with 50 μg/ml ampicillin in either LB_{amp} medium or on LB_{amp} agar plates.

3.4.3. Heat Shock Transformation of Plasmid DNA into *E.coli* DH5α

For transformation of plasmid DNA into *E.coli* 100 ng plasmid DNA or 5 μl of ligation mixture was added to 50 μl competent *E.coli* (chapter 3.4.1) and the mixture incubated at 4°C for 30 min. After heat shock at 42°C for 90 sec the mixture was incubated at 4°C for 2 min. 400 μl LB medium was added and cells incubated at 37°C under shaking and aliquots plated onto LB_{amp} agar plates and incubated at 37°C over night.

3.4.4. Single Colony Picking

After incubation of transformed *E.coli* DH5α on agar plates (chapter 3.4.3) single colonies were picked, transferred into LB_{amp} medium and incubated over night at 37°C on a shaker. Plasmid DNA was then isolated (chapter 3.5.9).

3.5. Molecular Biology Methods

3.5.1. Isolation of Genomic DNA

Genomic DNA (gDNA) was isolated from $5 * 10^6 - 10^7$ freshly thawed cells (chapter 3.3.4) using the QIAamp DNA Mini Kit according to the manufacturer's protocol.

3.5.2. Determination of DNA Quantity and Quality

DNA concentration and purity was determined by measuring 1 μl DNA sample in a nanophotometer.

3.5.3. Polymerase Chain Reaction

To amplify the coding sequences of eGFP (from pCDH-EF1α-eFFly-T2A-eGFP, cloned by Michela Carlet), destroy the restriction enzyme site NheI, or introduce the restriction enzyme site AvrII polymerase chain reaction (PCR) was performed using the primers indicated in table 2.6 and 2.7 and either Pfu DNA Polymerase or Phusion High-Fidelity PCR Master Mix:

1x	Pfu Polymerase reaction buffer
50 - 100 ng	Plasmid DNA
100 pmol	Forward primer
100 pmol	Reverse primer
10 nmol	dNTPs (each)
2.5 U	Pfu Polymerase
up to 50 μl	H_2O

1x	Phusion High-Fidelity PCR Master Mix
50 - 100 ng	Plasmid DNA
25 pmol	Forward primer
25 pmol	Reverse primer
up to 50 μl	H_2O

The PCR was run with ProFlex PCR System applying the following program. Annealing temperatures were adjusted according to the melting temperatures of the primers (see table 2.6 and 2.7).

Temperature [°C]	Time	Cycles
95	2 min	1
95	30 sec	
55 - 60	1 min	35
72	1 min	
72	5 min	1

3.5.4. Repetitive Finger Printing Using PCR of Mitochondrial DNA

For regular authentication of PDX samples, distinct areas of mitochondrial DNA were sequenced and analysed for sample specific single nucleotide variants (Hutter et al., 2004).

GDNA of PDX cells was isolated (chapter 3.5.1) and DNA concentration measured (chapter 3.5.2). The hypervariable region 1 (HVR1) of the control region of mitochondrial DNA was amplified by PCR (chapter 3.5.3:

1x	GoTaq Polymerase reaction buffer
300 ng	gDNA
10 pmol	Forward primer
10 pmol	Reverse primer
10 nmol	dNTPs (each)
5 U	GoTaq Polymerase
up to 50 μl	H_2O

PCR was run with the following program:

Temperature [°C]	Time	Cycles
95	2 min	1
94	30 sec	
60	30 sec	35
72	30 sec	
72	5 min	1

PCR products were purified using the MinElute PCR Purificaiton kit according to manufacturer's protocol. 100 ng/μl purified PCR product were sent for Sanger sequencing using the

same primers as for PCR (chapter 3.5.10). Sequencing results were compared to the reference sequence of each patient sample to authenticate the sample.

3.5.5. Agarose Gel Electrophoresis

For separation of DNA fragments according to size agarose gel electrophoresis was performed using a 1% agarose gel. Agarose was added to TAE buffer, heated and 0.01% Midori Green added. The agarose solution was allowed to dry in a gel chamber with a comb. 5 μl of DNA ladder or up to 30 μl of samples mixed with 1x DNA loading dye were added to the pockets. Separation was performed in TAE buffer at 100 V for 40 min. Separation of DNA was analysed using a gel documentation station.

3.5.6. Extraction of DNA from Agarose Gels

For the extraction and purification of DNA fragments from agarose gels, the DNA was cut and NucleoSpin Gel and PCR Clean-Up kit was used according to manufacturer's protocol.

3.5.7. Restriction Enzyme Digest

PCR products and vectors were digested with the restriction enzymes indicated in table 2.8 and 2.9 at 37°C for 1 h to 2 h.

5 - 10 U	restriction enzyme
2 μg	DNA
1x	restriction enzyme buffer
up to 20 μl	H_2O

After restriction digest the efficiency was tested by agarose gel electrophoresis (chapter 3.5.5).

3.5.8. Ligation

For the ligation of digested DNA fragments (chapter 3.5.7) 100 ng of vector backbone and vector insert in a 1:3 ratio were used. The correct amount of vector insert was calculated using the following formula:

$$amount_{\ vector\ insert}\ [ng] = \frac{size_{\ vector\ insert}\ [kb]}{size_{\ vector\ backbone}\ [kb]} * amount_{\ vector\ backbone}\ [ng] * ratio$$

Ligation was performed with T4 ligase at 22°C for 1 h or 16°C over night.

1 μl	T4 ligase
100 ng	DNA vector backbone
	DNA vector insert
up to 10 μl	H_2O

3.5.9. Extraction of Plasmid DNA from *E.coli*

For plasmid DNA mini or midi preparations NucleoSpin Plasmid Easy Pure or NucleoBond Extra Midi kit, respectively, were used according to manufacturer's protocol.

3.5.10. Sanger Sequencing

Plasmids and PCR products were sequenced with GATC Biotech, Konstanz, Germany. 30 - 100 ng/μl DNA (chapter 3.5.9) or 20 μl of purified PCR product (chapter 3.5.3 and 3.5.6) and 10 pmol/μl primer were sent to sequencing.

3.5.11. Preparation of complex barcode plasmid library

Daniel Richter, Ludwig-Maximilians-Universität München, designed and cloned a barcode (BC) plasmid library.

The pCDH-EF1a-H2K^k-T2A-NGFR (w/oNheI, with AvrII) plasmid was digested with AvrII and KpnI-HF for 4 hours at 37°C:

10 U	AvrII
40 U	KpnI-HF
6 μg	DNA
1x	CutSmart buffer
up to 200 μl	H_2O

Digestion was followed by a SPRI bead clean-up using a 1:1 ratio as described elsewhere (Beckman Coulter, Inc., 2020). 1.25 μM HPLC purified, phosphorylated BC oligonucleotides were annealed in 0.5x NEBuffer 3.1 in a 80 μl reaction by heating to 90°C and decreasing the temperature by 0.1°C per 10 sec until 20°C. For cloning of the BC insert into the digested vector a cut-ligation was performed in four reactions overnight:

800 U	T4 ligase
10 U	AvrII
40 U	NheI-HF
500 ng	DNA vector backbone
0.01%	DNA vector insert (BC annealing product)
1.5 mM	ATP
1x	CutSmart buffer
up to 80 μl	H_2O

Cut-ligation was run with the following program:

Temperature [°C]	**Time**	**Cycles**
37	5 min	55
20	5 min	
37	30 min	1
80	20 min	1

After pooling of reactions, cut-ligation mixtures were transformed into NEB Stable Competent *E.coli* according to manufacturer's protocol. After 1 hour of outgrowth at 37°C 0.25% of bacteria were used for plating to determine overall transformation efficiencies by colony counts. The remaining transformed *E.coli* were cultured in LB_{amp} (chapter 3.4.2) and plasmids isolated using the PureYield Midi Prep kit according to Manufacturer's protocol.

3.6. Sequencing Analysis

3.6.1. Targeted Sequencing of Recurrently Mutated Genes

For sequencing of 68 recurrently mutated genes, I collaborated with Binje Vick, Helmholtz Zentrum München, Maja Rothenberg-Thurley, Klinikum der Universität München, and Laboratory for Functional Genome Analysis (LAFUGA), Ludwig-Maximilians-Universität München. Binje Vick provided $5*10^6 - 1*10^7$ frozen PDX AML cells over serial passages (PDX AML-491: first to tenth engraftment round; AML-661: first to fifth engraftment round). gDNA was isolated of primary patient's material (chapter 3.1.1) as well as PDX AML cells using the QIAamp DNA Mini kit and QIACube.

Coding regions or hotspot areas of 68 recurrently mutated genes were sequenced as previously described (Metzeler et al., 2016). In brief, sequencing libraries were generated by Maja Rothenberg-Thurley using a custom targeted, muliplexed amplicon-based approach from 100 - 250 ng gDNA. Samples were paired-end sequenced by Stefan Krebs from LAFUGA using a Illumina MiSeq instrument: (i) 250 bases for the first read of the sample, (ii) 8 bases to read the i7 index and (iii) 250 bases for the second read of the sample.

Maja Rothenberg-Thurley performed data analysis using a custom data analysis pipeline based on Linux shell scripts as previously described (Metzeler et al., 2016). In brief, reads were quality trimmed and aligned to the human reference genome, version hg19, using BWA (Li and Durbin, 2009a). Single nucleotide variants (SNVs) and short insertions or deletions were called using VarScan 2 (Koboldt et al., 2012) and Pindel (Ye et al., 2009), respectively. Known and possible AML associated mutations were identified through review of public databases (COSMIC, version 70; dbSNP, version 138).

3.6.2. Barcode Sequencing and Data Analysis

For BC sequencing and analysis, I collaborated with Daniel Richter and LAFGUA, both Ludwig-Maximilians-Universität München. Cell pellets or viably frozen cells (chapter 3.3.4) were provided to Daniel Richter.

Daniel Richter isolated gDNA using either DNeasy Blood & Tissue kit ($\geq 10^6$ cells) or DNeasy Micro kit ($< 10^6$ cells) according to manufacturer's protocol. Isolated gDNA was quantified using QuantiT PicoGreen dsDNA assay.

Barcodes were extracted using an adapted strategy from SiMSen-seq (Ståhlberg et al., 2017). For each sample library preparations were carried out in technical triplicates. In brief, 3 – 5 μl of gDNA were used as input for a first PCR reaction in 10 μl volume using 0.1 U Phusion II HotStart polymerase and 40 nM primers targeting the sequences of the lentiviral insert surrounding the expressed barcode and carrying unique molecular identifiers (table 2.6 and 2.7):

Temperature [°C]	Time	Cycles
98	30 sec	1
98	10 sec	
62	10 min	2-12
72	30 sec	

The reaction was inactivated by adding 20 μl Actinase E in 1x TE buffer in a final concen-

tration of 45 ng/μl and incubating at 65°C for 15 min followed by heat inactivation at 95°C for 15 min. Subsequently, for each technical replicate two downstream PCRs, each in 40 μl, were carried out using Q5 HotStart High Fidelity Polymerase, 10 μl of the previous reaction as template and 400 nM primers carrying indexed Illumina adapter sequences and indices to enable sequencing on Illumina sequencers:

Temperature [°C]	Time	Cycles
98	3 min	1
80	10 sec	20-33
72	30 sec	
76	30 sec	
ramping of 0.2/sec	30 sec	

Samples were cleaned up using SPRI beads at a ratio of 0.8:1 (Beckman Coulter, Inc., 2020) and reactions of the same technical replicates were pooled when eluting with 20 μl buffer EB. As a quality control 5 μl of one replicate per sample were run on a 1.5% agarose gel for visual inspection. Finally, all prepared libraries were quantified using a QuantiT PicoGreen dsDNA assay and pooled based on their concentration. Final library pools were quantified using a Bioanalyzer 2100 with High Sensitivity DNA Kits.

Library pools were single-end sequenced by Stefan Krebs from LAFUGA using a HiSeq1500 sequencer: (i) 150 bases to read the sample, (ii) 8 bases to obtain the i7 index and (iii) 8 bases to read the i5 index.

Raw fastq files were demultiplexed using deML to separate reads derived from different samples (Renaud et al., 2015). Specific barcode sequences were extracted from the reads using bartender (Zhao et al., 2018). For low complexity samples barcodes were clustered based on their Hamming distance either using bartender or Starcode (Zhao et al., 2018; Zorita et al., 2015). Data was further processed and plotted using R, including the packages tidyverse and ggplot2 (Wickham et al., 2019; Wickham, 2016).

3.6.3. Exome Sequencing and Data Analysis

For exome sequencing and analysis, I collaborated with LAFUGA and Ilse Valtierra, both Ludwig-Maximilians-Universität München. PDX AML cells were thawed (one replicate per SCC; chapter 3.3.4), depleted of murine cells (chapter 3.3.11) and cell pellets were provided to LAFUGA.

Sylvia Mallok from LAFUGA isolated gDNA of PDX AML SCCs and primary patient samples using the QIAamp DNA Blood Mini Kit and quantified DNA content using Nanodrop and Qubit dsDNA HS Assay Kit. gDNA was sheared and exome libraries prepared and multiplexed for sequencing using the SureSelect Human All Exon V6 kit. Shearing of gDNA was performed with a Covaris M220 instrument instead of a Covaris instrument of the E or S series. KAPAHiFi PCR kit was used instead of Herculase II Fusion DNA Polymerase kit

Libraries were paired-end sequenced by Stefan Krebs from LAFUGA using a HiSeq1500 sequencer: (i) 100 bases for the first read of the sample, (ii) 9 bases to read the i7 index and (iii) 100 bases for the second read of the sample.

Ilse Valtierra mapped paired-end 100 bp whole exome sequencing reads using BWA-MEM version 0.7.15-r1140 (Li, 2013). Whole exome sequencing data of primary patient samples from diagnosis, relapse 1 and relapse 2 as well as complete remission and BM donor samples, performed by LAFUGA and analysed by Ilse Valtierra previously (unpublished), were used. Reads from primary patient samples were mapped to the human reference genome, version hg19, whereas reads from the 12 PDX AML SCCs were mapped to a concatenated human-mouse reference genome (hs37d5 - GRCm38) and reads mapping to standard human chromosomes were extracted with samtools version 1.8 (Li et al., 2009b). Using the complete remission and BM donor samples as normal control, SNVs and indels were called following the GATK best practices with MuTect2, version 3.6 (Cibulskis et al., 2013; Van der Auwera et al., 2013). GATK HaplotypeCaller v3.6 was used to call single-nucleotide polymorphisms (SNPs) and germline indels in PDX AML SCC and primary patient samples (Poplin et al., 2018). The ExAC release 0.3.1 was used as a polymorphism reference (Lek et al., 2016). Ilse Valtierra filtered the SNPs per sample according to the GATK best practices by removing SNPs with a quality depth < 2, a Fisher strand test > 60, mean quality < 40, MQRankSum < -12.5, and ReadPosRankSum < -8.0. Indels were filtered with quality depth < 2, a Fisher strand test > 60, and ReadPosRankSum < -20.0. A core set of heterozygous SNPs across samples was defined by the intersection of all SNPs and indels that passed the filters in the diagnosis and full remission samples, were annotated in ExAC and had a minimum coverage of 20 reads.

For phylogenetic inference of the PDX AML SCCs, Ilse Valtierra extracted allele counts of SNVs that passed the MuTect2 filters in all PDX AML SCCs using the Rsamtools package, version 2.2.1 (Morgan et al., 2019). Since PDX AML SCCs originated from a single cell, fixed somatic variants of each sample were expected. Ilse Valtierra made a binary matrix of SNV detection per sample, which was set to 1 if the SNV had a variant allele frequency > 0.3 in one

PDX AML SCC or > 0.05 in a patient sample. With the Jaccard (binary) distance she used hierarchical clustering (complete) to group PDX AML SCCs. The clustering dendrogram was converted into a phylogenetic tree using the ape package (Paradis and Schliep, 2019).

For the analysis of copy number variants (CNVs), the MARATHON pipeline was applied to call allele-specific CNVs on the exome data (Urrutia et al., 2018) using the CODEX2 and FALCON-X packages (Jiang et al., 2018; Chen et al., 2017). The pipeline requires the coverage per allele per sample at heterozygous SNP sites. The core set of heterozygous SNPs from the initial diagnosis and remission exomes was given as input to CODEX2 to normalize the coverage on the primary patient and PDX AML SCC samples with respect to the three control remission samples. Chromosomal regions with allele-specific copy number differences between each tumour-control pair based on the coverage at heterozygous SNPs, which were observed in both samples, were called using FALCON-X. Copy number estimates were homogenized along stretches of 1 Mbp and segments were delimited based on a $\Delta\text{CN} = 0.3$ yielding copy number values for the major and minor copy per tumour-control pair. In order to yield a unique set that was well supported by all controls, with a homogeneous copy number annotation along the largest possible segments, Ilse Valtierra first obtained the intersection of CNV regions per sample that were called against each control. Then, she merged the intersected CNV regions of all samples using the reduce() function of the GenomicRanges R package (Lawrence et al., 2013) and filtered any segments below 10 Mbp in length. Ilse Valtierra extracted all the separate segments with the disjoin() function of GenomicRanges and merged any adjacent segments that were below 1 Mbp in length o establish segments within the merged regions that had different copy number values among samples. She additionally merged larger segments to the small ones if they were present in less than 3 samples, or more than 12 (out of 15), which enabled keeping regional differences in copy number, while preserving the structure of major CNV events that were shared by multiple samples. The final copy number that was reported per segment corresponds to the mean between the copy number values per control produced by FALCON-X; this mean copy number was weighted by the length of the original CN reported on the sample, where a CN = 1 was assigned to the genomic ranges that were not annotated in the original FALCON-X output of the sample. Ilse Valtierra extracted the genes from the final CNV regions based on the GRCh37.75 annotation, importing the corresponding GTF file as a txdb object in R. ENSEMBL gene identifiers were converted to their gene names and Entrez Gene ID with the biomaRt package v2.42.0 (Durinck et al., 2009, 2005). The ReactomePA package was used to perform pathway enrichment analysis of the genes in CNV regions (Yu

and He, 2016).

3.6.4. DNA Methylation Array

For DNA methylation analysis, I collaborated with Bianka Ksienzyk, Vindi Jurinovic and Tobias Herold, all Klinikum der Universität München, and the Genomics and Proteomics Core Facility, Deutsches Krebsforschungszentrum Heidelberg. PDX AML cells were thawed (one replicate per SCC; chapter 3.3.4), depleted of murine cells (chapter 3.3.11), lysed in 60 μl RLT buffer with 1% β-mercaptoethanol per $1 * 10^6$ cells, stored at $-20°$C and provided to Bianka Ksienzyk.

Bianka Ksienzyk isolated gDNA using the QIAamp DNA Mini kit and QIACube and provided 1 μg gDNA in a concentration of 25 ng/μl to the Deutsches Krebsforschungszentrum Heidelberg. There samples were treated with bisulfite and sequenced with the Infinium MethylationEPIC BeadChip according to manufacturer's protocol analysing over 850,000 CpG islands.

Vindi Jurinovic and Tobias Herold performed data analysis using the R-package minfi (version 1.32.0). The raw methylation data were preprocessed with the preprocessIllumina function using default parameter values, and M values were used for subsequent analyses. t-SNE plots were created with the R-package Rtsne (version 0.15).

3.6.5. Transcriptome Sequencing (SCRB-Seq)

For transcriptomic analysis by single cell RNA barcoding and sequencing (SCRB-seq), I collaborated with Johannes Bagnoli and LAFUGA, both Ludwig-Maximilians-Universität München, Vindi Jurinovic and Tobias Herold, both Klinikum der Universität München. PDX AML cells were thawed (3 - 4 replicates per SCC; chapter 3.3.4), 2,000 fluorochrome expressing cells sorted into a 96-well plate (chapter 3.3.12), lysed in 50 μl RLT buffer with 1% β-mercaptoethanol, stored at $-80°$C and provided to Johannes Bagnoli.

Johannes Bagnoli used a modified SCRB-seq protocol (Ziegenhain et al., 2017) for library preparation as described by Ebinger et al. (2020). In brief, proteinase K was used to digest proteins and RNA was cleaned up with help of SPRI beads (22% polyethylene glycol). DNase I treatment for 15 min at RT removed DNA and cDNA was generated by oligo-dT primers with sample specific barcodes and unique molecular identifiers (UMIs). Excess primers were digested with Exonuclease I, cDNA was amplified using KAPA HiFi HotStart polymerase and pooled. Nextera libraries were generated using the Nextera XT kit and 3' end enriched with

a custom P5 primer. Libraries were cleaned using a 2% E-Gel Agarose EX gel and Monarch DNA Gel Extraction kit according to manufacturer's protocol.

Libraries were paired-end sequenced by LAFUGA using Illumina HiSeq 1500: (i) 16 bases to obtain cellular barcodes and (ii) 50 bases to read parts of the cDNA fragment.

Data analyses was performed by Vindi Jurinovic and Tobias Herold. Raw fastq files were processed as described by Ebinger et al. (2020). In brief, data was demultiplexed with deML (Renaud et al., 2015) and processed with zUMIs 2.4.5b (Parekh et al., 2018). Data was mapped against the concatenated human (hg38) and murine genome (mm10) using STAR 2.6.0a (Dobin et al., 2013). Genes were annotated with Ensembl (GRCh38.84/GRCm38.75) and cellular barcodes used for sample identification. Two samples were excluded because their library size was less than 50,000. Genes with less than 1 count per million reads in more than 2 (out of 3) of cases were excluded from the analysis. Raw data were normalized with the voom function from the R package limma (version 3.42.2). This package was also used for differential gene expression analyses. The p-values were adjusted with the Benjamini-Hochberg method and all adjusted p-values $p < 0.05$ were considered significant. t-SNE plots were created with the R-package Rtsne (version 0.15). Gene set enrichment analysis was used to test the enrichment of different pathways from the Hallmark gene sets database. The p-values were adjusted with Benjamini-Hochberg method and the adjusted p-values $p < 0.05$ considered significant.

3.7. Statistical Analysis

All statistical analyses in this study were performed with the GraphPad Prism 7 software or RStudio software. Two-tailed t-test with Benjamini and Hochberg correction for multiple testing was applied to test significant differences between calculated PDX AML SCC burden of untreated and treated leukaemias engrafted in mice. Ordinary one-way ANOVA with Tukey correction for multiple testing was used to test significant differences in PDX AML SCC size after treatment normalised to untreated control. Ordinary two-way ANOVA with Tukey correction was applied to test significant differences of relative growth of PDX AML SCCs in competitive *in vivo* experiments. Repeated measure two-way ANOVA with Sidak correction for multiple testing was applied to test significant differences in BLI curves with and without treatment pressure.

4. Results

Acute myeloid leukaemia (AML) is a haematopoietic malignancy characterised by not only inter-patient diversity but also considerable intra-patient heterogeneity, both genetically and functionally. This heterogeneity presents a major challenge in the successful treatment of AML patients since response rates differ not only between individual patients but also within a patient's tumour. The most adverse cancer cells within the patient's leukaemia determine therapy response and, thus, prognosis.

In this work, I aimed at a better understanding of the genetically, epigenetically and functionally diverse subpopulations present within an individual tumour in order to find and characterise challenging subclones. Ultimately, the goal is to find putative targets for therapeutic approaches.

Towards this aim, established patient-derived xenograft (PDX) AML cells were utilized to generate single cell clones (SCCs) derived from one individual patient. These PDX AML SCCs were characterised genetically, epigenetically and transcriptionally. Moreover, they were analysed functionally focusing on homing capacity, growth behaviour and therapy response in order to find challenging subclones and to correlate this to genetic and transcriptional traits.

4.1. Characterisation of PDX AML Samples

In the hosting lab, more than 20 serially transplantable and transducable PDX AML samples have been established (Binje Vick, Helmholtz Zentrum München), of which 13 samples were used within this study (table 4.1) (Ebinger et al., 2020; Vick et al., 2015). All patients suffered from high-risk or relapsed AML of different karyotypes, genotypes, and clinical histories and, thus, represent highly aggressive forms of AML with poor prognosis. Of note, PDX AML-491 and AML-661 were derived from the same patient at first and second relapse, respectively.

Table 4.1. Clinical characteristics of AML samples.

Sample	Disease stage	Age[#] [years]	Sex	Cytogenetics	Mutations[$]
AML-346	Rel 1	1	f	int. del(5q)(13q)	*CKIT*
AML-356	Rel 1	5	m	n.d.	*KRAS*, *U2AF1*
AML-358	Rel 2	9	m	n.d.	*FLT3-ITD*
AML-372	Rel 1	42	m	complex, incl. -17	*KRAS*, *TP53*
AML-388	ID	57	m	KMT2A-AF6	*KRAS*, *CEBPZ*
AML-393	Rel 1	47	f	KMT2A-AF10	*BCOR*, *KRAS*
AML-415	Rel 2	69	f	normal	*DNMT3A*, *NPM1*, *FLT3-ITD*, *IDH1*
AML-491	Rel 1	53	f	del(7)(q21)	*DNMT3A*, *BCOR*, *NRAS*, *KRAS*, *ETV6*, *PTPN11*, *RUNX1*
AML-538	Rel 1	68	f	CN	*DNMT3A*, *IDH1*
AML-573	Rel 1	64	f	t(5;11)(p1;q13)	*DNMT3A*, *FLT3-ITD*, *IDH2*, *WT1*
AML-579	Rel 1	51	m	CN	*DNMT3A*, *NPM1*, *FLT3-ITD*, *IDH1*
AML-602	Rel 1	40	f	complex	*DNMT3A*, *TET2*, *FLT3-ITD*, *NPM1*, *CEBPA*, *JAK1*
AML-661	Rel 2	55	f	del(7)(q21)	*DNMT3A*, *BCOR*, *NRAS*, *ETV6*, *PTPN11*, *RUNX1*, *EZH2*

[#] when the primary AML sample was obtained; [$] mutations detected by targeted sequencing in PDX AML cells; ID = initial diagnosis; Rel = relapse; f = female; m = male; int = interstitial; del = deletion; CN = cytogenetically normal; n.d. = not determined.

4.1.1. Passaging Times, Homing Capacity and Stem Cell Frequencies of PDX AML Samples

In order to study inter-patient heterogeneity, functional characterisation of PDX AML samples regarding growth velocity, homing capacity and stem cell frequency was performed. This data has partly been published in Ebinger et al. (2020).

To characterise growth behaviour, *in vivo* passaging times were determined for selected PDX AML samples. Here, $5 * 10^5 - 5 * 10^6$ PDX AML cells were injected into up to 100 mice per sample and the time from transplantation until overt leukaemia, meaning first signs of disease,

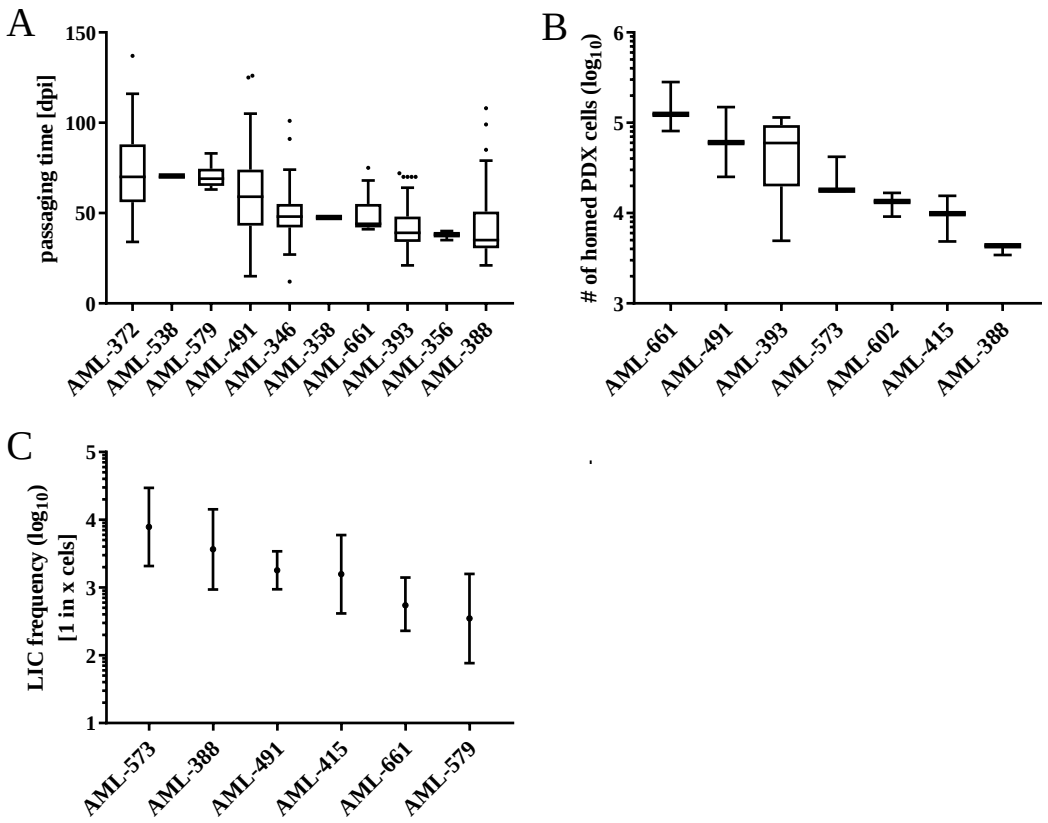

Figure 4.1. Passaging times, homing and stem cell frequencies of PDX AML samples. **(A)** $5 * 10^5 - 5 * 10^6$ PDX AML cells were injected per mouse. Passaging times from transplantation until overt leukaemia was analysed. Box plots of at least 4 and up to 100 mice per sample are depicted. **(B)** $1 * 10^7$ PDX AML cells were injected per mouse. The number of PDX AML cells homing to the bone marrow (BM) was determined after 2 or 3 days by flow cytometry. Box plots of at least 3 mice are shown. Data was generated together with Sarah Ebinger, Helmholtz Zentrum München. **(C)** PDX AML cells were transplanted into mice in limiting dilutions at numbers indicated in table A.1 - A.3. Positive engraftment was determined by bioluminescence *in vivo* imaging (BLI) and/or flow cytometry. Leukaemia-initiating cell (LIC) frequency was calculated using the ELDA software (Hu and Smyth, 2009). Mean $\pm$ 95% CI is depicted. Data has been partly published in Ebinger et al. (2020).
dpi = days post injection; LIC = leukaemia-initiating cell; CI = confidence interval.

was measured. Passaging time is a representative measure for the growth of the leukaemia. Median passaging times of different samples ranged from 35 days to 70 days between samples, a 2-fold difference between the analysed samples (figure 4.1A). Of note, I also observed major intra-sample heterogeneity; the interquartile range within individual samples was up to 31 days (PDX AML-491, median: 49 days, interquartile range: 43 - 74 days).

As a second parameter the number of PDX AML cells homing into the murine bone marrow (BM) was ascertained. $1 * 10^7$ PDX AML cells freshly isolated from a donor mouse were injected into next recipient mice. Two to three days after transplantation, mice were sacrificed and whole BM analysed by flow cytometry to determine the absolute number of homed PDX AML cells. Within this time period, cells injected into the murine blood stream travel to and

interact with the murine niche. This process is accompanied by migration, adhesion, cell-stroma and cell-cell interactions enabling them to survive the new environment and, eventually, proliferate. The median number of homed cells ranged dramatically with an almost 30-fold difference between samples (4,347 - 124,176 PDX AML cells; figure 4.1B), indicating again the inter-sample heterogeneity. The interquartile range was also large with a difference of up to 201,331 cells (PDX AML-661, median: 124,176 cells, interquartile range: 80,890 - 282,221 cells), displaying the intra-sample heterogeneity already seen in the passaging times.

Next, the stem cell frequency of PDX AML cells was studied. Here, PDX AML cells were injected into groups of mice at decreasing cell numbers in a limiting dilution transplantation assay (LDTA) (table A.1 - A.3). This experimental setup is the gold standard to determine the number of cells needed for engraftment of one single cell, the so-called leukaemia-initiating cell (LIC) frequency. LICs are a surrogate for leukaemia stem cells (LSCs), which are by definition able to repopulate the disease (see chapter 1.2.3). Mean LIC frequencies differed between PDX AML samples with a more than 20-fold difference (1 in 7,853 - 1 in 351 cells; figure 4.1C), again confirming the observed inter-sample heterogeneity.

4.1.2. *In Vivo* Chemotherapy Response of PDX AML Samples

One of the most important aspects determining a patient's clinical outcome is the initial response rate towards chemotherapy. Even though most patients initially respond towards treatment with tumour burden dropping below 5% of blasts in the BM (80 - 90% for favourable, 40 - 80% for intermediate and $<$50% for adverse risk category), incomplete or no response might occur and is correlated to poor prognosis (Ravandi et al., 2018, 2017; Othus et al., 2016; Estey, 2014; Buckley et al., 2013).

In order to mimic the variety of clinical response towards treatment and to identify challenging, treatment-resistant leukaemic cells, *in vivo* therapy of mice engrafted with PDX AML cells can be employed. Here, PDX AML cells, transduced with a luciferase for monitoring of leukaemic growth and sensitive follow-up of tumour burden by bioluminescence *in vivo* imaging (BLI) (Ebinger et al., 2020; Vick et al., 2015), were transplanted into groups of mice. When leukaemia had developed to a substantial burden (total flux = $5.7 * 10^8 - 1.2 * 10^{10}$ photons/sec; figure 4.2), animals were repetitively treated with cytarabine (Ara-C), an anti-proliferative chemotherapeutic commonly used in the clinics and acting as a cytosine analogue inhibiting DNA and RNA sythesis (Galmarini et al., 2001), and leukaemic burden was monitored by BLI (figure 4.2A, see chapter 1.4.2). With the repository of PDX AML samples established by the

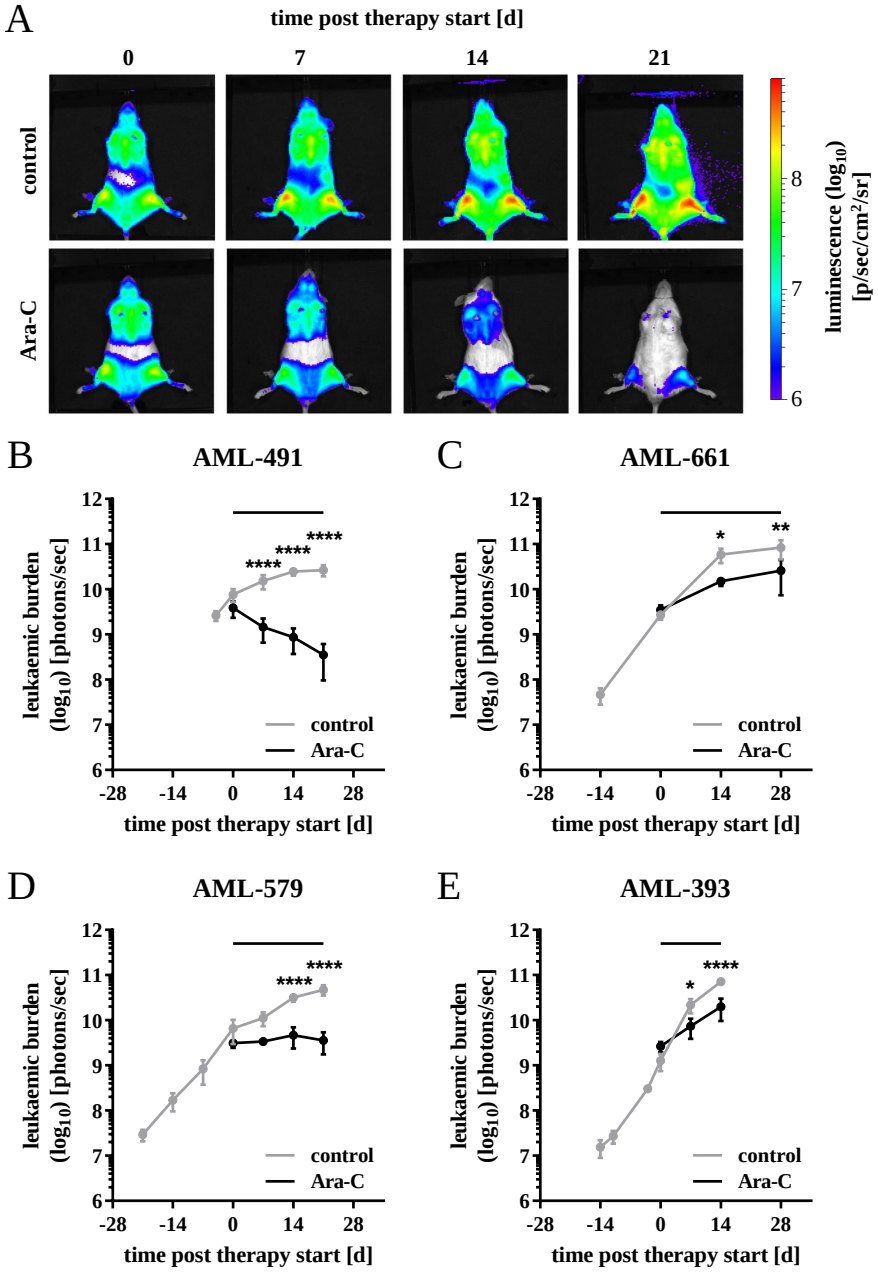

Figure 4.2. Cytarabine (Ara-C) response of PDX AML samples. $8.4 * 10^5 - 5 * 10^6$ PDX AML cells were transplanted into groups of mice and growth monitored by BLI every week. At a total flux of $5.7 * 10^8 - 1.2 * 10^{10}$ photons/sec, animals were left untreated (control, grey) or treated with 100 mg/kg Ara-C on days 2 - 5 of the week (Ara-C, black). Chemotherapy was applied every week for two weeks (AML-393, (E)) or three weeks (AML-491, (A,B); AML-579, (D)). Alternatively, mice were treated in a bi-weekly rhythm for four weeks (AML-661, (C)). **(A)** Examplary imaging pictures are shown for two representative mice engrafted with PDX AML-491, one untreated and one treated with Ara-C. **(B-E)** Quantification of BLI is depicted (mean ± SD). Data for PDX AML-661 (C) was generated by Binje Vick, Helmholtz Zentrum München. Significance was tested by two-way ANOVA with Sidak correction. If not indicated otherwise, the comparison was not significant.
d = days; * = $p < 0.05$; ** = $p < 0.01$; **** = $p < 0.0001$.

hosting lab I was able to model complete response (PDX AML-491, figure 4.2B), partial re-

sponse (PDX AML-579, figure 4.2D) as well as resistance (PDX AML-661 and AML-393, figure 4.2CE) towards chemotherapy, displaying funtional inter-patient heterogeneity. Of note, PDX AML-491 and AML-661, the first and second relapse of the same patient, respectively, show differential Ara-C response with PDX AML-491 being sensitive and AML-661 being resistant towards treatment. This finding demonstrates not only functional intra-patient heterogeneity but also evolution over time towards a more aggressive phenotype.

In vivo treatment response rates as well as growth rates, homing capacities and stem cell frequencies of AML xenografts has shown functional inter- and intra-patient heterogeneity strengthening the value of the PDX AML model to investigate tumour heterogeneity. Additionally to functional intra-patient heterogeneity, I now analysed genetic heterogeneity within one AML patient.

4.1.3. Genetic Heterogeneity of PDX AML-491 and AML-661

Since PDX AML-491 and AML-661, the first and second relapse of the same patient, have demonstrated functional heterogeneity regarding growth behaviour, homing capacity, stem cell frequency and therapy response, the genetic composition of this leukaemia was analysed in more detail. Unfortunately, cells from initial diagnosis of the same patient did not engraft in mice and, thus, could not be analysed in this study as a xenograft. Patient cells at initial diagnosis, first and second relapse as well as untransduced and transduced PDX AML cells over several passages were sequenced for 68 recurrently mutated genes (Maja Rothenberg-Thurley, Klinikum der Universität München; LAFUGA, Ludwig-Maximilians-Universität München; Binje Vick, Helmholtz Zentrum München) (Metzeler et al., 2016). The patient's leukaemia consisted of a major clone, indicated by mutations with a variant allele frequency (VAF) of around 50%, and also minor clones, characterized by mutations with a low VAF (figure 4.3). The major clone comprised mutations in the epigenetic regulators *DNMT3A*, a DNA methyltransferase (Chaudry and Chevassut, 2017; Chen and Chan, 2014), and *BCOR*, a co-repressor involved in histone modification and apoptosis (de Rooij et al., 2015; Tiacci et al., 2012), mutations in the transcription factors *ETV6* (Feurstein and Godley, 2017; Wang et al., 2014) and *RUNX1* (Hayashi et al., 2017; Harada and Harada, 2009) as well as a mutation in *PTPN11*, a protein-tyrosine phosphatase (Renneville et al., 2008; Tartaglia et al., 2005). Furthermore, subclonal mutations could be detected in the epigenetic regulator *EZH2*, a histone methyltransferase (Kim and Roberts, 2016; Shih et al., 2012), as well as in proteins involved in signalling pathways such as *KRAS* and *NRAS*, proto-oncogenes and small GTPases (Renneville et al., 2008; Bos, 1989),

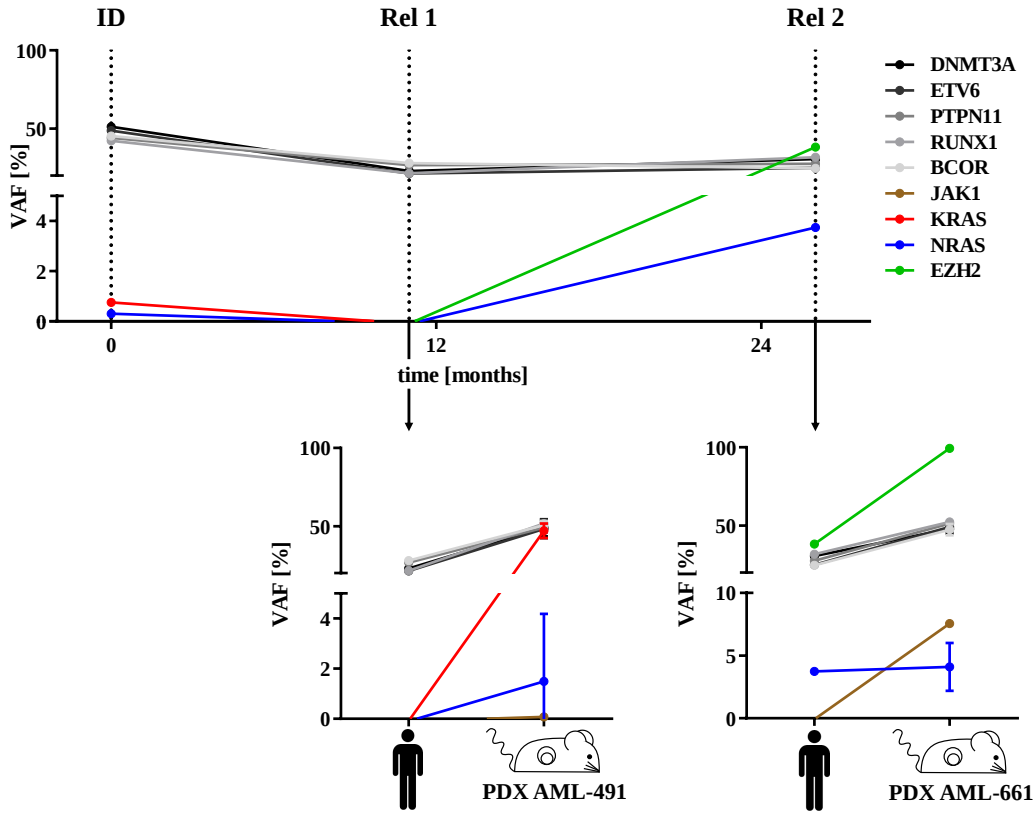

Figure 4.3. Genetic characterisation of primary AML patient cells and PDX AML-491 and AML-661 cells by targeted sequencing. Upper panel: Patients' AML cells were harvested by BM puncture or blood sampling at time of initial diagnosis (ID), relapse 1 (Rel 1) or relapse 2 (Rel 2). Targeted sequencing of 68 recurrently mutated genes in AML was performed. Variant allele frequency (VAF) of detected mutations is depicted. **Lower panel:** Cells from the first and second relapse were transplanted into mice, from now on referred to as PDX AML-491 (left) and AML-661 (right), respectively. PDX cells were harvested from murine BM after several rounds of re-passaging (AML-491: first to tenth engraftment round; AML-661: first to fifth engraftment round) and also after lentiviral transduction (AML-491: n = 9; AML-661: n = 3). Targeted sequencing was performed as for patient cells. Mean VAF ± SD is shown. PDX AML cells were provided by Binje Vick, Helmholtz Zentrum München, and both primary and PDX AML samples were prepared and data analysed by Maja Rothenberg-Thurley, Klinikum der Universität München and sequenced by LAFUGA, Ludwig-Maximilians-Universität München.
ID = initial diagnosis; Rel = relapse; VAF = variant allele frequency.

and *JAK1*, a tyrosine kinase (Xiang et al., 2008; Jeong et al., 2008) (figure 4.3 upper panel). The *EZH2* mutation was only detectable within cells of the second relapse, whereas the *KRAS* mutation was not detectable within cells of the first and second relapse.

When cells of the first relapse engrafted in mice (PDX AML-491), we found that mutations within *KRAS* and *NRAS*, detectable within cells of initial diagnosis with subclonal VAFs (*KRAS*: 0.8%, *NRAS*: 0.3%), were detectable in PDX AML cells at increased VAFs (*KRAS*: 35.5%, *NRAS*: 8.2%), suggesting the engraftment of minor clones (figure 4.3 lower panel, left). These VAFs were stable during passaging and lentiviral transduction. Interestingly, the muta-

tions in *KRAS* and *NRAS* could not be detected in primary cells from the first relapse, indicating that these mutations were below detection threshold at this tumour stage. When cells of the second relapse engrafted in mice (PDX AML-661), the *EZH2* mutation increased in frequency to almost 100%, indicating a homozygous mutation or a loss of heterozygosity (LOH) as well as an engraftment advantage of a subclone (VAF = 38.3% to 98.8%) (figure 4.3 lower panel, right). Additionally, subclonal mutations in *NRAS* and *JAK1* were detectable in PDX AML-661 cells. As for PDX AML-491, the VAFs of those mutations were stable during passaging and lentiviral transduction. In summary, some subclones within the primary patient's samples were capable of engrafting in immunocompromised mice, outcompeting even the main clone detected in the patient.

Taken together, PDX AML-491 and AML-661 represent a sample pair from the first and second relapse of the same patient, which does not only show functional inter- and intra-sample variety but also genetic subclones, of which several successfully engrafted in mice. Thus, this sample pair presents a suitable tool to study genetic and functional intra-tumour heterogeneity.

4.2. Generation of PDX AML Single Cell Clones

In order to study intra-patient heterogeneity, it is necessary to clearly distinguish individual subclones from each other. One possibility to guarantee the clonality of the examined leukaemia population is to generate single cell clones (SCCs), each originating from one individual patient-derived AML cell. These PDX AML SCCs do not only have the advantage of a known ancestry and, thus, defined genetic alterations, but also enable examination of their functional characteristics due to the serially transplantable nature of PDX cells.

Due to the demonstrated genetic and functional diversity of PDX AML-491 and AML-661 (chapter 4.1), the sample pair was regarded suitable for the study of clonal heterogeneity in AML and, thus, the generation and characterisation of PDX AML SCCs.

4.2.1. Genetic Barcoding and Limiting Dilution Transplantation of PDX AML Cells

In order to generate PDX AML SCCs, LDTAs were performed (figure 4.4AC and table A.4). Here, bulk PDX AML-491 or AML-661 cells were isolated from donor mice and lentivirally transduced with a genetic barcode (BC) pool (designed and cloned by Daniel Richter, Ludwig-Maximilians-Universität München, figure 4.4AB). This genetic BC pool, consisting of a semi-random nucleotide sequence, enables marking of cells with individual BCs and, thus, allows

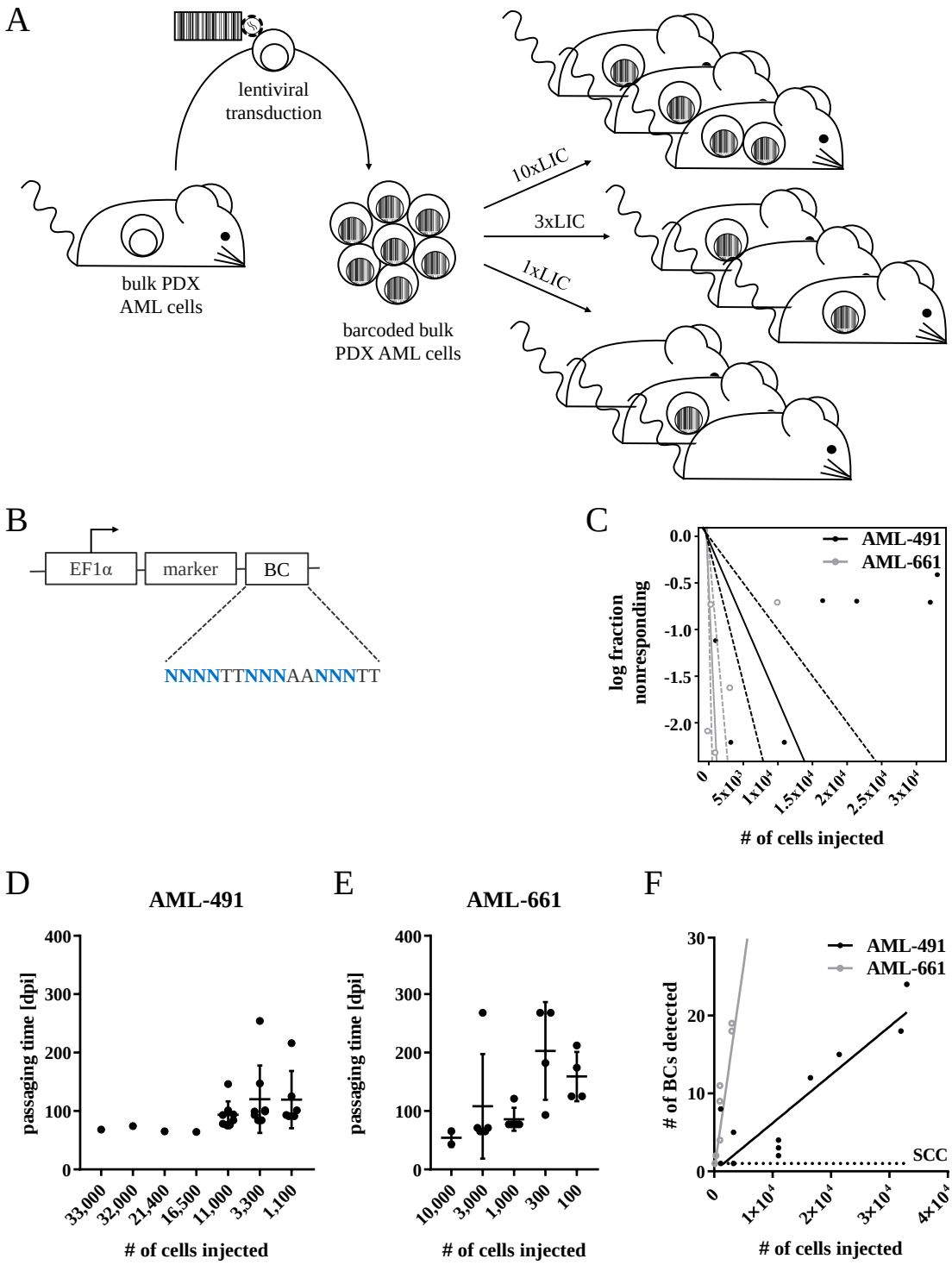

Figure 4.4. Generation and validation of PDX AML single cell clones (SCCs). (A) Experimental procedure; bulk PDX AML-491 or AML-661 cells were isolated from donor mice, transduced *ex vivo* with a lentiviral barcode (BC) pool and after 4 - 6 days sorted for marker expression. Barcoded cells were re-injected into groups of mice close to and above LIC frequency as determined in figure 4.1 and table A.1-A.3 (PDX AML-491: n = 33; PDX AML-661: n = 14). **(B)** Schematic of barcoding construct; a marker for positive selection and a genetic BC consisting of a semi-random nucleotide sequence with 10 random nucleotides are expressed under the elongation factor 1α (EF1α). The construct was designed and cloned by Daniel Richter, Ludwig-Maximilians-Universtität München.
(Legend continued on the next page.)

Figure 4.4. Generation and validation of PDX AML single cell clones (SCCs). (C) Positive engraftment with PDX AML-491 (black) or AML-661 cells (grey) was determined by flow cytometry and LIC frequency was calculated using the ELDA software (Hu and Smyth, 2009) (see figure A.4). Mean ± 95% CI is depicted. **(D,E)** Passaging times of engrafted mice from transplantation of PDX AML-491 (D) or AML-661 (E) cells until overt leukaemia was analysed. One dot represents one mouse. Mean ± SD is shown. **(F)** Leukaemic populations of mice engrafted with PDX AML-491 (black) or AML-661 (grey) were sequenced for the genetic BC. One dot represents one mouse. Sample preparation and data analysis was performed by Daniel Richter, Ludwig-Maximilians-Universität München; sequencing was done by LAFUGA, Ludwig-Maximilians-Universität München.
LIC = leukemia initiating cell; # = number; dpi = days post injection; BC = barcode; CI = confidence interval.

distinguishing single cells and their descendants from each other on DNA level. After transduction of the BC pool, cells were sorted for the marker expressed together with the BC and injected into groups of mice close to and above LIC frequency (PDX AML-491: n = 33; PDX AML-661: n = 19; table A.4), as pre-determined before (see figure 4.1C and table A.1 - A.3). The outgrowth of PDX AML cells was followed up by regular flow cytometric analysis of murine peripheral blood. Of the 52 mice injected, 42 animals showed engraftment of human cells (80.8%; PDX AML-491: 26/33 (78.8%); PDX AML-661: 16/19 (84.2%)). LIC frequencies were determined (figure 4.4C) and showed a more than 10-fold difference between PDX AML-491 (mean: 1 in 5,810 cells) and AML-661 (mean: 1 in 525 cells).

Analysis of time from injection of PDX AML cells to end-stage leukaemia revealed that decreasing cell numbers resulted in increasing passaging times, both for PDX AML-491 and AML-661 (figure 4.4DE).

To investigate the clonality of engrafted PDX AML cells, i.e. the number of clones constituting the end-stage leukaemia population, Daniel Richter sequenced PDX AML cells isolated from murine BM. The amount of genomically integrated genetic BCs detected per mouse showed a clear correlation to the number of cells injected per mouse (figure 4.4F). Additionally, Daniel Richter confirmed PDX AML populations arising from one single cell, as characterised by the integration of one individual BC, which, therefore, are termed PDX AML SCCs (n = 15; PDX AML-491: n = 11; PDX AML-661: n = 4; table 4.2).

In summary, 15 PDX AML SCCs of PDX AML-491 and AML-661 were successfully generated and were subsequently used to characterise intra-tumour heterogeneity.

4.2.2. Expansion and Fluorochrome Marking of PDX AML Single Cell Clones

In order to enable functional characterisation of the individual PDX AML SCCs, I aimed at marking each SCC with an individual combination of fluorochromes. PDX AML SCCs were expanded in serial transplantations and lentivirally transduced with constructs carrying (i) a lu-

ciferase and one of four fluorochromes or (ii) a fluorochrome alone (figure 4.5A-C). Luciferase was used for BLI and, thus, facilitated monitoring of tumour outgrowth or decline during *in vivo* treatment experiments (see chapter 1.4.2). Colour marking similar to RGB marking (see chapter 1.5.2) allowed competitive *in vivo* transplantation experiments, thereby reducing the number of animals needed and mouse-to-mouse variations. In this work, PDX AML SCCs were transduced with lentiviruses so they expressed a defined colour combination of up to four fluorochromes, allowing discrimination of, theoretically, 15 populations by flow cytometry (figure 4.5DE). Colour marked PDX AML SCC cells were enriched by FACS sorting, expanded and viable frozen for all consequent experiments within this study.

From the 15 PDX AML SCCs, 13 SCCs were expanded. Two PDX AML SCCs with low sequencing depth in BC analyses were not expanded. Unfortunately, one PDX AML-491 SCC failed to re-engraft, presumably due to a low frequency of barcoded cells within the initial population.

Table 4.2. Expansion and fluorochrome marking of PDX AML SCCs.

Sample	# of cells injected	# of SCCs	# of expanded SCCs	# of re-engrafted SCCs
AML-491	3,300	7	5	4
	1,100	4	4	4
AML-661	100	4	4	4

Taken together, I was able to successfully generate and colour mark twelve PDX AML SCCs of the same patient. These PDX AML SCCs were hereinafter characterised on multiple levels: regarding genetics, epigenetics and transcription levels as well as regarding functionality, i.e. homing capacity, growth behaviour, stem cell frequency and response towards various therapies.

4.3. Genetic, Epigenetic and Transcriptomic Characterisation of PDX AML Single Cell Clones

As a first step, expanded and flurochrome marked PDX AML SCCs were characterized regarding genetics, epigenetics and transcriptome in order to define differences between the PDX AML SCCs.

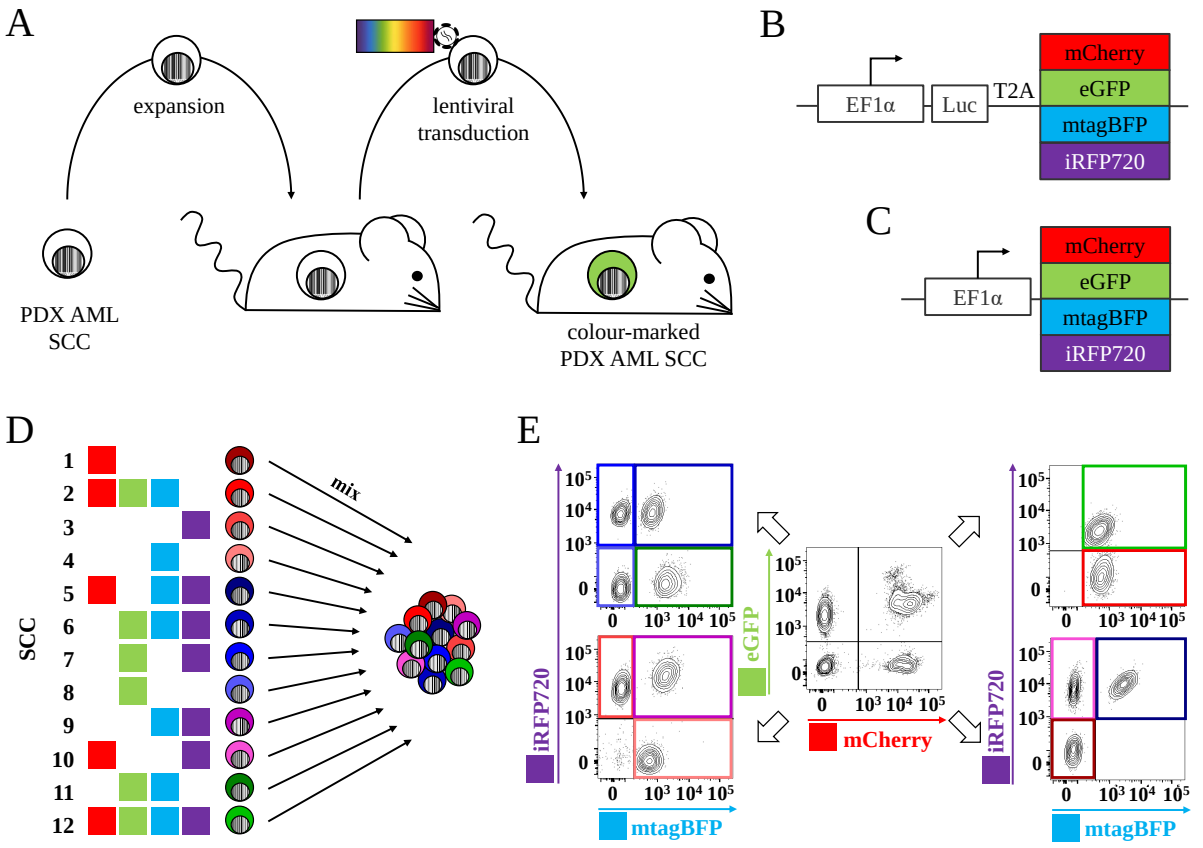

Figure 4.5. Expansion and fluorochrome marking of PDX AML SCCs. **(A)** Experimental procedure; verified PDX AML SCCs were expanded in mice. Re-isolated cells were transduced *ex vivo* with up to four lentiviral constructs encoding different fluorochromes, sorted for fluorochrome expression and re-injected into next recipient mice for amplification of cells. **(B,C)** Schematic of lentiviral constructs; a luciferase (Luc) and one of four fluorochromes (mCherry, eGFP, mtagBFP, iRFP720), separated by T2A for equimolar expression, were expressed under the EF1α promotor (B); alternatively, only fluorochromes were expressed (C). **(D)** Schematic of colour combination for each of the 12 SCCs used in this work; red = mCherry, green = eGFP, blue = mtagBFP, purple = iRFP720. Different colour combinations facilitate the mixing of all PDX AML SCCs for competitive experiments. **(E)** Schematic flow cytometry gating strategy to discriminate all twelve PDX AML SCCs in a competitive experiment.
EF1α = elongation factor 1α.

4.3.1. Targeted Sequencing Displayed an Enriched Capability of *NRAS*^{Q61K} Mutated Cells to Generate PDX AML Single Cell Clones

First, I performed targeted Sanger sequencing of known subclonal mutations of the patient and PDX sample pair, namely *KRAS*^{G12A}, *NRAS*^{Q61K}, *EZH2*^{A692G} and *JAK1*^{V658F}. These mutations in *KRAS*, *NRAS*, *EZH2* and *JAK1* are used as ”molecular markers” for the distinction of individual AML subclones rather than mutations responsible for an observed functional phenotype.

Table 4.3. Targeted sequencing of PDX AML SCCs for known subclonal mutations of the patient.

Sample	SCC	*KRAS*^{G12A}	*NRAS*^{Q61K}	*EZH2*^{A692G}	*JAK1*^{V658F}
AML-491	1	**wt/mut**	wt/wt	wt/wt	wt/wt
	2	**wt/mut**	wt/wt	wt/wt	wt/wt
	3	**wt/mut**	wt/wt	wt/wt	wt/wt
	4	**wt/mut**	wt/wt	wt/wt	wt/wt
	5	wt/wt	**wt/mut**	wt/wt	wt/wt
	6	wt/wt	**wt/mut**	wt/wt	wt/wt
	7	wt/wt	**wt/mut**	wt/wt	wt/wt
	8	wt/wt	**wt/mut**	wt/wt	wt/wt
AML-661	9	wt/wt	**wt/mut**	**Δ/mut**	wt/wt
	10	wt/wt	**wt/mut**	**Δ/mut**	wt/wt
	11	wt/wt	wt/wt	**Δ/mut**	wt/wt
	12	wt/wt	wt/wt	**Δ/mut**	wt/wt

This colour code will be used throught the thesis.

Targeted sequencing showed that 4 / 8 PDX AML-491 SCCs (SCC 1 - SCC 4) harboured a heterozygous mutation in the *KRAS* gene (*KRAS*^{G12A}; table 4.3 and figure 4.6A). Furthermore, a heterozygous mutation in the *NRAS* gene (*NRAS*^{Q61K}) was present in 4 / 8 PDX AML-491 SCCs (SCC 5 - SCC 8; table 4.3 and figure 4.6A). Both the *KRAS* and *NRAS* mutations are associated with several types of solid cancers, e.g. colorectal cancer and melanoma, respectively (Angelino et al., 2016; Peeters et al., 2013), but are also present in 12% of AML patients (The Cancer Genome Atlas Research Network, 2013). These mutations lead to an activation of the small GTPase and, consequently, to i.a. increased MAPK signalling (Renneville et al., 2008). 4 / 4 PDX AML-661 SCCs (SCC 9 - SCC 12) carried a homozygous mutation in *EZH2* (*EZH2*^{A692G}; table 4.3 and figure 4.6A), indicating either a loss of heterozygosity (LOH) or, alternatively, the same mutation on both alleles. This mutation leads to a loss-of-function of the histone methyltransferase, which has been associated with treatment resistance in AML (Göllner et al., 2017). 2 / 4 PDX AML-661 SCCs (SCC 9 - SCC 10) additionally harboured the *NRAS* mutation (*NRAS*^{Q61K}) also found in patient cells and PDX AML-491 SCC 5 - SCC 8 (table 4.3 and figure 4.6A). In the generated PDX AML SCCs *KRAS*^{G12A} mutation was mutually exclusive with *NRAS*^{Q61K} and *EZH2*^{A692G} mutations, whereas *NRAS*^{Q61K} and *EZH2*^{A692G} mutations could co-occur (table 4.3 and figure 4.6A).

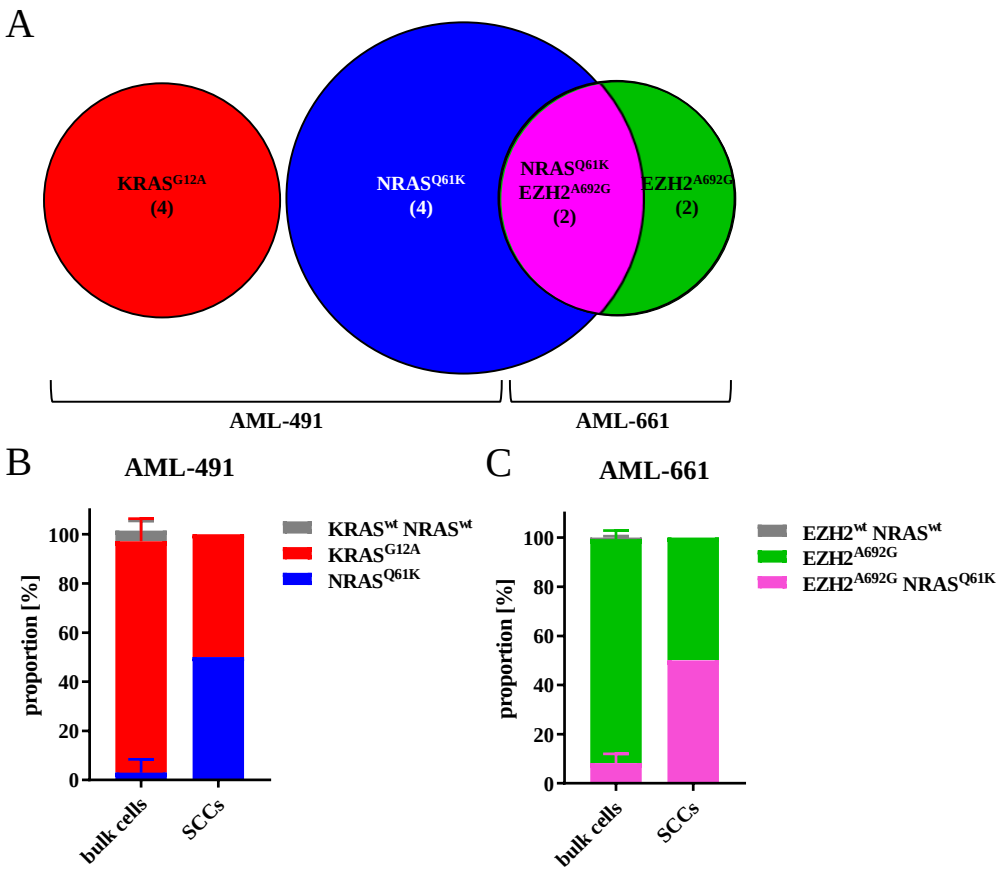

Figure 4.6. Targeted sequencing of PDX AML SCCs for known subclonal mutations. **(A)** Cells of the 12 PDX AML SCCs generated were analysed by targeted Sanger sequencing concerning known subclonal mutations within *KRAS*, *NRAS*, *EZH2* and *JAK1* (see table 4.3). The confirmed mutations and amount of PDX AML SCCs bearing these mutations are depicted; red = $KRAS^{G12A}$ (n = 4), blue = $NRAS^{Q61K}$ (n = 4), pink = $EZH2^{A692G}$ $NRAS^{Q61K}$ (n = 2), green = $EZH2^{A692G}$(n = 2). **(B,C)** Proportion of bulk PDX AML-491 (B) and AML-661 (C) cells harbouring mutations within depicted genes (data from figure 4.3) was compared to frequency of the same mutations in PDX AML SCCs. $NRAS^{Q61K}$ bulk PDX AML-661 cells were assumed to also be $EZH2^{A692G}$ mutated. For bulk cells mean ± SD is depicted.

Next, the ratio of $NRAS^{Q61K}$ PDX AML SCCs was compared to the ratio of this mutation within bulk PDX AML cells over several passages as measured by targeted sequencing (Maja Rothenberg-Thurley, Klinikum der Universität München; LAFUGA, Ludwig-Maximilians-Universität München; Binje Vick, Helmholtz Zentrum München). Interestingly, even though the VAF of the $NRAS^{Q61K}$ mutation was far below 50% in both PDX AML-491 and AML-661 cells over several rounds of passaging indicating that only a small subclone harboured this mutation, 50% of the PDX AML SCCs carried the mutation in both samples (figure 4.6BC). These data suggests that $NRAS^{Q61K}$ cells have a higher capacity to generate PDX AML SCCs.

Taken together, the twelve PDX AML SCCs generated in this study originated from at least four genetically distinct subclones of the same patient.

4.3.2. Exome Sequencing Confirmed Four Genetically Distinct Clones Represented by PDX AML Single Cell Clones

In order to examine the genetic architecture of the PDX AML SCCs in more detail, exome sequencing was performed (LAFUGA and Ilse Valtierra, both Ludwig-Maximilians-Universität München).

Ilse Valtierra's analyses confirmed the four genetically distinct clones determined by Sanger sequencing (chapter 4.3.1, figure 4.7A). In analyses of copy number variations (CNVs), a deletion of parts of chromosome 7 was detected in all PDX AML SCCs, affecting the *EZH2* gene and leading to LOH of this region (figure 4.7B and A.1). Moreover, rearrangements of chromosome 6 were identified in the primary patient sample of the second relapse and all four PDX AML-661 SCCs (SCC 9 - SCC 12; figure 4.7B and A.1). Additionally, PDX AML SCC 11 and SCC 12 harbouring the $EZH2^{A692G}$ mutation displayed a q-arm deletion of chromosome 17 (figure 4.7B and A.1), resulting in enrichment of HOX signalling, epigenetic regulation, oxidative stress induced senescence, transcription and translation (figure 4.7C, examplary for PDX AML SCC 11).

In summary, exome sequencing confirmed that the generated PDX AML SCCs originated from four genetically distinct subclones of one individual AML patient.

4.3.3. DNA Methylation Analysis Revealed Clustering of PDX AML Single Cell Clones According to Mutational Phenotype

Addtionally to the genetic characterisation of PDX AML SCCs (chapter 4.3.1 and 4.3.2), samples were analysed concerning DNA methylation signatures (Bianka Ksienzyk, Tobias Herold and Vindi Jurinovic, all Klinikum der Universität München; Genomics and Proteomics Core Facility, Deutsches Krebsforschungszentrum Heidelberg).

Vindi Jurinovic's and Tobias Herold's analysis showed clustering of PDX AML SCCs according to the genetic mutations detected (chapter 4.3.1 and 4.3.2) with the largest difference represented by the $EZH2^{A692G}$ mutation (figure 4.8). Since the $EZH2^{A692G}$ mutation arose in the patient during disease progression from first to second relapse, it, subsequently, is only present in PDX AML-661 SCCs. This finding might indicate that the biggest divergence seen in DNA methylation is due to evolution in the patient.

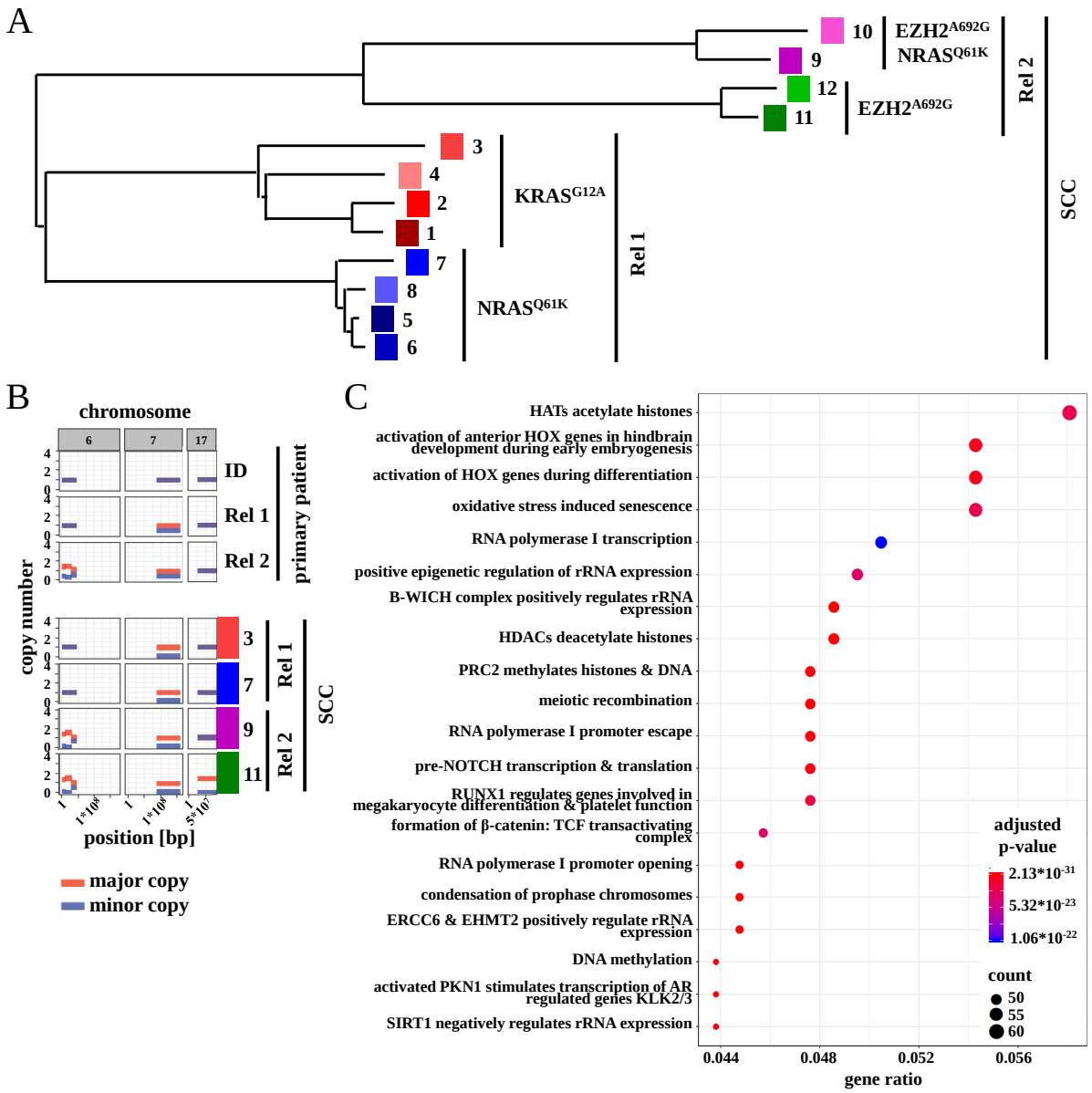

Figure 4.7. Exome sequencing of PDX AML SCCs. gDNA was isolated from every PDX AML SCC and exome libraries preped for 100 bp paired-end sequencing (sample preparation by LAFUGA, Ludwig-Maximilians-Universität München). Data was demultiplexed and analysed by Ilse Valtierra, Ludwig-Maximilians-Universität München, using existing whole exome sequencing data from primary patient's material (initial diagnosis (ID), relapse 1 (Rel 1) and relapse 2 (Rel2) as well as complete remission samples) as control. **(A)** A phylogenetic tree was generated using analyses of single nucleotide variants (SNVs) of whole exome sequencing of PDX AML SCCs. **(B)** Copy number variants (CNVs) were analysed using ID and complete remission samples as control. CNVs of chromosome 6, 7 and 17 are depicted for primary patient's material and PDX AML SCC 3 (*KRAS*^{G12A}), SCC 7 (*NRAS*^{Q61K}), SCC 9 (*EZH2*^{A692G} *NRAS*^{Q61K}) and SCC 11 (*EZH2*^{A692G}) as representative PDX AML SCCs for their genetic group. CNV analyses of all chromosomes and all samples are depicted in figure A.1. **(C)** Pathway enrichment analysis of genes in CNV regions differing in PDX AML SCC 11 (*EZH2*^{A692G}) compared to all other PDX AML SCC.

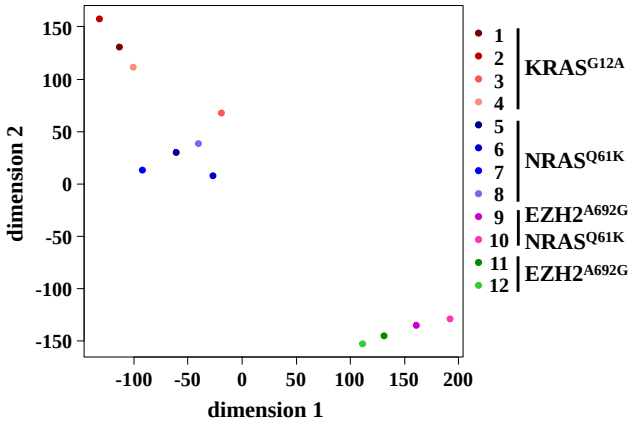

Figure 4.8. Methylation array of PDX AML SCCs. gDNA was isolated from every PDX AML SCC, bisulfite treated and sequenced with the Infinum MethylationEPIC BeadChip (sample preparation by Bianka Ksienzyk and Tobias Herold, both Klinikum der Universität München, and sequencing by Genomics and Proteomics Core Facility, Deutsches Krebsforschungszentrum Heidelberg). Data was analysed by Vindi Jurinovic, Klinikum der Universität München, and Tobias Herold. t-SNE plot of all PDX AML SCCs is depicted. Every dot represents one sample.
t-SNE = t-distributed stochastic neighbour embedding.

4.3.4. Transcriptome Sequencing Revealed Clustering of PDX AML Single Cell Clones According to Mutational Phenotype

To extent the characterisation of the twelve PDX AML SCCs, transcriptomic analysis was performed using RNA barcoding and sequencing (SCRB-seq; Johannes Bagnoli, LAFUGA, both Ludwig-Maximilians-Universität München, Vindi Jurinovic and Tobias Herold, both Klinikum der Universität München).

Similar to DNA methylation analysis PDX AML SCCs clustered according to the genetic mutations detected (chapter 4.3.1 and 4.3.2) with the largest difference represented by the *EZH2*^{A692G} mutation (figure 4.9A). Interestingly, PDX AML SCC 9 and SCC 10, harbouring both the *EZH2*^{A692G} and *NRAS*^{Q61K} mutations, were enriched for i.a. apoptosis, P53 pathway and IL6-JAK-STAT3 signalling compared to PDX AML SCC 11 and SCC 12, harbouring both only the *EZH2*^{A692G} mutation (figure 4.9B and A.2).

Taken together, both DNA methylation and transcriptomic analyses revealed clustering of PDX AML SCCs according to their genetic differences defined by mutations in *KRAS*, *NRAS* and *EZH2*.

Genetic, epigenetic and transcriptomic characterisation of the twelve PDX AML SCCs demonstrated that four genetically distinct subclones from one individual patient's leukaemia are represented by the SCCs. Furthermore, PDX AML SCCs cluster in epigenetic and transcriptomic analyses according to their genotype illustrating the homogeneity of the PDX AML SCCs with

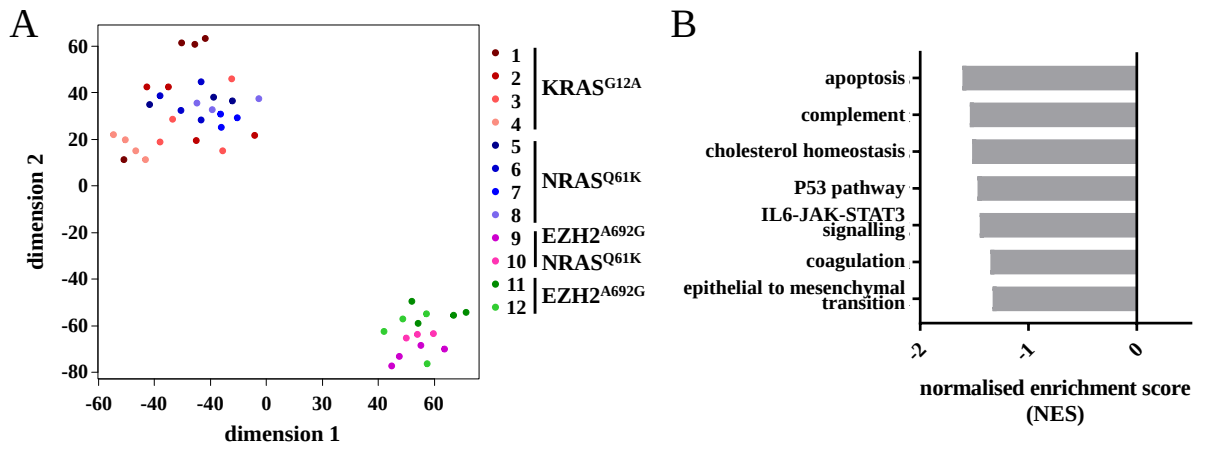

Figure 4.9. Transcriptome sequencing (SCRB-seq) of PDX AML SCCs. RNA of PDX AML SCCs (3 - 4 replicates) was isolated, cDNA generated and libraries prepared for 50 bp sequencing using a modified single cell RNA barcoding and sequencing (SCRB-seq) protocol (sample preparation by Johannes Bagnoli, Ludwig-Maximilians-Universität München, and sequencing by LAFUGA, Ludwig-Maximilians-Universität München). Data was analysed by Vindi Jurinovic and Tobias Herold, both Klinikum der Universität München. **(A)** t-SNE plot of all PDX AML SCCs is depicted. Every dot represents one sample. **(B)** Significantly enriched hallmark pathways (nominal p-value ≤ 0.05) comparing PDX AML SCC 11 and SCC 12 (both *EZH2*^{A692G}) to SCC 9 and SCC 10 (both *EZH2*^{A692G} *NRAS*^{Q61K}).
bp = base pair; t-SNE = t-distributed stochastic neighbour embedding.

the same genetic characteristics. The isolation of these genetically, epigenetically and transcriptomically diverse subclones confirms not only the presence of subclones within an individual AML but also demonstrates the evolution a patient's leukaemia may undergo over time.

4.4. Functional Characterisation of PDX AML Single Cell Clones

Even though many studies exist about the genetic and epigenetic heterogeneity in AML (Waanders et al., 2020; Li et al., 2016b; Burrell and Swanton, 2014; Corces-Zimmerman et al., 2014a; Marusyk et al., 2012; Hanahan and Weinberg, 2011), studies about functional intra-tumour diversity are scarce, especially regarding a precise association of genetic and functional traits (de Boer et al., 2018). The PDX AML SCCs generated in this study allow characterising intra-patient heterogeneity not only genetically but also correlating genetic, epigenetic and transcriptomic differences to a functional phenotype. Such functional characterisation, e.g. regarding stemness, growth behaviour and therapy response, may enable the discovery of adverse subclones within an individual patient responsible for treatment resistance and relapse and to link this adversity to the molecular origin potentially identifying new therapeutic targets.

4.4.1. Limiting Dilution Transplantation Assays Revealed an Increased Stem Cell Frequency in *NRAS^{Q61K}* Cells

The first unexpected and remarkable discovery in this project was that *NRAS^{Q61K}* PDX AML cells showed an increased capacity to generate PDX AML SCCs compared to *NRAS^{wt}* PDX AML cells, both in PDX AML-491 and AML-661 cells. One possible explanation for this observed phenotype is an increased stem cell frequency of these subclones. To test this hypothesis, PDX AML SCC 3 (*KRAS^{G12A}*) and SCC 7 (*NRAS^{Q61K}*) were transplanted into groups of mice in a LDTA to determine and compare the LIC frequency of these PDX AML SCCs (table A.5).

Interestingly, analysis of engraftment capacity revealed an 13-fold higher LIC frequency of PDX AML SCC 7 (*NRAS^{Q61K}*; estimate: 1 in 1,725) over SCC 3 (*KRAS^{G12A}*; estimate: 1 in 21,878, p = 0.0009; figure 4.10).

This increased stem cell frequency might explain the increased capacity of *NRAS^{Q61K}* or *EZH2^{A692G} NRAS^{Q61K}* PDX AML cells compared to *NRAS^{wt}* cells to generate SCCs.

4.4.2. Competitive *In Vivo* Homing Assay of PDX AML Single Cell Clones Displayed Successful Homing of All Single Cell Clones

One characteristic of adversity is intensive interaction of leukaemic cells with the BM niche, since the surrounding environment may present an effective protectorate from elimination through chemotherapeutics (Ebinger et al., 2016; Duan et al., 2014; Boyerinas et al., 2013; Ishikawa et al., 2007).

One technique to study niche interactions of PDX AML cells is the homing assay (see chapter 4.1). Successful homing to the murine BM niche after injection of cells into the systemic blood stream is chaperoned by migration, adhesion and leukaemia-niche interactions, processes relevant for tumour survival.

To reduce mouse numbers and to have comparable conditions for the studied PDX AML SCCs, homing was examined in a competitive manner. Here, PDX AML SCCs were mixed and transplanted into mice (n = 6; figure 4.11A). After three days, mice were sacrificed, BM was analysed by flow cytometry for fluorochrome expressing PDX AML SCCs and ratios of each PDX AML SCC compared to input ratios. In three independent experiments with between four and ten PDX AML SCCs mixed in various ratios it became apparent that all analysed SCCs were able to home to the murine BM (figure 4.11B-D).

Successful homing of all analysed PDX AML SCCs demonstrates a comparable capability

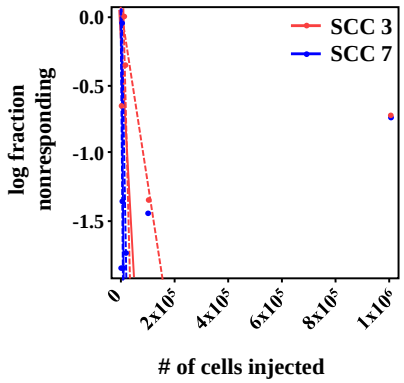

Figure 4.10. LIC frequency of one *KRAS*^{G12A} and one *NRAS*^{Q61K} PDX AML SCC. PDX AML SCC 3 (*KRAS*^{G12A}) and SCC 7 (*NRAS*^{Q61K}) cells were thawed, cultured *in vitro* for four days and sorted for fluorochrome expression. Cells were transplanted into mice in limiting dilutions at numbers indicated in table A.5. Positive engraftment was determined by BLI after up to 9 weeks post transplantation. LIC frequency and statistical significance (Chi-square test) was calculated using the ELDA software (Hu and Smyth, 2009). Mean ± 95% CI is depicted; p = 0.0009.

of all SCCs to proficiently migrate to and adhere to the murine BM niche.

4.4.3. Analysis of Growth Behaviour and Proliferation Identified *EZH2*^{A692G} PDX AML Single Cell Clones as Fast Growing

Another measure of adversity of AML subclones is growth behaviour. Fast growing subclones are disadvantageous since they may lead to rapid disease progression and, thus, shorter survival of patients.

4.4.3.1. Competitive Transplantation of PDX AML Single Cell Clones Uncovered *EZH2*^{A692G} Single Cell Clones as the Most Aggressively Growing Clones

To study *in vivo* growth behaviour of PDX AML SCCs with reduced mouse-to-mouse variation, a competitive transplantation assay was performed. Here, PDX AML SCCs were mixed and injected into groups of mice (n = 6) (figure 4.12A). Animals were sacrificed at defined time points according to leukaemic burden (figure 4.12AB) and murine BM was analysed by flow cytometry.

After transplantation of eleven PDX AML SCCs representing all four genetic subclones of the patient's AML in a 1:1 ratio, it became evident that PDX AML SCC 11 and SCC 12 (both *EZH2*^{A692G}) overgrew all other SCCs within the first 2.5 weeks (figure 4.12C). Interestingly, PDX AML SCC 5 (*NRAS*^{Q61K}) was not detectable in 3 / 6 mice or constituted only up to 0.15% of PDX AML cells already at low leukaemic burden (day 17) indicating a growth disadvantage of this PDX AML SCC. When the four PDX AML-661 SCCs (SCC 9 - SCC 12; two

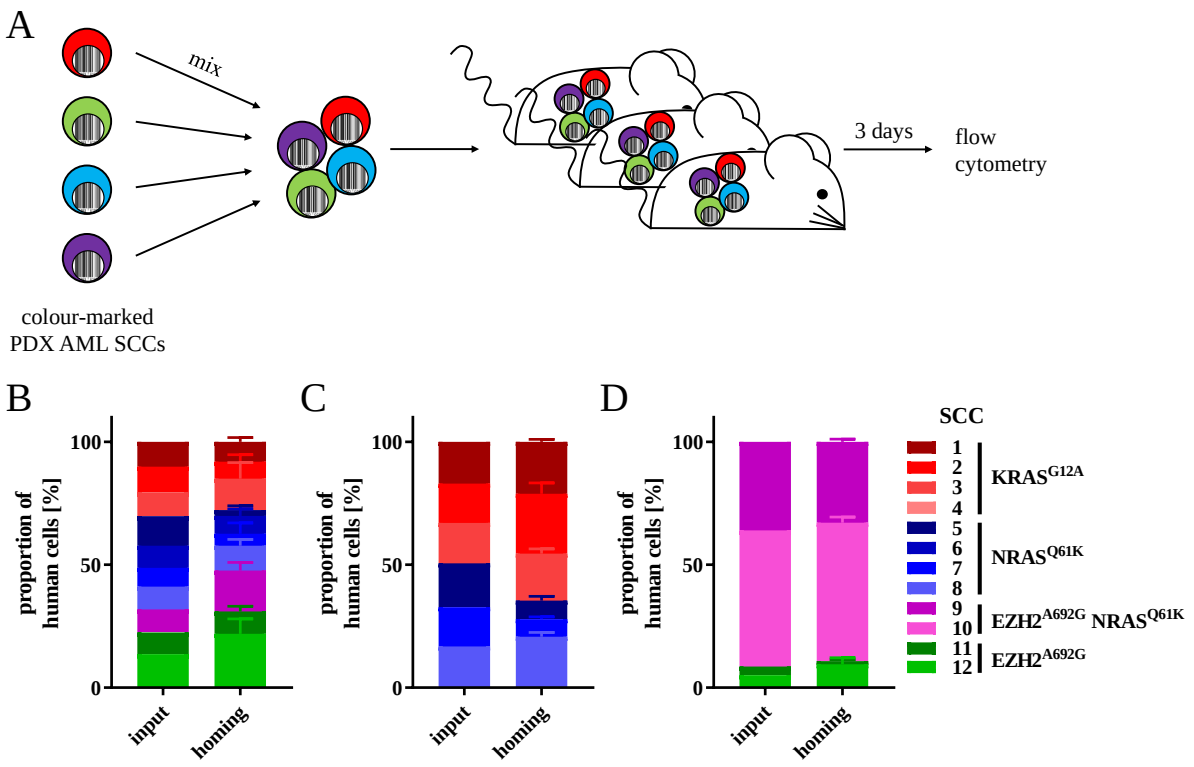

Figure 4.11. Competitive *in vivo* homing of PDX AML SCCs. **(A)** Experimental procedure; fluorochrome marked PDX AML SCCs were thawed, cultured *in vitro* for 4 days and sorted for viable fluorochrome marked cells. Cells were mixed at different ratios and $2 * 10^5 - 6.4 * 10^5$ cells were injected into groups of mice (n = 6). Animals were sacrificed 3 days after transplantation and murine BM analysed via flow cytometry. **(B-D)** Relative ratio of individual PDX AML SCCs within the mixture of ten (B; SCC 1 - SCC 3, SCC 5 - SCC 9, SCC 11, and SCC 12), six (C; SCC 1 - SCC 3, SCC 5, SCC 7 and SCC 8), or four PDX AML SCCs (D; SCC 9 - SCC 12) at time of injection (input; n = 1) and re-isolation (homing; n = 6). For time point homing mean ± SD is depicted.

EZH2^{A692G} *NRAS*^{Q61K} and two *EZH2*^{A692G} SCCs) where transplanted into groups of mice in an approximately 9:1 ratio, the growth advantage of PDX AML SCC 11 and SCC 12 (both *EZH2*^{A692G}) could be confirmed (figure 4.12D).

Taken together, competitive *in vivo* growth revealed that PDX AML SCC 11 and SCC 12 (both *EZH2*^{A692G}) had a clear growth advantage over the other PDX AML SCCs in competitive transplantation assays.

4.4.3.2. Competitive *In Vivo* Proliferation Assay of PDX AML Single Cell Clones Shows That Growth Behaviour Correlates with Proliferation

Even though competitive *in vivo* experiments represent a sensitive readout to measure growth behaviour, they do not distinguish between proliferation and apoptosis rate of PDX AML SCCs. One possibility to measure proliferation is to stain cells with the proliferation sensitive dye carboxyfluorescein succinimidyl ester (CFSE); reduction of the mean fluorescence intensity

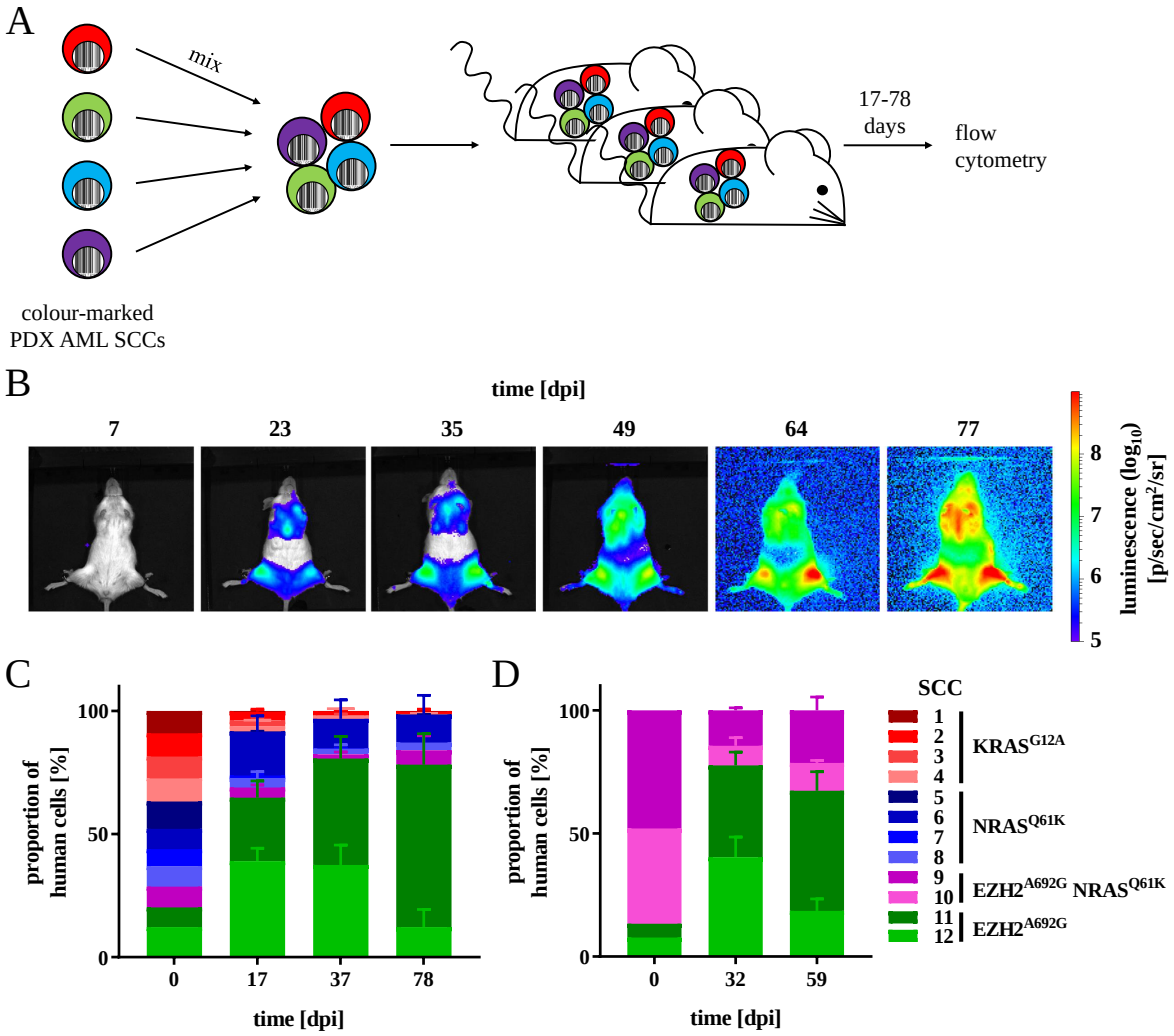

Figure 4.12. Competitive *in vivo* growth of PDX AML SCCs. **(A)** Experimental procedure; fluorochrome marked PDX AML SCCs were thawed, cultured *in vitro* for 4 days and sorted for viable fluorochrome marked cells. Cells were mixed at different ratios and $2 * 10^5 - 3 * 10^5$ cells were injected into groups of mice. Tumour outgrowth was regularly monitored by BLI. Animals were sacrificed 17 - 78 days after transplantation and murine BM was analysed via flow cytometry. **(B)** Representative imaging pictures of mice injected with a mix of eleven PDX AML SCCs (SCC 1 - SCC 9, SCC 11, and SCC 12) are shown. **(C,D)** Relative ratio of individual PDX AML SCCs within a mixture of eleven (C; SCC 1 - SCC 9, SCC 11, and SCC 12), or four PDX AML SCCs (D; SCC 9 - SCC 12; two independent experiments) at time of injection (0 dpi; n = 1) and re-isolation at indicated time points (17 - 78 dpi; n = 5 - 6) is depicted. For time points mean ± SD is depicted. Statistical significance was tested with two-way ANOVA with Tukey correction (see tables A.6- A.8).
dpi = days post injection.

(MFI) of CFSE distinctly correlates with the proliferation rate (Quah and Parish, 2010; Hawkins et al., 2007). Additionally, CFSE content of PDX acute leukaemia (AL) cells can be employed to measure and identify a low-cycling and quiescent subpopulation of PDX AL cells called label-retaining cells (LRC) (Ebinger et al., 2020, 2016). LRC are defined as cells within three

bisections of the MFI of non-proliferating cells indicating less than three cell doublings as described by Ebinger et al. (2020, 2016).

To determine proliferation rates and the ratio of LRC within the PDX AML SCCs, I combined the already established CFSE staining with the competitive *in vivo* approach, performing a competitive *in vivo* CFSE assay for the first time. Here, PDX AML SCCs transgenic for the fluorochromes mCherry, mtagBFP and/or iRFP720 were mixed, stained with CFSE and transplanted into mice (n = 6; figure 4.13A). After ten days animals were sacrificed, murine BM was analysed by flow cytometry and CFSE MFI as well as ratio of LRC determined for each PDX AML SCC (figure 4.13AB).

Proliferation and ratio of LRC was analysed exemplary for PDX AML SCC 3 ($KRAS^{G12A}$), SCC 10 ($EZH2^{A692G}$ $NRAS^{Q61K}$) and SCC 11 ($EZH2^{A692G}$). After ten days of *in vivo* growth engraftment was verified by BLI (figure 4.14A). Flow cytometric analysis of the expressed fluorochromes proofed again the growth advantage of PDX AML SCC 11 ($EZH2^{A692G}$) over SCC 3 ($KRAS^{G12A}$) and SCC 10 ($EZH2^{A692G}$ $NRAS^{Q61K}$; figure 4.14B). Absolute number of PDX AML SCC cells was calculated by flow cytometric analysis (figure 4.14E).

CFSE MFI was determined for each PDX AML SCC (figure 4.14C) and correlation to the absolute number of PDX AML SCC cells analysed (figure 4.14F). A visible relationship between the two parameters could be observed illustrating proliferation as the main process responsible for the variable growth rates of PDX AML SCCs.

Additionally, ratio of LRC was determined for each PDX AML SCC (figure 4.14D) and correlated to absolute number of PDX AML SCC cells analysed (figure 4.14G). A distinct correlation between the two parameters could be observed indicating a close interrelationship between the fraction of quiescent and low-cycling PDX AML cells to *in vivo* growth.

In summary, both loss of the proliferation sensitive dye CFSE and the fraction of dormant LRC correlated with and validated growth behaviour seen in competitive *in vivo* experiments. These results are in line with the results shown in chapter 4.4.3.1, where $EZH2^{A692G}$ SCCs overgrew all other SCCs. Therefore, I conclude that within this individual AML patient, subclones with a more aggressive growth behaviour exist.

4.4.4. *In Vivo* Therapy of PDX AML Single Cell Clones with Cytarabine Identified $EZH2^{A692G}$ Single Cell Clones as Partially Resistant

Supplementary to the ability to adhere to the BM niche and to proliferate efficiently, drug resistance represents one of the major factors defining adversity of leukaemia subclones. Partial

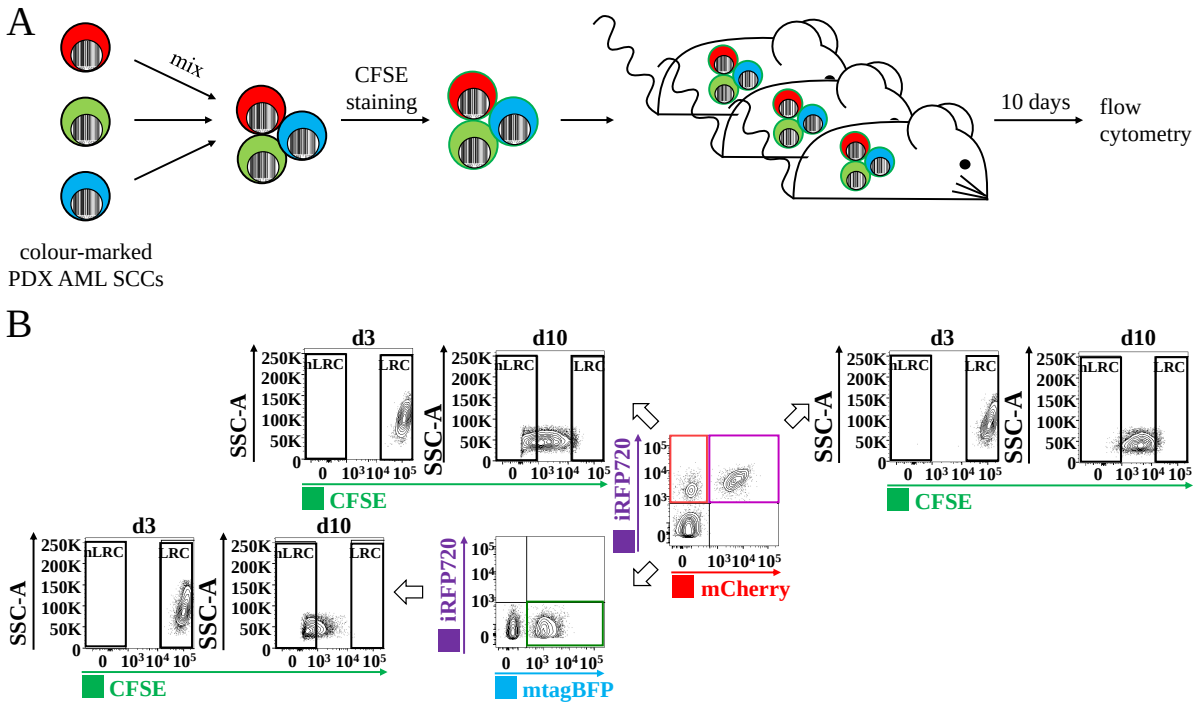

Figure 4.13. Schematic of competitive carboxyfluorescein succinimidyl ester (CFSE) assay of PDX AML SCCs. (A) Experimental procedure; three fluorochrome marked PDX AML SCCs were isolated from donor mice, mixed, stained with carboxyfluorescein succinimidyl ester (CFSE) and $1 * 10^7$ cells were injected into groups of mice. Animals were sacrificed after ten days and murine BM was analysed via flow cytometry. **(B)** Flow cytometry gating strategy; PDX AML SCCs were distinguished by their fluorochrome expression. For each PDX AML SCC the CFSE content was analysed. The CFSE MFI after three days of *in vitro* culture of the PDX AML SCCs was taken as starting value. Cells within three bisections, indicating up to three cell doublings, were defined as label-retaining cells (LRC), whereas seven or more bisections were defined as non-LRC as described by Ebinger et al. (2020, 2016).
CFSE = carboxyfluorescein succinimidyl ester; LRC = label-retaining cells; nLRC = non label-retaining cells.

or complete failure to respond to treatment as well as the ability to re-induce the tumour causing relapse are leading factors for patients' poor prognosis (Ravandi et al., 2017; Othus et al., 2016; Buccisano et al., 2006). Additionally, these phenomena are a testimony to intra-tumour heterogeneity (see chapter 1.1.3 and 1.3).

4.4.4.1. Competitive *In Vivo* Therapy of PDX AML Single Cell Clones with Cytarabine Revealed *EZH2*^{A692G} Single Cell Clones as Partially Resistant

To examine the response towards Ara-C, one of the most commonly used drugs to treat AML, competitive *in vivo* experiments were performed with the PDX AML SCCs, additionally reducing mouse numbers as well as mouse-to-mouse variations. Again PDX AML SCCs were mixed and transplanted into groups of mice, which were either left untreated or treated with a drug of choice (figure 4.15).

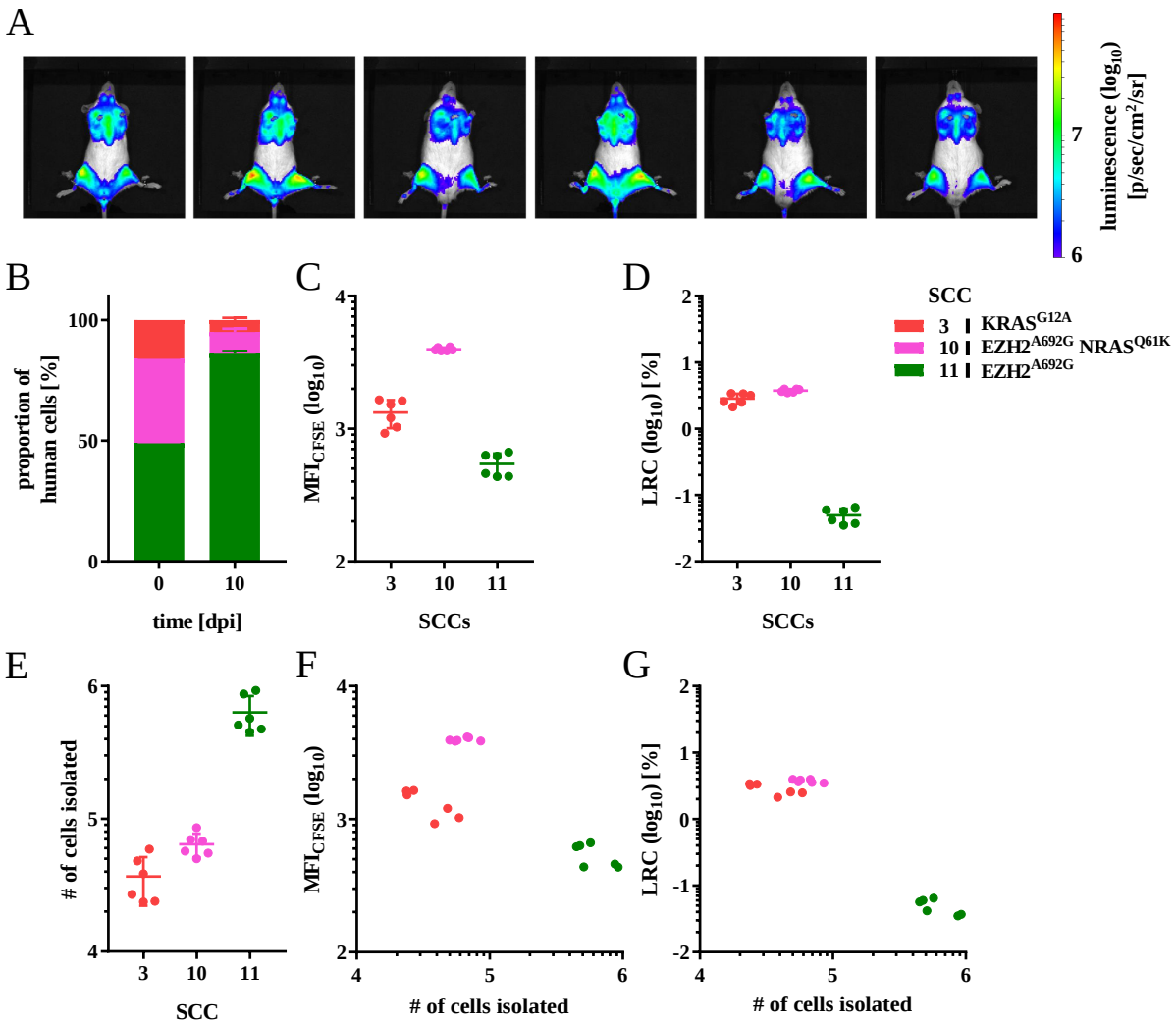

Figure 4.14. Competitive CFSE assay of PDX AML SCCs. Experimental procedure was performed as described in figure 4.13. A mix of three PDX AML SCCs (SCC 3, SCC 10 and SCC 11) was stained with CFSE and $1 * 10^7$ cells were injected into mice (n = 6). **(A)** Imaging pictures of the mice at day 10 are shown. **(B)** Relative ratio of individual PDX AML SCCs within the mixture at time of injection (0 dpi; n = 1) and re-isolation (10 dpi; n = 6) are depicted (mean ± SD). **(C)** CFSE mean fluorescence intensitiy (MFI) of PDX AML SCCs at day 10 was determined by flow cytometry (mean ± SD). One dot represents one mouse. **(D)** Ratio of LRC within the whole population of each individual PDX AML SCCs is shown (mean ± SD). One dot represents one mouse. **(E)** Absolute number of PDX AML SCC cells was counted for every mouse by flow cytometry and is shown as mean ± SD. One dot represents one mouse. **(F)** Correlation of number of PDX AML SCC cells as depicted in (E) with CFSE MFI of individual PDX AML SCCs as depicted in (C). One dot represents one mouse. **(G)** Correlation of number of PDX AML SCC cells as depicted in (E) with the ratio of LRC within the whole population of each individual PDX AML SCC as depicted in (D). One dot represents one mouse.
dpi = days post injection; MFI = mean fluorescence intensity; CFSE = carboxyfluorescein succinimidyl ester; LRC = label-retaining cells.

In the first competitive *in vivo* treatment experiment a mix of eleven PDX AML SCCs was injected into groups of mice (n = 4 - 6). For PDX AML SCC 10 fluorochrome-marking was not ready yet, therfore, it was not included in this experiment. When BLI reached a defined leukaemic burden (total flux = $2.2 * 10^8 - 3.0 * 10^9$ photons/sec), mice were treated with Ara-C

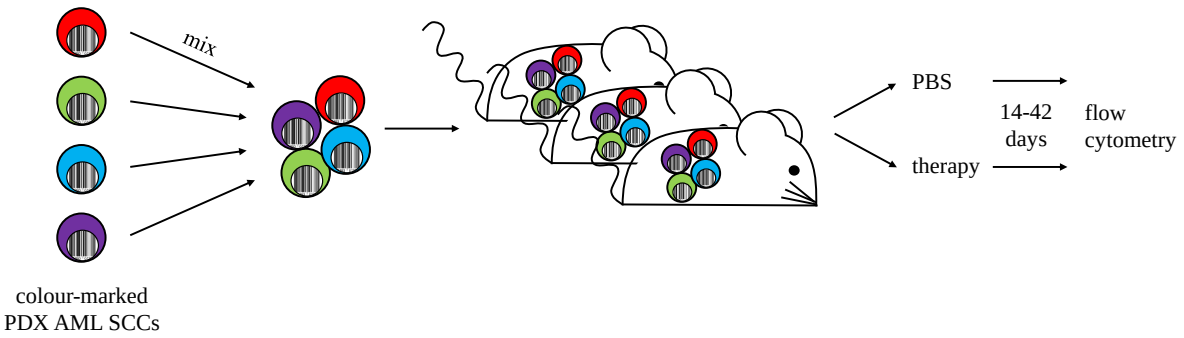

Figure 4.15. Schematic experimental procedure of competitive *in vivo* therapy of PDX AML SCCs. Experimental procedure; fluorochrome marked PDX AML SCCs were thawed, cultured *in vitro* for four days and sorted for viable fluorochrome marked cells. Cells were mixed and injected into groups of mice. Tumour outgrowth was regularly monitored by BLI. At defined leukaemic burden animals were either left untreated or treated with a drug of choice. After 14 - 42 days of therapy, mice were sacrificed and murine BM was analysed by flow cytometry.

over a period of six weeks alternating one week with four doses (days 2 - 5) and one week of rest. Leukaemic burden was measured repeatedly by BLI and quantified (figure 4.16AB). A significant, but minor decrease of leukaemia burden was observed when mice were treated with Ara-C as compared to control (42 days after therapy start: total flux = $7.68 * 10^{10}$ photons/sec vs. total flux = $1.27 * 10^{10}$ photons/sec, $p < 0.0001$). After treatment stop mice were sacrificed and murine BM was analysed by flow cytometry for fluorochrome composition. PDX AML SCC 11 and SCC 12 (both $EZH2^{A692G}$) constituted 99.1% of human cells in treated animals in comparison to 78.2% in untreated mice (figure 4.16C). To calculate the individual leukaemic burden of each PDX AML SCC, the total leukaemic burden of animals at end of therapy as measured by BLI was multiplied with the relative ratio of each PDX AML SCC. This calculated individual PDX AML SCC burden demonstrates the reduction of every SCC in the treatment group compared to the control group (figure 4.16D). To analyse the relative effect of chemotherapy on each individual PDX AML SCC, treatment response was normalised to untreated controls for every PDX AML SCC (figure 4.16E) and summarised according to genetic classification of PDX AML SCCs (figure 4.16F). This competitive *in vivo* experiment evidently exposes differences in Ara-C response rates, namely a strong sensitivity of all four $NRAS^{Q61K}$ and one $EZH2^{A692G}$ $NRAS^{Q61K}$ PDX AML SCCs (mean of normalised PDX AML SCC size = 0.0027 and 0.0009, respectively), an intermediate response rate of all four $KRAS^{G12A}$ PDX AML SCCs (mean of normalised PDX AML SCC size = 0.0876) and a partial resistance of $EZH2^{A692G}$ PDX AML SCCs (mean of normalised PDX AML SCC size = 0.1883).

Similarly, a competitive *in vivo* therapy trial was performed with a mix of the two $EZH2^{A692G}$

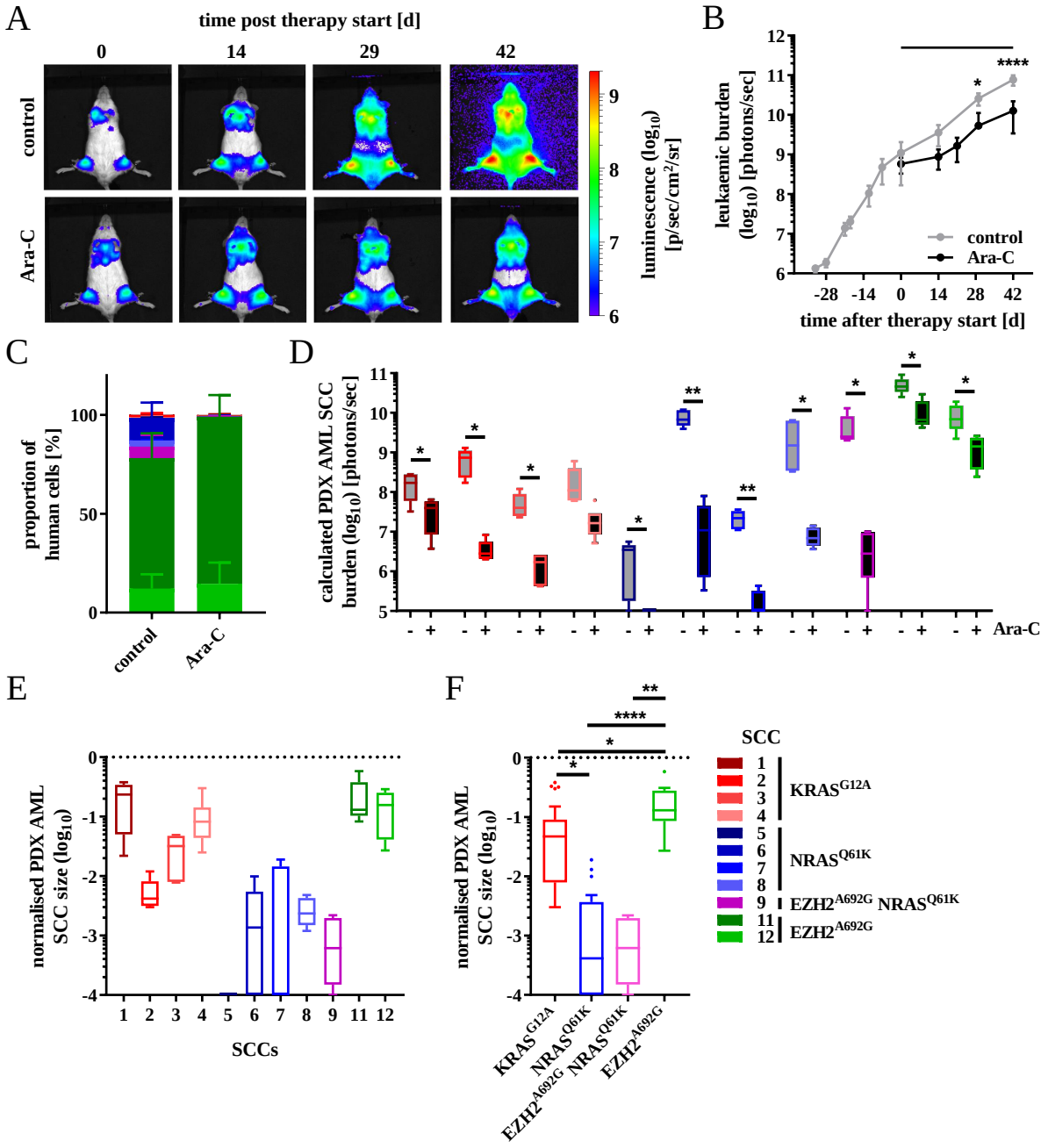

Figure 4.16. Competitive *in vivo* cytarabine (Ara-C) therapy of eleven PDX AML SCCs. Experimental procedure was performed as described in figure 4.15. A mix of eleven PDX AML SCCs (SCC 1 - SCC 9, SCC 11 and SCC 12; $2 * 10^5$ cells per mouse) was injected into groups of mice. At total flux of $2.2 * 10^8 - 3.0 * 10^9$ photons/sec animals were either left untreated (control) or treated with 100 mg/kg Ara-C on days 2 - 5 in a bi-weekly rhythm for six weeks (Ara-C). **(A)** Imaging pictures of one representative control and Ara-C treated mouse are shown. **(B)** Quantification of BLI of control (grey) and Ara-C treated mice (black) is depicted (mean ± SD; n = 5 - 12). Statistical significance was tested with two-way ANOVA with Sidak correction. If not indicated otherwise, the test was not significant. **(C)** Relative ratio of individual PDX AML SCCs within the mixture of SCCs of control and Ara-C treated mice. Mean ± SD is depicted.
(Legend continued on the next page.)

Figure 4.16. Competitive *in vivo* cytarabine (Ara-C) therapy of eleven PDX AML SCCs. (D) PDX AML SCC burden was calculated for every mouse using the relative ratio of each individual PDX AML SCC as depicted in (C) multiplied with the BLI quantification of each mouse as depicted in (B) and is shown as box plots. Statistical significance was tested with t-test with Benjamini and Hochberg correction. If not indicated otherwise, the test was not significant. **(E)** Calculated PDX AML SCC burden of Ara-C treated mice as depicted in (D) was normalised to SCC burden of control animals and is shown as box plots. Statistical significance was tested between all PDX AML SCCs by one-way ANOVA with Tukey correction (see table A.9). **(F)** Normalised calculated PDX AML SCC burden as depicted in (E) was summarized according to genotype and is depicted as box plots. Statistical significance was tested by one-way ANOVA with Tukey correction. If not indicated otherwise, the test was not significant.
Ara-C = cytarabine; d = days; * = $p < 0.05$; ** = $p < 0.01$; **** = $p < 0.0001$.

NRAS^{Q61K} and the two *EZH2*^{A692G} PDX AML SCCs. Quantification of BLI displayed a significant decrease in tumour burden when mice were treated with Ara-C for a period of four weeks with four doses per week (days 2 - 5) compared to untreated control animals (28 days after therapy start: total flux = $5.50 * 10^9$ photons/sec vs. total flux = $5.10 * 10^{10}$ photons/sec, $p < 0.0001$; figure 4.17A). Murine BM was analysed for fluorochrome composition displaying a relative enrichment of PDX AML SCC 11 and SCC 12 (both *EZH2*^{A692G}) under Ara-C treatment in comparision to untreated control (mean = 88.1% vs. mean = 24.3%; figure 4.17B). Again, BLI quantification of animals and ratio of PDX AML SCCs in the mixture was used to calculate the leukaemic burden of each individual PDX AML SCC showing a significant response of all SCCs towards Ara-C (figure 4.17C). When PDX AML SCC burden after Ara-C therapy was normalised to untreated control for each individual SCC (figure 4.17D) and summarised according to the genetic classification (figure 4.17E), it became evident that *EZH2*^{A692G} *NRAS*^{Q61K} PDX AML SCCs respond towards Ara-C treatment (mean of normalised PDX AML SCC size = 0.0149); on the contrary, *EZH2*^{A692G} PDX AML SCCs are partially resistant towards Ara-C therapy in this competitive *in vivo* experiment (mean of normalised PDX AML SCC size = 0.4439; $p < 0.0001$) (figure 4.17E) confirming the effects already seen in figure 4.16.

Therefore, I conclude that the *EZH2*^{A692G} PDX AML SCCs (SCC 11 and SCC 12) represent an adverse clone within the patient's leukaemia.

4.4.4.2. *In Vivo* Therapy of Single PDX AML Single Cell Clones Confirmed the Partial Resistance of *EZH2*^{A692G} Single Cell Clones

In order to validate the chemotherapy responses observed in figures 4.16 - 4.17, individual PDX AML SCCs were injected in a non-competitive experiment into groups of mice (n = 2 - 3), which were either left untreated or treated with Ara-C for a period of four weeks with four

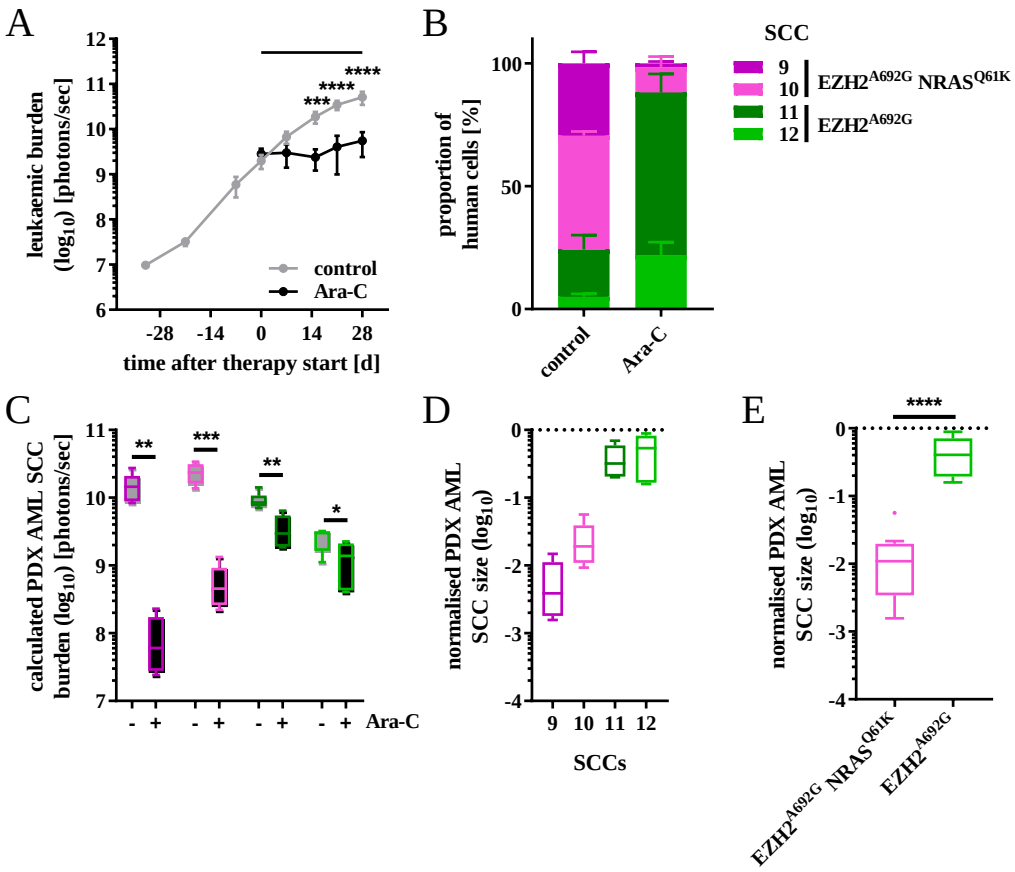

Figure 4.17. Competitive *in vivo* cytarabine (Ara-C) therapy of four PDX AML SCCs. Experimental procedure was performed as described in figure 4.15. A mix of four PDX AML SCCs (SCC 9 - SCC 12; $3.0 * 10^5$ cells per mouse) was injected into groups of mice. At total flux of $4.9 * 10^8 - 3.2 * 10^9$ photons/sec animals were either left untreated (control) or treated with 100 mg/kg Ara-C on days 2 - 5 for four weeks (Ara-C). **(A)** Quantification of BLI of control (grey) and Ara-C treated mice (black) is depicted (mean ± SD; n = 5 - 12). Statistical significance was tested with two-way ANOVA with Sidak correction. If not indicated otherwise, the test was not significant. **(B)** Relative ratio of individual PDX AML SCCs within the mixture of SCCs of control and Ara-C treated mice. Mean ± SD is depicted. **(C)** PDX AML SCC burden was calculated for every mouse using the relative ratio of each individual PDX AML SCC as depicted in (B) multiplied with the BLI quantification of each mouse as depicted in (A) and is shown as box plots. Statistical significance was tested with t-test with Benjamini and Hochberg correction. **(D)** Calculated PDX AML SCC burden of Ara-C treated mice as depicted in (C) was normalised to SCC burden of control animals and is shown as box plots. Statistical significance was tested between all PDX AML SCCs by one-way ANOVA with Tukey correction (see table A.10). **(E)** Normalised calculated PDX AML SCC burden as depicted in (D) was summarized according to genotype and is shown as box plots. Statistical significance was tested by one-way ANOVA with Tukey correction.

Ara-C = cytarabine; d = days; * = $p < 0.05$; ** = $p < 0.01$; *** = $p < 0.001$; **** = $p < 0.0001$.

doses per week (days 2 - 5). Here, one partially resistant and one sensitive PDX AML SCC were chosen, namely PDX AML SCC 11 (*EZH2*^{A692G}) and SCC 9 (*EZH2*^{A692G} *NRAS*^{Q61K}), respectively. While PDX AML SCC 11 (*EZH2*^{A692G}) displayed a significant, but mild reduction of leukaemic burden after four weeks of treatment (day 28 post therapy start: to-

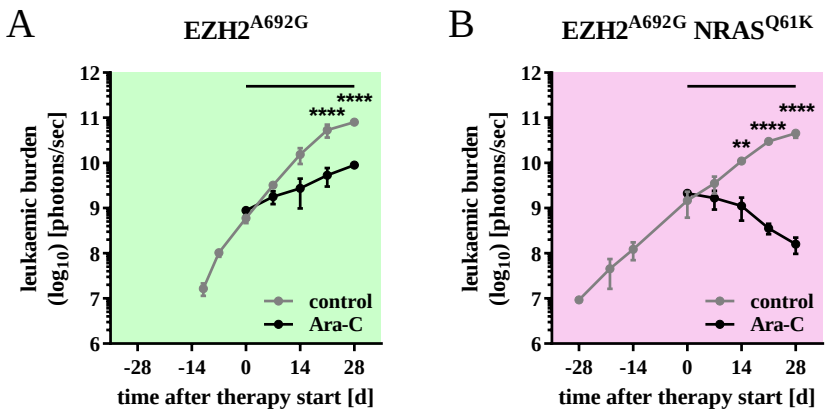

Figure 4.18. ***In vivo*** **cytarabine (Ara-C) therapy response validation of two PDX AML SCCs.** $3.75 * 10^5$ PDX AML SCC 11 cells (*EZH2*^{A692G}) **(A)** or $3.2 * 10^5$ PDX AML SCC 9 cells (*EZH2*^{A692G} *NRAS*^{Q61K}) **(B)** were injected into groups of mice (n = 2 - 3). Tumour outgrowth was regularly monitored by BLI. At total flux of $4.5 * 10^8 - 2.5 * 10^9$ photons/sec animals were either left untreated (control, grey) or treated with 100 mg/kg Ara-C on days 2 - 5 for four weeks (Ara-C, black). Quantification of BLI signals is depicted (mean ± SD). Statistical significance was tested with two-way ANOVA with Sidak correction. If not indicated otherwise, the test was not significant.
d = days; ** = $p < 0.01$; **** = $p < 0.0001$.

tal flux = $9.00 * 10^9$ photons/sec vs. total flux = $8.03 * 10^{10}$ photons/sec, $p < 0.0001$; figure 4.18A) and, hence, partial resistance, PDX AML SCC 9 (*EZH2*^{A692G} *NRAS*^{Q61K}) showed a significant and increased reduction of leukaemic burden (28 days post therapy start: total flux = $1.60 * 10^8$ photons/sec vs. total flux = $4.57 * 10^{10}$ photons/sec, $p < 0.0001$; figure 4.18B) and, thus, therapy sensitivity.

These results validate the partial Ara-C resistance of *EZH2*^{A692G} PDX AML SCCs in comparison to the other SCCs in an independent and differently executed experiment.

4.4.5. *In Vivo* Chemotherapy of PDX AML Single Cell Clones Identified *EZH2*^{A692G} Single Cell Clones as Partially Sensitive towards 5-Azacitidine

Even though Ara-C has been one of the most frequently used drugs for the treatment of AML patients in the last 30 years (De Kouchkovsky and Abdul-Hay, 2016; Döhner et al., 2015), recent advances in AML research have led to the introduction of novel therapeutic drugs (see chapter 1.1.2). Among those are targeted therapies such as FLT3 kinase inhibitors (Stone et al., 2018, 2017), hypomethylating agents (HMAs) like 5-azacitidine (Aza) and decitabine (Estey, 2018; Fenaux et al., 2009), as well as molecular inhibitors such as the Bcl-2 inhibitor venetoclax (DiNardo et al., 2018; Wei et al., 2018).

4.4.5.1. *In Vivo* Therapy of One *EZH2*^{A692G} PDX AML Single Cell Clone with Venetoclax and 5-Azacitidine Uncovered a Partial Sensitivity towards 5-Azacitidine

A first step was to identify drugs potentially capable of eliminating the Ara-C resistant *EZH2*^{A692G} PDX AML SCCs. Here, individual PDX AML SCC 11 (*EZH2*^{A692G}) was injected in a non-competitive experiment into groups of mice (n = 3), which were either left untreated or treated with clinically relevant drugs, namely venetoclax and Aza. While treatment with venetoclax over a period of three weeks with five doses per week (days 1 - 5) showed no effect on leukaemic burden (21 days post therapy start; total flux = $1.01 * 10^{10}$ photons/sec vs. total flux = $1.53 * 10^{10}$ photons/sec, p = 0.1359; figure 4.19A), therapy with Aza over a period of four weeks with three doses per week (days 1, 3 and 5) displayed a significant reduction of tumour burden (28 days post therapy start: total flux = $1.36 * 10^{8}$ photons/sec vs. total flux = $1.53 * 10^{10}$ photons/sec, $p < 0.0001$; figure 4.19B) indicating a partial sensitivity towards Aza.

4.4.5.2. Competitive *In Vivo* Therapy of *EZH2*^{A692G} and *EZH2*^{A692G} *NRAS*^{Q61K} PDX AML Single Cell Clones Displayed Similar Responses

To broaden the characterization of PDX AML SCCs regarding response towards Aza, a competitive *in vivo* experiment was performed as described in chapter 4.4.4.1 and figure 4.15. Here, a mix of the two *EZH2*^{A692G} *NRAS*^{Q61K} and the two *EZH2*^{A692G} PDX AML-661 SCCs was transplanted into groups of mice (n = 5). When leukaemic burden reached a defined BLI signal (total flux = $2.80 * 10^{8}$ - $4.50 * 10^{9}$ photons/sec), mice were either left untreated or treated with Aza over a period of four weeks with three doses per week (days 1, 3 and 5) and tumour burden was repeatedly monitored by BLI (figure 4.20A). BLI quantification displayed significant reduction of leukaemic burden under Aza therapy compared to control (28 days post therapy start: total flux = $1.65 * 10^{9}$ photons/sec vs. total flux = $4.28 * 10^{10}$ photons/sec, $p < 0.0001$. Murine BM was analysed for fluorochrome composition after treatment stop showing no differences in the relative ratio of PDX AML SCCs with and without Aza therapy (figure 4.20B). BLI quantification of animals and ratio of PDX AML SCCs in the mixture was used to calculate the leukaemic burden of individual PDX AML SCCs showing a significant reduction of all four tested PDX AML SCCs under therapy (figure 4.20C). Calculated PDX AML SCC burden after Aza therapy was normalised to untreated control in each individual PDX AML SCC (figure 4.20D) and summarised according to mutational status of *NRAS* (figure 4.20E). Here, it became evident that all four analysed PDX AML SCCs had a similar response rate towards

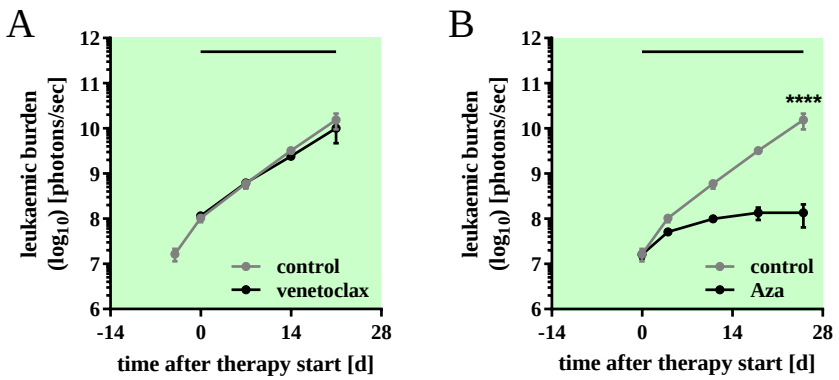

Figure 4.19. ***In vivo*** **Treatment of one** $EZH2^{A692G}$ **PDX AML SCC with venetoclax or 5-azacitidine (Aza).** $3.75 * 10^5$ PDX AML SCC 11 cells ($EZH2^{A692G}$) were injected into groups of mice (n = 3). Tumour outgrowth was regularly monitored by BLI. **(A)** At total flux of $8.6 * 10^7 - 1.3 * 10^8$ photons/sec animals were either left untreated (control, grey) or treated with 100 mg/kg venetoclax on days 1 - 5 for three weeks (venetoclax, black). **(B)** At total flux of $1.2 * 10^7 - 2.2 * 10^7$ photons/sec animals were either left untreated (control, grey) or treated with 5 mg/kg Aza on days 1, 3 and 5 for four weeks (Aza, black). Quantification of BLI signals is depicted (mean $\pm$ SD). Statistical significance was tested with two-way ANOVA with Sidak correction. If not indicated otherwise, the test was not significant.
**** = $p < 0.0001$.

treatment with Aza and, thus, are partially sensitive.

In summary, *in vivo* therapy of PDX AML-661 SCCs with Aza exposed a partial sensitivity of all tested PDX AML SCCs independent from their reponse rate towards Ara-C.

Altogether, I was able to generate SCCs derived from AML xenografts of two time points, the first and second relapse, of one individual patient. These PDX AML SCCs could be analysed not only on a genetic, epigenetic and transcriptomic level but they were also characterized functionally in competitive *in vivo* experiments regarding homing, growth, quiescence and chemotherapy response.

The functional characterization of the PDX AML SCCs generated and fluorochrome marked in this work allows the identification of an *in vivo* fast proliferating and partially Ara-C resistant subclone, represented by PDX AML SCC 11 and 12 ($EZH2^{A692G}$), which respond partially towards Aza. This adverse functional phenotype could be correlated to genetic alterations such as a q-arm deletion of chromosome 17 linked to an enrichment in HOX signaling, epigenetic regulation, oxidative stress induced senescence, transcription and translation. As a next step, it would be of particular interest to investigate the mechanisms responsible for this adverse phenotype. Here, knock-down, knock-out, knock-in or re-expression experiments could be performed in order to identify the molecular alterations responsible for the fast growing and Ara-C resistant phenotype and, thus, pinpointing putative targets for novel treatment options.

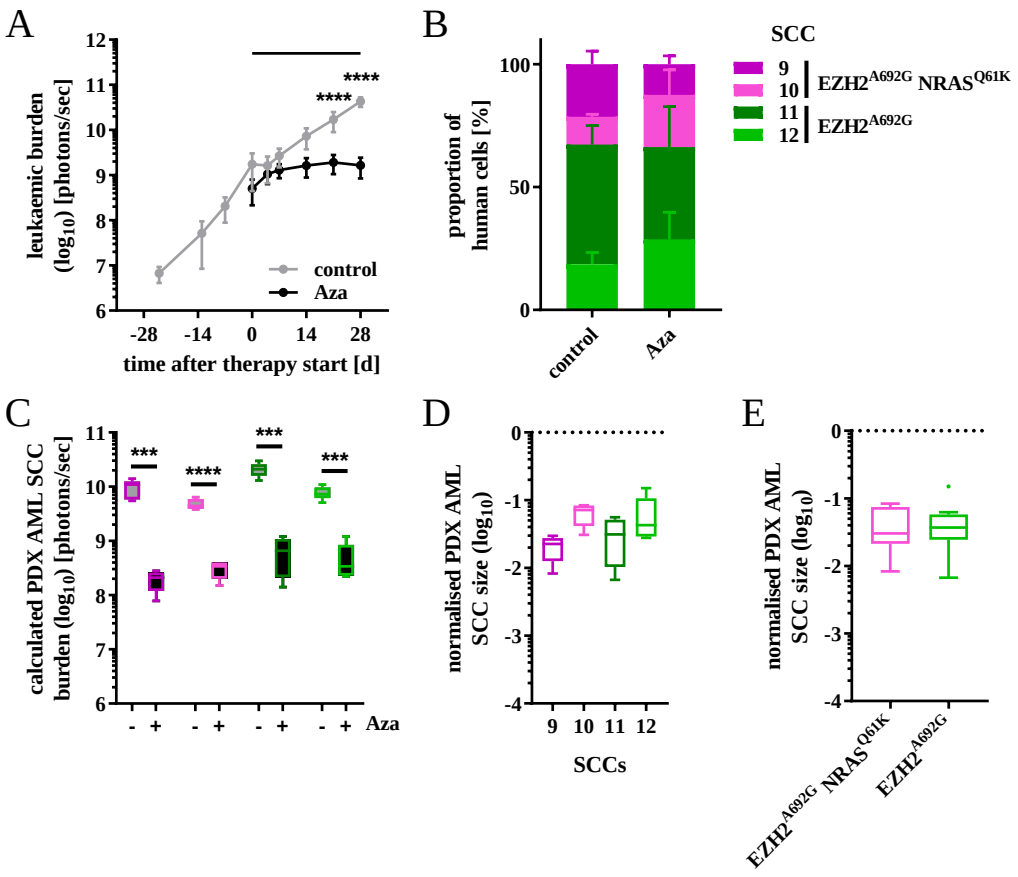

Figure 4.20. Competitive *in vivo* 5-azacitidine (Aza) therapy of four PDX AML SCCs. Experimental procedure was performed as described in figure 4.15. A mix of four PDX AML SCCs (SCC 9 - SCC 12; $2.6 * 10^5$ cells per mouse) was injected into groups of mice. At total flux of $2.8 * 10^8 - 4.5 * 10^9$ photons/sec animals were either left untreated (control) or treated with 5 mg/kg Aza on days 1, 3 and 5 for four weeks (Aza,). **(A)** Quantification of BLI of control (grey) and Aza treated mice (black) is depicted (mean ± SD; n = 5 - 12). Statistical significance was tested with two-way ANOVA with Sidak correction. If not indicated otherwise, the test was not significant. **(B)** Relative ratio of individual PDX AML SCCs within the mixture of SCCs of control and Aza treated mice. Mean ± SD is depicted. **(C)** PDX AML SCC burden was calculated for every mouse using the relative ratio of each individual PDX AML SCC as depicted in (B) multiplied with the BLI quantification of each mouse as depicted in (A) and is shown as box plots. Statistical significance was tested with t-test with Benjamini and Hochberg correction. **(D)** Calculated PDX AML SCC burden of Aza treated mice as depicted in (C) was normalised to SCC burden of control animals and is shown as box plots. Statistical significance was tested between all PDX AML SCCs by one-way ANOVA with Tukey correction. If not indicated otherwise, the test was not significant. **(E)** Normalised calculated PDX AML SCC burden as depicted in (D) was summarized according to genotype and is shown as box plots. Statistical significance was tested by one-way ANOVA with Tukey correction. If not indicated otherwise, the test was not significant.
Aza = 5-azacitidine; d = days; *** = $p < 0.001$; **** = $p < 0.0001$.

5. Discussion

Clonal Heterogeneity presents a major challenge in the successful treatment of acute myeloid leukaemia (AML) since the most adverse subclone within a patient's leukaemia determines clinical outcome and prognosis. However, the biology of unfavourable subclones is currently not well understood and correlation of functional traits of AML subpopulations to genetic, epigenetic and transcriptomic features is still scarce (de Boer et al., 2018).

In this study, I generated and characterised twelve AML populations derived from one single stem cell (single cell clones, SCCs) of one individual AML patient using the patient-derived xenograft (PDX) mouse model. Four genetically distinct subclones of the patient were represented by the PDX AML SCCs, which could also be discriminated within DNA methylation and transcriptomic analyses. Functional *in vivo* characterisation revealed a fast growing and cytarabine (Ara-C) resistant clone which carried an $EZH2^{A692G}$ mutation as well as a partial loss of chromosome 17.

5.1. Genetic and Functional Inter- and Intra-Patient Heterogeneity Are Challenging Clinical Characteristics of Acute Myeloid Leukaemia

As the biological origins of AML are diverse, it is a disease with considerable inter-patient heterogeneity (Döhner et al., 2017, 2015; The Cancer Genome Atlas Research Network, 2013). Cytogenetic alterations, genetic mutations and epigenetic changes differ from patient to patient resulting in a complex disease entity characterised by a broad range of clinical response rates towards chemotherapy and prognosis (Döhner et al., 2017, 2015; The Cancer Genome Atlas Research Network, 2013; Schlenk et al., 2008). Complex karyotype, specific rearrangements, e.g. *KMT2A*-rearrangements and *BCR-ABL1* translocation, as well as certain mutations, e.g. in *RUNX1* and *TP53*, have been associated with worse clinical outcome and a relapse incidence of $>$90% and, thus, are categorised as adverse (Döhner et al., 2017, 2015; Estey, 2014). In contrast, *RUNX1-RUNX1T1* translocation as well as mutated *NPM1* without *FLT3-ITD* are considered favourable with a relapse incidence of 35-40% (Döhner et al., 2017, 2015; Estey,

2014). In addition to the major inter-patient heterogeneity presented in AML, the disease can evolve over time; relapsed leukaemia often differs from diagnosis, e.g. concerning mutational patterns (Greif et al., 2018; Boyd et al., 2018; Corces-Zimmerman et al., 2014a; Klco et al., 2014; Krönke et al., 2013). Genetic alterations as well as gene expression patterns may be lost or gained over time adding more complexity (Greif et al., 2018; Boyd et al., 2018; Corces-Zimmerman et al., 2014a; Klco et al., 2014; Krönke et al., 2013).

In this study the PDX model of AML was applied since it enables repetitive *in vitro* and *in vivo* studies using patient-derived cells of diverse origin, thereby facilitating studies on patient-to-patient heterogeneity. Even though the PDX AML samples examined in this work present highly aggressive forms of leukaemia, they still vary concerning cytogenetics (normal karyotype, single translocations or complex karyotype) and display a wide spectrum of genetic alterations commonly seen in AML patients (see chapter 4.1). Additionally to these genetic differences, functional variation was observed between the samples regarding *in vivo* growth, homing to the murine bone marrow (BM), stemness and drug response (see chapter 4.1). With this broad range of genetically and functionally diverse samples, the PDX AML model exhibits advantages both over studies conducted with cell lines and with primary AML samples. On the one hand, cell lines have accumulated unphysiological mutations over time leading to transcriptomic and proteomic alterations (Liu et al., 2019b; Ben-David et al., 2019; Fasterius and Szigyarto, 2018; Pan et al., 2009); furthermore, clonality is reduced over time *in vitro* (Belderbos et al., 2017). On the other hand, patients' primary AML samples are favoured for studies on genetic heterogeneity, but as they rarely proliferate *in vitro*, functional examination is difficult (Brenner et al., 2019); moreover, material is limited impeding repetitive studies. Thus, the PDX model presents a suitable and advantageous alternative.

In addition to the considerable inter-patient diversity detected in AML, major intra-patient heterogeneity has been observed (Chen et al., 2019; Yilmaz et al., 2019; de Boer et al., 2018; Ding et al., 2012). Acute leukaemia (AL) subclones display differences in genetics such as translocations and mutations as well as epigenetics (Chen et al., 2019; Rothenberg-Thurley et al., 2018; Shlush et al., 2017; Corces et al., 2016; Ding et al., 2012). Furthermore, diversity has been observed regarding differentiation and stemness (Caiado et al., 2016; Kreso and Dick, 2014), proliferation (Ebinger et al., 2020, 2016; Kreso and Dick, 2014; Saito et al., 2010), niche interactions (Belderbos et al., 2017; Elder et al., 2017; Verovskaya et al., 2014) as well as therapy response (de Boer et al., 2018; Caiado et al., 2016; Kreso and Dick, 2014). This intra-patient heterogeneity presents a major challenge in the successful treatment of AML patients

since therapy may not eradicate all subclones and, eventually, leads to relapse (Shlush et al., 2017; Burrell and Swanton, 2014).

In line with published data, functional intra-patient variability has been observed within the PDX AML models used in this work regarding growth behaviour, homing to the murine BM as well as chemotherapy response, especially for the main samples of this work, PDX AML-491 and AML-661, xenografts of the first and second relapse of the same patient (see chapter 4.1). Furthermore, for this PDX AML sample pair targeted sequencing of known AML mutations has demonstrated the presence of genetically diverse subclones already detected in the patient's primary cells, of which some, but not all, were able to engraft into immunocompromised mice (see chapter 4.1). Enhanced engraftment capability of minor subclones has been described previously (Sandén et al., 2020; Shlush et al., 2017; Klco et al., 2014). These differences of AML clones in their ability to engraft has been connected to heterogeneity regarding stemness (Sandén et al., 2020; Caiado et al., 2016; Townsend et al., 2016; Kreso and Dick, 2014). Furthermore, AML subclones capable of engrafting and overgrowing other clones in mice have been associated with treatment resistance and relapse (Sandén et al., 2020; Shlush et al., 2017; Klco et al., 2014). However, even though xenografts might skew the clonal composition of the primary patient's leukaemia, the PDX model still presents a suitable tool to study intra-patient heterogeneity, which enables correlation of genetic and functional differences of AML subpopulations.

In summary, the PDX model of AML presents a suitable tool to investigate not only inter- but also intra-patient heterogeneity.

5.2. Generation of Barcoded and Fluorochrome Marked PDX AML Single Cell Clones Enables Genetic and Functional Studies of Cancer Clonality

One potential methodical approach to study intra-tumour heterogeneity and clonality is genetic barcoding. Here, individual cells are lenti- or retrovirally marked with an exclusive genetic barcode (BC) allowing sensitive and reliable discrimination of individual cells and their descendants over space and time (Bramlett et al., 2020; Adair et al., 2020; Belderbos et al., 2017; Elder et al., 2017; Bystrykh and Belderbos, 2016; Bystrykh et al., 2014). Several groups have applied genetic barcoding in PDX models of acute lymphoblastic leukaemia (ALL) to study engraftment, proliferation, clonal expansion and dynamics (Jacobs et al., 2019; Belderbos et al.,

2017; Elder et al., 2017; Verovskaya et al., 2014). Engraftment of leukaemic cells in various organs has been analysed, sometimes even over time and serial transplantation showing clonal skewing in different organs and loss of clonality when small cell numbers where serially transplanted (Jacobs et al., 2019; Belderbos et al., 2017; Elder et al., 2017; Verovskaya et al., 2014). Furthermore, stem cell differentiation of human cord blood cells transplanted into immunocompromised mice has been analysed with the use of genetic BCs (Cheung et al., 2013). In this work genetic barcoding was utilised in combination with limiting dilution transplantation assay (LDTA) to determine the clonality of human AML populations engrafted in the murine BM after transplantation in order to generate AML populations derived from one individual stem cell (single cell clones, SCCs; see chapter 4.2). Thus, genetic barcoding can be used to determine the stem cell, or in AML the leukaemia-initiating cell (LIC), frequency as previously described (Elder et al., 2017). This approach might present an alternative to LDTAs to determine the LIC frequency of AL samples. On the one hand, genetic barcoding does not require transplantation of limiting numbers of AL cells but can be performed with high cell numbers; thus, it might present a more accurate readout for the stem cell frequency. On the other hand, standard LDTAs don't depend on viral transduction of a BC, which might not only be impossible for some samples but might also introduce skewing of subclones, as it is unclear whether all subpopulations can be transduced with the same efficiency. However, a precise comparison of LDTA and genetic barcoding for the determination of LIC frequency has not yet been reported.

A second approach to study intra-sample heterogeneity is red/green/blue (RGB) fluorochrome marking. In RGB marking cells are genetically labeled with a combination of fluorochromes (van der Heijden et al., 2019; Finkenzeller, 2016; Abramowski et al., 2015; Gomez-Nicola et al., 2014; Weber et al., 2012, 2011). Specific colour codes, either through random integration of fluorochromes or defined fluorochrome combinations, enable distinction of individual living cells (Maetzig et al., 2018, 2017; Finkenzeller, 2016; Weber et al., 2012, 2011). RGB marking has been utilised to study spatiotemporal clonal dynamics in various types of cancer, e.g. colorectal cancer, osteosarcoma, neuroendocrine-carcinoma and leukaemia, as well as healthy tissues such as brain and liver (van der Heijden et al., 2019; Gambera et al., 2018; Cornils et al., 2017; Abramowski et al., 2015; Gomez-Nicola et al., 2014; Cornils et al., 2014). In this work pre-defined colour combinations were used to discriminate the generated PDX AML SCCs in functional assays (see chapter 4.2). In contrast to genetic barcoding RGB marking allows analysing viable cells, which can be re-transplanted into mice or sorted for fluorochrome expression and functionally characterised further. Additionally, flow cytometric readout does

not demand time-consuming preparation of samples as does sequencing, but instead can be performed within minutes. Therefore, RGB fluorochrome marking presented an easy to handle readout of mixtures of the PDX AML SCCs.

To utilise the advantages of both genetic barcoding and RGB marking, I combined the two strategies in this study in order to analyse intra-patient heterogeneity: (i) genetic barcoding to determine if an outgrown leukaemia originated from one single cell, which is not feasible using RGB marking and (ii) RGB marking to facilitate functional *in vivo* analyses, which is challenging using genetic barcoding. To my knowledge, this is the first study combining these two approaches within an PDX AML model.

Using genetic barcoding and RGB marking I successfully generated fluorochrome marked PDX AML SCCs in order to resolve and decipher the clonal heterogeneity present in AML. Generated PDX AML SCCs represented genetically distinct subclones of the patient (see chapter 4.3), which displayed functional differences regarding *in vivo* growth and drug response (see chapter 4.4). Even though not all AML subclones of the patient sample, which were identified by panel sequencing of 68 recurrently mutated genes (see chapter 4.1), were represented by the PDX AML SCCs, with this approach it is still feasible to unravel the clonal architecture of an individual leukaemia and to extricate and study the most adverse subclone(s) from the clonal mixture. Yet, every model underestimates the intra-patient clonal complexity. To my knowledge de Boer et al. (2018) have been the only other group to resolve AML heterogeneity by isolating individual subclones. They used individual expression of plasma membrane proteins to sort AML subclones in order to characterise them genetically and functionally (de Boer et al., 2018). Surface protein expression correlated not only to genetically diverse subclones, but was also associated to specific regulatory phenotypes and functional characteristics regarding growth behaviour, stemness, engraftment and therapy response (de Boer et al., 2018). In comparison to the generation of PDX AML SCCs this technique has one main advantages: patients' primary material is used directly without requiring established AML xenografts. However, more than one subclone might upregulate a specific plasma membrane protein impeding isolation of individual subclones. Additionally, primary patients' material is limited restricting functional *in vivo* and *in vitro* analyses. In contrast, since every PDX AML SCC generated in this study originated from one individual stem cell, they certainly and reliably represent individual subclones. Furthermore, PDX AML SCCs can be expanded *in vivo* enabling virtually limitless functional studies. Therefore, both methods, isolation of subclones by plasma membrane protein expression and generation of PDX AML SCCs, present novel and suitable

resources to study intra-tumour heterogeneity and to identify the most challenging subclone(s), and, thus, complement each other.

In order to characterise functional differences between the generated PDX AML SCCs, competitive *in vivo* transplantation assays were applied (see chapter 4.4). First, this reduces mouse numbers extensively since mixes of PDX AML SCCs are injected into animals. Second, mouse-to-mouse variations can be avoided. In fact, several groups have employed competitive approaches to study tumour heterogeneity and clonality, either by transplanting BC or RGB marked heterogeneous cancer populations into animals (van der Heijden et al., 2019; Gambera et al., 2018; Belderbos et al., 2017; Elder et al., 2017; Cornils et al., 2017) or by mixing of RGB fluorochrome marked subpopulations (Maetzig et al., 2017; Finkenzeller, 2016). On the one hand, the latter technique has the advantage of defined colour combinations for every clone enabling enhanced discrimination of subpopulations. On the other hand, this method is limited to defined, e.g. monoclonal, cell populations as single clones cannot without doubt be discriminated by colour marking. Competitive *in vitro* and *in vivo* assays with clones marked with defined fluorochrome combinations, as was also performed in this study, have revealed not only outgrowth of subclones, but also differences in drug sensitivity (Maetzig et al., 2017; Finkenzeller, 2016). In this study competitive *in vivo* transplantation assays have been successfully applied to compare homing frequency, growth behaviour and treatment response. As a matter of fact, I observed differences in growth rates of PDX AML SCCs whereas all PDX AML SCCs were capable of successfully homing to the murine BM (see chapter 4.4). Additionally, differences in sensitivity to the anti-proliferative agent Ara-C, a chemotherapeutic drug commonly used for the treatment of AML patients, were discovered (see chapter 4.4). In a similar approach to the one used in this study Finkenzeller (2016) showed functional differences regarding *in vivo* growth as well as drug sensitivity in competitive *in vivo* assays of ALL subclones isolated by RGB marking of bulk PDX ALL cells.

Next, heterogeneity concerning dormancy was analysed. To this end, competitive transplantation assays were combined with carboxyfluorescein succinimidyl ester (CFSE) staining as previously described (Ebinger et al., 2020, 2016). To my knowledge, this is the first time that CFSE staining was performed in a competitive *in vivo* assay. Reduction of the CFSE dye as well as the ratio of label-retaining cells (LRC) was analysed in three PDX AML SCCs and could be correlated to the calculated leukaemic burden of the respective PDX AML SCCs. Since CFSE is used to detect proliferation (Quah and Parish, 2010; Lyons, 2000), the first observation was to be expected. However, quiescent cells, e.g. defined as LRC, have been associated

with chemotherapy resistance in AL (Ebinger et al., 2020; Thomas and Majeti, 2017; Pollyea and Jordan, 2017; Ebinger et al., 2016). Thus, one would expect an Ara-C resistant subclone to be enriched in low-cycling LRC, which could not be observed in this work. Therefore, other mechanisms of drug resistance must be responsible for the chemoresistance observed. Possible explanations include genetic alterations associated with chemotherapy resistance, e.g. *TP53* or *RUNX1* mutation, or *FLT3-ITD* (Döhner et al., 2015; Konig and Levis, 2015; Renneville et al., 2008; Wattel et al., 1994). Moreover, loss-of-function or decreased expression of epigenetic regulators like EZH2 and KDM6A have been associated to resistance to cytotoxic drugs and tyrosine kinase inhibitors as well as reduced overall survival (Stief et al., 2019; Greif et al., 2018; Göllner et al., 2017).

Taken together, genetic barcoding was combined with RGB marking in order to generate fluorochrome marked PDX AML SCCs. These PDX AML SCCs were then analysed genetically and functionally in competitive *in vivo* assays in order to better understand the clonal heterogeneity of AML.

5.3. Genetic, Epigenetic and Transcriptomic Characterisation of PDX AML Single Cell Clones Revealed Four Distinct AML Subclones

As a first step, the twelve generated PDX AML SCCs were characterised genetically, epigenetically and transcriptomically.

Targeted Sanger sequencing as well as exome sequencing revealed the presence of four genetically distinct leukaemic subpopulations represented by the PDX AML SCCs, which can be defined by the following mutations, which are used as ”molecular markers” for the distinction of individual AML subclones: $KRAS^{G12A}$ (4/12), $NRAS^{Q61K}$ (4/12), $EZH2^{A692G}$ (2/12) and $EZH2^{A692G}$ $NRAS^{Q61K}$ (2/12) (see chapter 4.3). RAS GTPases are known protooncogenes involved in proliferation, differentiation, cell survival and apoptosis and associated with diverse types of cancer such as pancreatic adenocarcinoma and colon cancer (Drosten and Barbacid, 2020; Jakob et al., 2012; Renneville et al., 2008; Minamoto et al., 2000; Bos, 1989). Mutations in *KRAS* or *NRAS* have been observed in 12% of AML patients at time of initial diagnosis and commonly affect codons 12, 13 or 61 resulting in constitutive activation of the GTPase and its downstream pathways (The Cancer Genome Atlas Research Network, 2013; Renneville et al., 2008). In fact, the *KRAS* and *NRAS* mutations seen in the AML sample pair mainly used for this study, PDX AML-491 and AML-661, affect codon 12 and 61, respectively, leading to an

amino acid change from glycine to alanine (G12A) and glutamine to lysine (Q61K), respectively. Even though *RAS* mutations are drivers in many types of solid cancers (Jakob et al., 2012; Renneville et al., 2008; Minamoto et al., 2000; Bos, 1989), they could not be correlated to AML patients' treatment response or outcome (Yang et al., 2013; Renneville et al., 2008; Bowen et al., 2005). *EZH2*, the subclonal mutation detected in PDX AML-661, encodes an epigenetic regulator, in particular, a histone H3K27 methyltransferase (Sashida and Iwama, 2017). Both tumour suppressor gene and oncogenic mutations of *EZH2* have been described in haematopoietic malignancies and are often accompanied by complete or partial deletion of chromosome 7 (Basheer et al., 2019; Skoda and Schwaller, 2019; Sashida and Iwama, 2017; Wang et al., 2013; Morin et al., 2010; Abdel-Wahab and Levine, 2010); this deletion was also observed in exome sequencing of PDX AML-491 and AML-661 SCCs (see chapter 4.3). Mutations in *EZH2* have been seen in 1.5% of AML patients at time of initial diagnosis, whereas loss of chromosome 7 or del(7q) have been described for 10% of AML cases (The Cancer Genome Atlas Research Network, 2013). Epigenetic regulation by *EZH2* has been observed to influence self-renewal and cell differentiation (Lund et al., 2014). Loss-of-function of this epigenetic regulator has been associated with increased drug resistance and, thus, adverse prognosis of patients with myeloid malignancies (Kikuchi et al., 2018; Göllner et al., 2017; Sashida and Iwama, 2017; Sashida et al., 2014). In this study $KRAS^{G12A}$, $NRAS^{Q61K}$ and $EZH2^{A692G}$ mutations are used as "molecular markers" rather than mutations responsible for an observed functional phenotype.

Next, PDX AML SCCs were analysed epigenetically. Analysis of DNA methylation showed clustering of PDX AML SCCs according to the genetic mutations detected with the largest difference between PDX AML SCCs with or without $EZH2^{A692G}$ mutation (see chapter 4.3). Since the $EZH2^{A692G}$ mutation arose in the patient during disease progression from first to second relapse, subsequently, it is only present in PDX AML-661 SCCs. This indicates that the biggest difference seen in DNA methylation occurred due to evolution in the patient's AML between first and second relapse. Indeed, it has been demonstrated that epigenetic variety increases during disease progression in leukaemia implying an increased evolutionary fitness of the cancer (de Boer et al., 2018; Caiado et al., 2016; Li et al., 2016b; Corces et al., 2016; Li et al., 2014; Landau et al., 2014). Additionally, Figueroa et al. (2010) have demonstrated that DNA methylation patterns can be used to cluster patients into AML subtypes. Since clustering of patients' individual leukaemias according to DNA methylation can be performed, this could also be done for subclones within a patient's AML as was observed in this study. To my knowl-

edge, the present study is first in showing clustering of AML subclones on DNA methylation level. Furthermore, epigenetic intra-patient heterogeneity has been associated with inferior outcome in AML (Caiado et al., 2016; Li et al., 2016a,b; Corces-Zimmerman et al., 2014a). Indeed, PDX AML-661 bulk cells have shown a more adverse phenotype compared to PDX AML-491 bulk cells which might partly be accounted to epigenetic variation. In particular, PDX AML-661 demonstrated increased homing capacity, faster passaging time, a higher stem cell frequency and resistance towards treatment with the chemotherapeutic drug Ara-C (see chapter 4.4). In general, the importance of epigenetic alterations in AML has been acknowledged in the last years leading to the approval of epigenetic drugs, such as hypomethylating agents (HMAs) for the treatment of AML, which has shown promising effects, especially in elderly patients with low blast count (20% - 30%) (Estey, 2018; Döhner et al., 2017; Schoofs and Müller-Tidow, 2011).

Last, transcriptomic differences were analysed between PDX AML SCCs. Similar to DNA methylation analysis clustering of PDX AML SCCs according to the genetic mutations could be observed, again with the largest difference represented by the $EZH2^{A692}$ mutation (see chapter 4.3), which arose in the patient during disease progression from first to second relapse. In fact, major changes in gene expression, both up- and down-regulation, have been observed during disease progression in AML patients from diagnosis to relapse possibly explaining the differences between PDX AML-491 and AML-661 SCCs (Bachas et al., 2015; Van den Heuvel-Eibrink et al., 2002). Distinct gene expression signatures could even be associated to worse prognosis of both adult and paediatric AML patients (Herold et al., 2018; Yagi et al., 2003), Furthermore, gene expression signatures have also been used to group patients into AML subtypes and even to identify new subtypes (Lavallée et al., 2016; Jongen-Lavrencic et al., 2008). Similarly, PDX AML SCCs clustered according to their genetic subclone enabling identification of leukaemic subpopulations through transcriptome profiling. Indeed, de Boer et al. (2018) presented distinct gene expression patterns for isolated AML subclones in bulk RNA sequencing. Furthermore, first attempts have been made to combine single-cell RNA sequencing with genotyping in order to distinuish AML cells from healthy BM cells and to demonstrate variability in gene expression between AML subclones status (van Galen et al., 2019; Petti et al., 2019).

Taken together, the twelve generated PDX AML SCCs represent four genetically distinct subclones, which could also be discriminated in DNA methylation and transcriptome analyses.

5.4. Functional Characterisation of PDX AML Single Cell Clones Uncovered Major Intra-Patient Heterogeneity in Stem Cell Frequency, Growth Behaviour and Therapy Response and Could Be Correlated to Genetic and Transcriptomic Alterations

In this study, we aimed at characterising the generated PDX AML SCCs not only on genetic, epigenetic and transcriptomic level but also functionally in order to ultimately link these types of analyses to define the most adverse subclone.

The first functional phenomenon observed in the present work was a clear overrepresentation of $NRAS^{Q61K}$ PDX AML SCCs; while this mutation was only present in a small percentage of bulk PDX AML-491 and AML-661 cells, 50% of PDX AML SCCs carried the mutation (see chapter 4.3). This increased capability of $NRAS^{Q61K}$ AML cells to generate PDX AML SCCs in comparison to $NRAS^{wt}$ AML cells could be correlated to an increased stem cell frequency, exemplary observed in one $NRAS^{Q61K}$ PDX AML SCC compared to one $KRAS^{G12A}$ PDX AML SCC (see chapter 4.4). Variability of engraftment capacity between leukaemic subclones into immunocompromised mice has been described previously and has been associated to heterogeneity in the stem cell frequency (Sandén et al., 2020; de Boer et al., 2018; Shlush et al., 2017; Caiado et al., 2016; Townsend et al., 2016; Klco et al., 2014; Kreso and Dick, 2014). $NRAS^{G12V}$ mutation, another common activating *RAS* mutation (Renneville et al., 2008), in particular, has been described to have a high self-renewal capability, which is commonly associated with leukaemic stem cells (LSCs), in the context of murine KMT2A-AF9 rearranged AML (Sachs et al., 2020, 2014). However, a high self-renewal capability has been associated to reduced proliferation, both for murine KMT2A-AF9 rearranged AML as well as human preleukaemic haematopoietic stem cells (HSCs) and LSCs (Sachs et al., 2020; Lechman et al., 2016; Essers et al., 2009; Foudi et al., 2009). Furthermore, Li et al. (2013a) have described a bimodal effect of the $NRAS^{G12D}$ mutation in HSCs regarding division with an increased proliferation frequency in some but a reduced division potential in other HSCs leading to a high proliferation rate as well as self-renewal capacity upon serial transplantation. This bi-modal effect could explain not only why $NRAS^{Q61K}$ PDX AML cells generated more PDX AML SCCs than $NRAS^{wt}$ PDX AML cells but also why $NRAS^{Q61K}$ cells are not lost during passaging of bulk PDX AML cells but outlast at subclonal level (see chapter 4.1).

Next, functional competitive *in vivo* analyses were performed. Successful homing of all PDX AML SCCs was observed (chapter 4.4), while differences concerning growth behaviour and

therapy response rates could be determined in this study. Interestingly, genetically distinct PDX AML SCCs, derived from PDX AML-491, which were either *KRAS*^{G12A} or *NRAS*^{Q61K} mutant, did not display major differences in growth rates or drug response towards Ara-C, indicating that the variability observed on genetic, epigenetic and transcriptomic levels did not influence these functional characteristics (chapter 4.4). However, *EZH2*^{A692G} PDX AML SCCs, derived from PDX AML-661, revealed fast growth and increased resistance towards treatment with Ara-C compared to all other PDX AML SCCs, determining this subclone as the most challenging clone of this individual AML patient (see chapter 4.4). Of note, *EZH2*^{A692G} *NRAS*^{Q61K} PDX AML SCCs, derived from PDX AML-661 as well, were functionally similar to *KRAS*^{G12A} and *NRAS*^{Q61K} PDX AML SCCs, even though marked differences could be observed on genetic, epigenetic and transcriptomic level. Thus, it can be assumed that the *EZH2*^{A692G} mutation is not causative for the observed Ara-C resistance, even though loss-of-function of EZH2 has been correlated to drug resistance (Kikuchi et al., 2018; Göllner et al., 2017; Sashida and Iwama, 2017; Sashida et al., 2014). Interestingly, exome sequencing uncovered a deletion of the q-arm of chromosome 17 (del(17q)) exclusively in the PDX AML SCCs carrying the *EZH2*^{A692G} mutation without *NRAS*^{Q61K} mutation. Even though del(17q) has been described for several types of cancers including colon, breast and ovarian cancer (Kawai et al., 2016; Radford et al., 1995; Cropp et al., 1993; Saito et al., 1993), little is known about its effect in AML. Van Limbergen et al. (2002) have observed del(17q) losses in 8% of MDS and AML patients with complex chromosomal aberrations in a purely descriptive study. However, studies are lacking about the effect of this particular deletion on leukaemia progression, treatment sensitivity or development of relapse. In this study, the partial deletion of chromosome 17 could be associated to an enrichment in HOX signalling, epigenetic regulation, oxidative stress induced senescence, transcription and translation (see chapter 4.3). In fact, deregulated HOX gene expression has been demonstrated in the majority of AML cases and HOX overexpression has been correlated to unfavourable prognosis (Alharbi et al., 2017; Andreeff et al., 2008; Argiropoulos and Humphries, 2007; Abramovich et al., 2005). Furthermore, epigenetic deregulation has been described as a major event in leukaemogenesis (Abdel-Wahab et al., 2011; Melnick, 2010; Oki and Issa, 2009). On the one hand, epigenetic regulators such as *DNMT3A*, *IDH1/2* and *TET2* are frequently mutated in AML (The Cancer Genome Atlas Research Network, 2013; Abdel-Wahab et al., 2011). On the other hand, dysregulation of DNA methylation and epigenetic intra-patient heterogeneity have been correlated to adverse prognosis of AML patients (Caiado et al., 2016; Li et al., 2016a,b; Corces-Zimmerman et al., 2014a; Melnick, 2010). Additionally,

LSCs were described to have excessive reactive oxygen species production and to evade cellular senescence by suppressing p38 MAPK signalling (Ye et al., 2015; Hole et al., 2013; Xiao et al., 2012; Zhou et al., 2010). Last, deregulation of transcriptome and proteome has been described as a major factor driving AML and can be used to classify AML patients according to their prognosis (Herold et al., 2018; Luczak et al., 2012; Greif et al., 2011; Balkhi et al., 2006). Furthermore, transcriptomic analyses have revealed enrichment of hallmarks such as apoptosis, P53 pathway and IL6-JAK-STAT3 signalling in Ara-C sensitive *EZH2*^{A692G} *NRAS*^{Q61K} PDX AML SCCs compared to Ara-C resistant *EZH2*^{A692G} SCCs. Indeed, induction of apoptosis has been shown to synergise with response towards Ara-C treatment in AML cells (Chromik et al., 2014), possibly explaining the sensitivity of *EZH2*^{A692G} *NRAS*^{Q61K} PDX AML SCCs towards treatment with Ara-C. Similarly, mutations in the tumour suppressor gene *TP53* are associated with Ara-C resistance and apoptosis and, thus, patients carrying such mutations are categorised as adverse (Döhner et al., 2017, 2015; Estey, 2014; Avramis et al., 1998; Wattel et al., 1994). In contrast, functional P53 and its downstream effectors may increase sensitivity towards treatment (McCubrey et al., 2007; Avramis et al., 1998). Moreover, increased STAT3 phosphorylation resulting from IL6 stimulation has been associated to induction of apoptosis and superior outcome of AML patients (Cao et al., 2015; Redell et al., 2013), providing a possible explanation for the Ara-C sensitivity of *EZH2*^{A692G} *NRAS*^{Q61K} PDX AML SCCs compared to *EZH2*^{A692G} SCCs. In summary, the partial deletion of chromosome 17 and the enriched pathways affected by this chromosomal loss might explain the adversity observed in *EZH2*^{A692G} PDX AML SCCs.

Last but not least, a partial response of the Ara-C resistant *EZH2*^{A692G} PDX AML SCCs towards the hypomethylating agent (HMA) 5-azacitidine (Aza) was observed in this study, which was comparable to the response rate of the Ara-C sensitive *EZH2*^{A692G} *NRAS*^{Q61K} PDX AML SCCs (see chapter 4.4). Aza is incorporated into RNA and, to a lower extend, into DNA during replication. On RNA level this leads to an inhibition of protein production (Stresemann and Lyko, 2008). Furthermore, Aza inhibits DNA methyltransferases, leading to hypomethylation of DNA and, thus, activation of suppressed genes such as tumour suppressor genes (Stresemann and Lyko, 2008; Jones et al., 1983). Aza and decitabine, another HMA with higher prevalence of DNA incorporation, have both been applied for the treatment of AML patients, especially of patients at older age, both alone and in combination with other drugs, e.g. cytarabine, showing similar or even improved outcomes to Ara-C treatment with reduced toxicity (Müller-Tidow et al., 2016; Dombret et al., 2015; Radujkovic et al., 2014; Kantarjian et al., 2012; Thomas

et al., 2011). Combination of Ara-C and Aza might have synergistic effects in the PDX AML model, eliminating also PDX AML SCCs resistant towards single drugs; however, this could not be adressed since combination of Ara-C and Aza was highly toxic in the immunocompromised mice.

In summary, I generated genetically diverse subclones from one individual patient's AML and discovered functional differences regarding stemness, proliferation and chemotherapy response. One adverse subclone was identified, characterised by fast growth and Ara-C resistance. This adverse subclone harboured a loss-of-function mutation in *EZH2* and partial deletion of chromosome 17 resulting in the deregulation of several cellular pathways invovled in leukaemogeneis and affecting prognosis in AML patients.

6. Conclusion and Outlook

Taken together, the PDX AML model does not only allow studying inter-patient but also intra-patient heterogeneity with its broad spectrum of genetically and functionally diverse samples.

Adopting genetic barcoding as well as RGB marking enabled the generation of PDX AML SCCs, which represented the heterogeneity observed in this AML patient. Generation of PDX AML SCCs has enabled not only functional characterisation of AML subclones but also description of genetic, epigenetic and transcriptomic changes. Thus, the generation of PDX AML SCCs presents a novel tool to correlate functional adversity, e.g. regarding growth behaviour or chemotherapy resistance, to the underlying responsible alterations and mechanisms.

In order to identify and characterise the molecular mechanism responsible for the drug resistance observed in one AML subclone genetic, transcriptomic and even proteomic changes need to be validated. With a CRISPR/Cas9 or shRNA library screen it would be possible to determine the alterations responsible for chemotherapy resistance. Furthermore, hits could be compared to patient data in the hope of correlating the adverse PDX AML SCCs to poor prognosis of patients. This might lead to the discovery of new therapeutic targets and, thus, might even improve treatment options for AML patients.

Bibliography

Abdel-Wahab, O. and Levine, R. L. (2010), 'Ezh2 mutations: mutating the epigenetic machinery in myeloid malignancies', *Cancer Cell* **18**(2), 105–107.

Abdel-Wahab, O., Patel, J. and Levine, R. L. (2011), 'Clinical implications of novel mutations in epigenetic modifiers in aml', *Hematology/Oncology Clinics* **25**(6), 1119–1133.

Abramovich, C., Pineault, N., Ohta, H. and Humphries, R. K. (2005), 'Hox genes: from leukemia to hematopoietic stem cell expansion', *ANNALS-NEW YORK ACADEMY OF SCIENCES* **1044**, 109.

Abramowski, P., Kraus, O., Rohn, S., Riecken, K., Fehse, B. and Schlueter, H. (2015), 'Combined application of rgb marking and mass spectrometric imaging facilitates detection of tumor heterogeneity', *Cancer Genomics-Proteomics* **12**(4), 179–187.

Adair, J. E., Enstrom, M. R., Haworth, K. G., Schefter, L. E., Shahbazi, R., Humphrys, D. R., Porter, S., Tam, K., Porteus, M. H. and Kiem, H.-P. (2020), 'Dna barcoding in nonhuman primates reveals important limitations in retrovirus integration site analysis', *Molecular Therapy-Methods & Clinical Development* .

Alharbi, R. A., Pandha, H. S., Simpson, G. R., Pettengell, R., Poterlowicz, K., Thompson, A., Harrington, K., El-Tanani, M. and Morgan, R. (2017), 'Inhibition of hox/pbx dimer formation leads to necroptosis in acute myeloid leukemia cells', *Oncotarget* **8**(52), 89566.

American Cancer Society (2020), 'Cancer facts & figures 2020', *Atlanta: American Cancer Society* .

Anderson, K., Lutz, C., Van Delft, F. W., Bateman, C. M., Guo, Y., Colman, S. M., Kempski, H., Moorman, A. V., Titley, I., Swansbury, J. et al. (2011), 'Genetic variegation of clonal architecture and propagating cells in leukaemia', *Nature* **469**(7330), 356.

Andreeff, M., Ruvolo, V., Gadgil, S., Zeng, C., Coombes, K., Chen, W., Kornblau, S., Baron, A. and Drabkin, H. (2008), 'Hox expression patterns identify a common signature for favorable aml', *Leukemia* **22**(11), 2041–2047.

Angelino, G., De Pasquale, M. D., De Sio, L., Serra, A., Massimi, L., De Vito, R., Marrazzo, A., Lancella, L., Carai, A., Antonelli, M. et al. (2016), 'Nras q61k mutated primary leptomeningeal melanoma in a child: case presentation and discussion on clinical and diagnostic implications', *BMC cancer* **16**(1), 512.

Arber, D. A., Orazi, A., Hasserjian, R., Thiele, J., Borowitz, M. J., Le Beau, M. M., Bloomfield, C. D., Cazzola, M. and Vardiman, J. W. (2016), 'The 2016 revision to the world health organization classification of myeloid neoplasms and acute leukemia', *Blood* **127**(20), 2391–2405.

Argiropoulos, B. and Humphries, R. (2007), 'Hox genes in hematopoiesis and leukemogenesis', *Oncogene* **26**(47), 6766–6776.

Avramis, V., Nandy, P., Kwock, R., Solorzano, M., Mukherjee, S., Danenberg, P. and Cohen, L. (1998), 'Increased p21/waf-1 and p53 protein levels following sequential three drug combination regimen of fludarabine, cytarabine and docetaxel induces apoptosis in human leukemia cells.', *Anticancer research* **18**(4A), 2327–2338.

Bachas, C., Schuurhuis, G. J., Zwaan, C. M., van den Heuvel-Eibrink, M. M., den Boer, M. L., de Bont, E. S., Kwidama, Z. J., Reinhardt, D., Creutzig, U., de Haas, V. et al. (2015), 'Gene expression profiles associated with pediatric relapsed aml', *PloS one* **10**(4).

Balkhi, M., Trivedi, A., Geletu, M., Christopeit, M., Bohlander, S., Behre, H. and Behre, G. (2006), 'Proteomics of acute myeloid leukaemia: cytogenetic risk groups differ specifically in their proteome, interactome and post-translational protein modifications', *Oncogene* **25**(53), 7041–7058.

Baron, J. and Wang, E. S. (2018), 'Gemtuzumab ozogamicin for the treatment of acute myeloid leukemia', *Expert review of clinical pharmacology* **11**(6), 549–559.

Barrett, D. M., Seif, A. E., Carpenito, C., Teachey, D. T., Fish, J. D., June, C. H., Grupp, S. A. and Reid, G. S. (2011), 'Non-invasive bioluminescent imaging of primary patient acute lymphoblastic leukemia: a strategy for pre-clinical modeling', *Blood* **118**(15), e112–e117.

Basheer, F., Giotopoulos, G., Meduri, E., Yun, H., Mazan, M., Sasca, D., Gallipoli, P., Marando, L., Gozdecka, M., Asby, R. et al. (2019), 'Contrasting requirements during disease evolution identify ezh2 as a therapeutic target in aml', *Journal of Experimental Medicine* **216**(4), 966–981.

Beckman Coulter, Inc. (2020), 'Agencourt ampure xp - pcr purification'.
URL: *https://www.beckman.com/techdocs/B37419AB/wsr-150180*

Belderbos, M. E., Koster, T., Ausema, B., Jacobs, S., Sowdagar, S., Zwart, E., de Bont, E., de Haan, G. and Bystrykh, L. V. (2017), 'Clonal selection and asymmetric distribution of human leukemia in murine xenografts revealed by cellular barcoding', *Blood* **129**(24), 3210–3220.

Ben-David, U., Beroukhim, R. and Golub, T. R. (2019), 'Genomic evolution of cancer models: perils and opportunities', *Nature Reviews Cancer* **19**(2), 97–109.

Ben-David, U., Siranosian, B., Ha, G., Tang, H., Oren, Y., Hinohara, K., Strathdee, C. A., Dempster, J., Lyons, N. J., Burns, R. et al. (2018), 'Genetic and transcriptional evolution alters cancer cell line drug response', *Nature* **560**(7718), 325.

Bhatia, M., Wang, J. C., Kapp, U., Bonnet, D. and Dick, J. E. (1997), 'Purification of primitive human hematopoietic cells capable of repopulating immune-deficient mice', *Proceedings of the national academy of Sciences* **94**(10), 5320–5325.

Bomken, S., Buechler, L., Rehe, K., Ponthan, F., Elder, A., Blair, H., Bacon, C., Vormoor, J. and Heidenreich, O. (2013), 'Lentiviral marking of patient-derived acute lymphoblastic leukaemic cells allows in vivo tracking of disease progression', *Leukemia* **27**(3), 718.

Bonnet, D. (2008), 'In vivo evaluation of leukemic stem cells through the xenotransplantation model', *Current protocols in stem cell biology* **7**(1), 3–2.

Bos, J. L. (1989), 'Ras oncogenes in human cancer: a review', *Cancer research* **49**(17), 4682–4689.

Bowen, D. T., Frew, M. E., Hills, R., Gale, R. E., Wheatley, K., Groves, M. J., Langabeer, S. E., Kottaridis, P. D., Moorman, A. V., Burnett, A. K. et al. (2005), 'Ras mutation in acute myeloid leukemia is associated with distinct cytogenetic subgroups but does not influence outcome in patients younger than 60 years', *Blood* **106**(6), 2113–2119.

Boyd, A. L., Aslostovar, L., Reid, J., Ye, W., Tanasijevic, B., Porras, D. P., Shapovalova, Z., Almakadi, M., Foley, R., Leber, B. et al. (2018), 'Identification of chemotherapy-induced leukemic-regenerating cells reveals a transient vulnerability of human aml recurrence', *Cancer Cell* **34**(3), 483–498.

Boyerinas, B., Zafrir, M., Yesilkanal, A. E., Price, T. T., Hyjek, E. M. and Sipkins, D. A. (2013), 'Adhesion to osteopontin in the bone marrow niche regulates lymphoblastic leukemia cell dormancy', *Blood, The Journal of the American Society of Hematology* **121**(24), 4821–4831.

Bramlett, C., Jiang, D., Nogalska, A., Eerdeng, J., Contreras, J. and Lu, R. (2020), 'Clonal tracking using embedded viral barcoding and high-throughput sequencing', *Nature Protocols* **15**(4), 1436–1458.

Brenner, A. K., Aasebø, E., Hernandez-Valladares, M., Selheim, F., Berven, F., Grønningsæter, I.-S., Bartaula-Brevik, S. and Bruserud, Ø. (2019), 'The capacity of long-term in vitro proliferation of acute myeloid leukemia cells supported only by exogenous cytokines is associated with a patient subset with adverse outcome', *Cancers* **11**(1), 73.

Brugman, M. H., Wiekmeijer, A.-S., van Eggermond, M., Wolvers-Tettero, I., Langerak, A. W., de Haas, E. F., Bystrykh, L. V., van Rood, J. J., de Haan, G., Fibbe, W. E. et al. (2015), 'Development of a diverse human t-cell repertoire despite stringent restriction of hematopoietic clonality in the thymus', *Proceedings of the National Academy of Sciences* **112**(44), E6020–E6027.

Buccisano, F., Maurillo, L., Gattei, V., Del Poeta, G., Del Principe, M., Cox, M., Panetta, P., Consalvo, M. I., Mazzone, C., Neri, B. et al. (2006), 'The kinetics of reduction of minimal residual disease impacts on duration of response and survival of patients with acute myeloid leukemia', *Leukemia* **20**(10), 1783.

Buckley, S., Appelbaum, F. and Walter, R. (2013), 'Prognostic and therapeutic implications of minimal residual disease at the time of transplantation in acute leukemia', *Bone marrow transplantation* **48**(5), 630.

Burrell, R. A. and Swanton, C. (2014), 'Tumour heterogeneity and the evolution of polyclonal drug resistance', *Molecular oncology* **8**(6), 1095–1111.

Busque, L., Buscarlet, M., Mollica, L. and Levine, R. L. (2018), 'Concise review: Age-related clonal hematopoiesis: Stem cells tempting the devil', *Stem Cells* **36**(9), 1287–1294.

Bystrykh, L. V. and Belderbos, M. E. (2016), Clonal analysis of cells with cellular barcoding: when numbers and sizes matter, *in* 'Stem Cell Heterogeneity', Springer, pp. 57–89.

Bystrykh, L. V., de Haan, G. and Verovskaya, E. (2014), Barcoded vector libraries and retroviral or lentiviral barcoding of hematopoietic stem cells, *in* 'Hematopoietic Stem Cell Protocols', Springer, pp. 345–360.

Caiado, F., Silva-Santos, B. and Norell, H. (2016), 'Intra-tumour heterogeneity–going beyond genetics', *The FEBS journal* **283**(12), 2245–2258.

Cancer Research UK (2020), 'Leukaemia (all subtypes combined) incidence statistics'.
URL: *https://www.cancerresearchuk.org/health-professional/cancer-statistics/statistics-by-cancer-type/leukaemia/incidence*

Cao, W., Liu, Y., Zhang, R., Zhang, B., Wang, T., Zhu, X., Mei, L., Chen, H., Zhang, H., Ming, P. et al. (2015), 'Homoharringtonine induces apoptosis and inhibits stat3 via il-6/jak1/stat3 signal pathway in gefitinib-resistant lung cancer cells', *Scientific reports* **5**, 8477.

Castaigne, S., Pautas, C., Terré, C., Raffoux, E., Bordessoule, D., Bastie, J.-N., Legrand, O., Thomas, X., Turlure, P., Reman, O. et al. (2012), 'Effect of gemtuzumab ozogamicin on survival of adult patients with de-novo acute myeloid leukaemia (alfa-0701): a randomised, open-label, phase 3 study', *The Lancet* **379**(9825), 1508–1516.

Cesano, A., Hoxie, J., Lange, B., Nowell, P., Bishop, J. and Santoli, D. (1992), 'The severe combined immunodeficient (scid) mouse as a model for human myeloid leukemias.', *Oncogene* **7**(5), 827–836.

Chaudry, S. F. and Chevassut, T. J. (2017), 'Epigenetic guardian: a review of the dna methyltransferase dnmt3a in acute myeloid leukaemia and clonal haematopoiesis', *BioMed research international* **2017**.

Chen, B.-F. and Chan, W.-Y. (2014), 'The de novo dna methyltransferase dnmt3a in development and cancer', *Epigenetics* **9**(5), 669–677.

Chen, H., Jiang, Y., Maxwell, K. N., Nathanson, K. L. and Zhang, N. (2017), 'Allele-specific copy number estimation by whole exome sequencing', *The annals of applied statistics* **11**(2), 1169.

Chen, J., Kao, Y.-R., Sun, D., Todorova, T. I., Reynolds, D., Narayanagari, S.-R., Montagna, C., Will, B., Verma, A. and Steidl, U. (2019), 'Myelodysplastic syndrome progression to acute myeloid leukemia at the stem cell level', *Nature medicine* **25**(1), 103.

Cheung, A. M., Nguyen, L. V., Carles, A., Beer, P., Miller, P. H., Knapp, D. J., Dhillon, K., Hirst, M. and Eaves, C. J. (2013), 'Analysis of the clonal growth and differentiation dynamics of primitive barcoded human cord blood cells in nsg mice', *Blood* **122**(18), 3129–3137.

Chromik, J., Safferthal, C., Serve, H. and Fulda, S. (2014), 'Smac mimetic primes apoptosis-resistant acute myeloid leukaemia cells for cytarabine-induced cell death by triggering necroptosis', *Cancer letters* **344**(1), 101–109.

Cibulskis, K., Lawrence, M. S., Carter, S. L., Sivachenko, A., Jaffe, D., Sougnez, C., Gabriel, S., Meyerson, M., Lander, E. S. and Getz, G. (2013), 'Sensitive detection of somatic point mutations in impure and heterogeneous cancer samples', *Nature biotechnology* **31**(3), 213.

Clappier, E., Gerby, B., Sigaux, F., Delord, M., Touzri, F., Hernandez, L., Ballerini, P., Baruchel, A., Pflumio, F. and Soulier, J. (2011), 'Clonal selection in xenografted human t cell acute lymphoblastic leukemia recapitulates gain of malignancy at relapse', *Journal of Experimental Medicine* **208**(4), 653–661.

Clevers, H. (2011), 'The cancer stem cell: premises, promises and challenges', *Nature medicine* **17**(3), 313.

ClinicalTrials.gov (2019*a*), 'Car-t cells therapy in relapsed/refractory acute myeloid leukemia (aml)'.
URL: *https://clinicaltrials.gov/ct2/show/NCT03473457*

ClinicalTrials.gov (2019*b*), 'Nivolumab in aml in remission at high risk for relapse'.
URL: *https://clinicaltrials.gov/ct2/show/NCT02532231*

ClinicalTrials.gov (2020), 'A study of the idh1 inhibitor ag-120 in combination with the checkpoint blockade inhibitor, nivolumab, for patients with idh1 mutated relapsed/refractory aml and high risk mds'.
URL: *https://clinicaltrials.gov/ct2/show/NCT04044209*

Corces, M. R., Buenrostro, J. D., Wu, B., Greenside, P. G., Chan, S. M., Koenig, J. L., Snyder, M. P., Pritchard, J. K., Kundaje, A., Greenleaf, W. J. et al. (2016), 'Lineage-specific and single-cell chromatin accessibility charts human hematopoiesis and leukemia evolution', *Nature genetics* **48**(10), 1193.

Corces-Zimmerman, M. R., Hong, W.-J., Weissman, I. L., Medeiros, B. C. and Majeti, R. (2014a), 'Preleukemic mutations in human acute myeloid leukemia affect epigenetic regulators and persist in remission', *Proceedings of the National Academy of Sciences* **111**(7), 2548–2553.

Corces-Zimmerman, M. R. and Majeti, R. (2014b), 'Pre-leukemic evolution of hematopoietic stem cells: the importance of early mutations in leukemogenesis', *Leukemia* **28**(12), 2276–2282.

Cornils, K., Thielecke, L., Hüser, S., Forgber, M., Thomaschewski, M., Kleist, N., Hussein, K., Riecken, K., Volz, T., Gerdes, S. et al. (2014), 'Multiplexing clonality: combining rgb marking and genetic barcoding', *Nucleic acids research* **42**(7), e56–e56.

Cornils, K., Thielecke, L., Winkelmann, D., Aranyossy, T., Lesche, M., Dahl, A., Roeder, I., Fehse, B. and Glauche, I. (2017), 'Clonal competition in bcrabl-driven leukemia: how transplantations can accelerate clonal conversion', *Molecular cancer* **16**(1), 120.

Cropp, C. S., Champeme, M.-H., Lidereau, R. and Callahan, R. (1993), 'Identification of three regions on chromosome 17q in primary human breast carcinomas which are frequently deleted', *Cancer research* **53**(23), 5617–5619.

Dagogo-Jack, I. and Shaw, A. T. (2018), 'Tumour heterogeneity and resistance to cancer therapies', *Nature reviews Clinical oncology* **15**(2), 81.

Daver, N., Basu, S., Garcia-Manero, G., Cortes, J. E., Ravandi, F., Jabbour, E. J., Hendrickson, S., Pierce, S., Ning, J., Konopleva, M. et al. (2016), 'Phase ib/ii study of nivolumab in combination with azacytidine (aza) in patients (pts) with relapsed acute myeloid leukemia (aml)'.

de Boer, B., Prick, J., Pruis, M. G., Keane, P., Imperato, M. R., Jaques, J., Brouwers-Vos, A. Z., Hogeling, S. M., Woolthuis, C. M., Nijk, M. T. et al. (2018), 'Prospective isolation and characterization of genetically and functionally distinct aml subclones', *Cancer cell* **34**(4), 674–689.

de Jonge-Peeters, S. D., Kuipers, F., de Vries, E. G. and Vellenga, E. (2007), 'Abc transporter expression in hematopoietic stem cells and the role in aml drug resistance', *Critical reviews in oncology/hematology* **62**(3), 214–226.

De Kouchkovsky, I. and Abdul-Hay, M. (2016), 'Acute myeloid leukemia: a comprehensive review and 2016 update', *Blood cancer journal* **6**(7), e441.

de Rooij, J. D., van den Heuvel-Eibrink, M. M., Hermkens, M. C., Verboon, L. J., Arentsen-Peters, S. T., Fornerod, M., Baruchel, A., Stary, J., Reinhardt, D., de Haas, V. et al. (2015), 'Bcor and bcorl1 mutations in pediatric acute myeloid leukemia', *haematologica* **100**(5), e194.

Desai, P., Mencia-Trinchant, N., Savenkov, O., Simon, M. S., Cheang, G., Lee, S., Samuel, M., Ritchie, E. K., Guzman, M. L., Ballman, K. V. et al. (2018), 'Somatic mutations precede acute myeloid leukemia years before diagnosis', *Nature medicine* **24**(7), 1015.

DiNardo, C. D., Pratz, K. W., Letai, A., Jonas, B. A., Wei, A. H., Thirman, M., Arellano, M., Frattini, M. G., Kantarjian, H., Popovic, R. et al. (2018), 'Safety and preliminary efficacy of venetoclax with decitabine or azacitidine in elderly patients with previously untreated acute myeloid leukaemia: a non-randomised, open-label, phase 1b study', *The lancet oncology* **19**(2), 216–228.

Ding, L., Ley, T. J., Larson, D. E., Miller, C. A., Koboldt, D. C., Welch, J. S., Ritchey, J. K., Young, M. A., Lamprecht, T., McLellan, M. D. et al. (2012), 'Clonal evolution in relapsed acute myeloid leukaemia revealed by whole-genome sequencing', *Nature* **481**(7382), 506.

Dobin, A., Davis, C. A., Schlesinger, F., Drenkow, J., Zaleski, C., Jha, S., Batut, P., Chaisson, M. and Gingeras, T. R. (2013), 'Star: ultrafast universal rna-seq aligner', *Bioinformatics* **29**(1), 15–21.

Döhner, H., Estey, E., Grimwade, D., Amadori, S., Appelbaum, F. R., Büchner, T., Dombret, H., Ebert, B. L., Fenaux, P., Larson, R. A. et al. (2017), 'Diagnosis and management of aml in adults: 2017 eln recommendations from an international expert panel', *Blood* **129**(4), 424–447.

Döhner, H., Weisdorf, D. J. and Bloomfield, C. D. (2015), 'Acute myeloid leukemia', *New England Journal of Medicine* **373**(12), 1136–1152.

Dombret, H., Seymour, J. F., Butrym, A., Wierzbowska, A., Selleslag, D., Jang, J. H., Kumar, R., Cavenagh, J., Schuh, A. C., Candoni, A. et al. (2015), 'International phase 3 study of azacitidine vs conventional care regimens in older patients with newly diagnosed aml with¿ 30% blasts', *Blood* **126**(3), 291–299.

Drosten, M. and Barbacid, M. (2020), 'Targeting the mapk pathway in kras-driven tumors', *Cancer Cell* **37**(4), 543–550.

Duan, C.-W., Shi, J., Chen, J., Wang, B., Yu, Y.-H., Qin, X., Zhou, X.-C., Cai, Y.-J., Li, Z.-Q., Zhang, F. et al. (2014), 'Leukemia propagating cells rebuild an evolving niche in response to therapy', *Cancer cell* **25**(6), 778–793.

Durinck, S., Moreau, Y., Kasprzyk, A., Davis, S., De Moor, B., Brazma, A. and Huber, W. (2005), 'Biomart and bioconductor: a powerful link between biological databases and microarray data analysis', *Bioinformatics* **21**(16), 3439–3440.

Durinck, S., Spellman, P. T., Birney, E. and Huber, W. (2009), 'Mapping identifiers for the integration of genomic datasets with the r/bioconductor package biomart', *Nature protocols* **4**(8), 1184.

Ebinger, S., Özdemir, E. Z., Ziegenhain, C., Tiedt, S., Alves, C. C., Grunert, M., Dworzak, M., Lutz, C., Turati, V. A., Enver, T. et al. (2016), 'Characterization of rare, dormant, and therapy-resistant cells in acute lymphoblastic leukemia', *Cancer cell* **30**(6), 849–862.

Ebinger, S., Zeller, C., Carlet, M., Senft, D., Bagnoli, J. W., Liu, W.-H., Rothenberg-Thurley, M., Enard, W., Metzeler, K. H., Herold, T. et al. (2020), 'Plasticity in growth behavior of patients' acute myeloid leukemia stem cells growing in mice.', *Haematologica* .

Ediriwickrema, A., Aleshin, A., Reiter, J. G., Corces, M. R., Köhnke, T., Stafford, M., Liedtke, M., Medeiros, B. C. and Majeti, R. (2020), 'Single-cell mutational profiling enhances the clinical evaluation of aml mrd', *Blood Advances* **4**(5), 943–952.

Elder, A., Bomken, S., Wilson, I., Blair, H. J., Cockell, S., Ponthan, F., Dormon, K., Pal, D., Heidenreich, O. and Vormoor, J. (2017), 'Abundant and equipotent founder cells establish and maintain acute lymphoblastic leukaemia', *Leukemia* **31**(12), 2577.

Essers, M. A., Offner, S., Blanco-Bose, W. E., Waibler, Z., Kalinke, U., Duchosal, M. A. and Trumpp, A. (2009), 'Ifnα activates dormant haematopoietic stem cells in vivo', *Nature* **458**(7240), 904–908.

Estey, E. H. (2014), 'Acute myeloid leukemia: 2014 update on risk-stratification and management', *American journal of hematology* **89**(11), 1063–1081.

Estey, E. H. (2018), 'Acute myeloid leukemia: 2019 update on risk-stratification and management', *American journal of hematology* **93**(10), 1267–1291.

Fasterius, E. and Szigyarto, C. A.-K. (2018), 'Analysis of public rna-sequencing data reveals biological consequences of genetic heterogeneity in cell line populations', *Scientific reports* **8**(1), 11226.

Fenaux, P., Mufti, G. J., Hellström-Lindberg, E., Santini, V., Gattermann, N., Germing, U., Sanz, G., List, A. F., Gore, S., Seymour, J. F. et al. (2009), 'Azacitidine prolongs overall survival compared with conventional care regimens in elderly patients with low bone marrow blast count acute myeloid leukemia', *Journal of Clinical Oncology* **28**(4), 562–569.

Feurstein, S. and Godley, L. A. (2017), 'Germline etv6 mutations and predisposition to hematological malignancies', *International journal of hematology* **106**(2), 189–195.

Figueroa, M. E., Lugthart, S., Li, Y., Erpelinck-Verschueren, C., Deng, X., Christos, P. J., Schifano, E., Booth, J., van Putten, W., Skrabanek, L. et al. (2010), 'Dna methylation signatures identify biologically distinct subtypes in acute myeloid leukemia', *Cancer cell* **17**(1), 13–27.

Finkenzeller, C. (2016), Patients' acute lymphoblastic leukemia cells show heterogeneous growth behavior and drug sensitivity in vivo, PhD thesis, lmu.

Fisher, R., Pusztai, L. and Swanton, C. (2013), 'Cancer heterogeneity: implications for targeted therapeutics', *British journal of cancer* **108**(3), 479.

Foudi, A., Hochedlinger, K., Van Buren, D., Schindler, J. W., Jaenisch, R., Carey, V. and Hock, H. (2009), 'Analysis of histone 2b-gfp retention reveals slowly cycling hematopoietic stem cells', *Nature biotechnology* **27**(1), 84.

Galmarini, C., Mackey, J. and Dumontet, C. (2001), 'Nucleoside analogues: mechanisms of drug resistance and reversal strategies', *Leukemia* **15**(6), 875.

Gambera, S., Abarrategi, A., González-Camacho, F., Morales-Molina, Á., Roma, J., Alfranca, A. and García-Castro, J. (2018), 'Clonal dynamics in osteosarcoma defined by rgb marking', *Nature communications* **9**(1), 3994.

Gerlinger, M., Horswell, S., Larkin, J., Rowan, A. J., Salm, M. P., Varela, I., Fisher, R., McGranahan, N., Matthews, N., Santos, C. R. et al. (2014a), 'Genomic architecture and evolution of clear cell renal cell carcinomas defined by multiregion sequencing', *Nature genetics* **46**(3), 225.

Gerlinger, M., McGranahan, N., Dewhurst, S. M., Burrell, R. A., Tomlinson, I. and Swanton, C. (2014b), 'Cancer: evolution within a lifetime', *Annual review of genetics* **48**, 215–236.

Gerlinger, M., Rowan, A. J., Horswell, S., Larkin, J., Endesfelder, D., Gronroos, E., Martinez, P., Matthews, N., Stewart, A., Tarpey, P. et al. (2012), 'Intratumor heterogeneity and branched evolution revealed by multiregion sequencing', *New England journal of medicine* **366**(10), 883–892.

Göllner, S., Oellerich, T., Agrawal-Singh, S., Schenk, T., Klein, H.-U., Rohde, C., Pabst, C., Sauer, T., Lerdrup, M., Tavor, S. et al. (2017), 'Loss of the histone methyltransferase ezh2 induces resistance to multiple drugs in acute myeloid leukemia', *Nature medicine* **23**(1), 69.

Gomez-Nicola, D., Riecken, K., Fehse, B. and Perry, V. H. (2014), 'In-vivo rgb marking and multicolour single-cell tracking in the adult brain', *Scientific reports* **4**, 7520.

Greif, P. A., Hartmann, L., Vosberg, S., Stief, S. M., Mattes, R., Hellmann, I., Metzeler, K. H., Herold, T., Bamopoulos, S. A., Kerbs, P. et al. (2018), 'Evolution of cytogenetically normal acute myeloid leukemia during therapy and relapse: An exome sequencing study of 50 patients', *Clinical Cancer Research* **24**(7), 1716–1726.

Greif, P., Eck, S., Konstandin, N., Benet-Pages, A., Ksienzyk, B., Dufour, A., Vetter, A., Popp, H., Lorenz-Depiereux, B., Meitinger, T. et al. (2011), 'Identification of recurring tumor-specific somatic mutations in acute myeloid leukemia by transcriptome sequencing', *Leukemia* **25**(5), 821–827.

Griessinger, E., Vargaftig, J., Horswell, S., Taussig, D. C., Gribben, J. and Bonnet, D. (2018), 'Acute myeloid leukemia xenograft success prediction: Saving time', *Experimental hematology* **59**, 66–71.

Grove, C. S. and Vassiliou, G. S. (2014), 'Acute myeloid leukaemia: a paradigm for the clonal evolution of cancer?', *Disease models & mechanisms* **7**(8), 941–951.

Habringer, S., Lapa, C., Herhaus, P., Schottelius, M., Istvanffy, R., Steiger, K., Slotta-Huspenina, J., Schirbel, A., Hänscheid, H., Kircher, S. et al. (2018), 'Dual targeting of acute leukemia and supporting niche by cxcr4-directed theranostics', *Theranostics* **8**(2), 369.

Hanahan, D. and Weinberg, R. A. (2011), 'Hallmarks of cancer: the next generation', *cell* **144**(5), 646–674.

Harada, Y. and Harada, H. (2009), 'Molecular pathways mediating mds/aml with focus on aml1/runx1 point mutations', *Journal of cellular physiology* **220**(1), 16–20.

Hausser, J. and Alon, U. (2020), 'Tumour heterogeneity and the evolutionary trade-offs of cancer', *Nature Reviews Cancer* pp. 1–11.

Hawkins, E. D., Hommel, M., Turner, M. L., Battye, F. L., Markham, J. F. and Hodgkin, P. D. (2007), 'Measuring lymphocyte proliferation, survival and differentiation using cfse time-series data', *Nature protocols* **2**(9), 2057.

Hayashi, Y., Harada, Y., Huang, G. and Harada, H. (2017), 'Myeloid neoplasms with germ line runx1 mutation', *International journal of hematology* **106**(2), 183–188.

Herold, T., Jurinovic, V., Batcha, A. M., Bamopoulos, S. A., Rothenberg-Thurley, M., Ksienzyk, B., Hartmann, L., Greif, P. A., Phillippou-Massier, J., Krebs, S. et al. (2018), 'A 29-gene and cytogenetic score for the prediction of resistance to induction treatment in acute myeloid leukemia', *haematologica* **103**(3), 456–465.

Hole, P. S., Zabkiewicz, J., Munje, C., Newton, Z., Pearn, L., White, P., Marquez, N., Hills, R. K., Burnett, A. K., Tonks, A. et al. (2013), 'Overproduction of nox-derived ros in aml promotes proliferation and is associated with defective oxidative stress signaling', *Blood, The Journal of the American Society of Hematology* **122**(19), 3322–3330.

Hope, K. J., Jin, L. and Dick, J. E. (2003), 'Human acute myeloid leukemia stem cells', *Archives of medical research* **34**(6), 507–514.

Hope, K. J., Jin, L. and Dick, J. E. (2004), 'Acute myeloid leukemia originates from a hierarchy of leukemic stem cell classes that differ in self-renewal capacity', *Nature immunology* **5**(7), 738.

Hortobagyi, G. (1997), 'Anthracyclines in the treatment of cancer', *Drugs* **54**(4), 1–7.

Hu, Y. and Smyth, G. K. (2009), 'Elda: extreme limiting dilution analysis for comparing depleted and enriched populations in stem cell and other assays', *Journal of immunological methods* **347**(1-2), 70–78.

Hutter, G., Nickenig, C., Garritsen, H., Hellenkamp, F., Hoerning, A., Hiddemann, W. and Dreyling, M. (2004), 'Use of polymorphisms in the noncoding region of the human mitochondrial genome to identify potential contamination of human leukemia-lymphoma cell lines', *The Hematology Journal* **5**(1), 61–68.

Hyo-eun, C. B., Ruddy, D. A., Radhakrishna, V. K., Caushi, J. X., Zhao, R., Hims, M. M., Singh, A. P., Kao, I., Rakiec, D., Shaw, P. et al. (2015), 'Studying clonal dynamics in response to cancer therapy using high-complexity barcoding', *Nature medicine* **21**(5), 440.

Ishikawa, F., Yoshida, S., Saito, Y., Hijikata, A., Kitamura, H., Tanaka, S., Nakamura, R., Tanaka, T., Tomiyama, H., Saito, N. et al. (2007), 'Chemotherapy-resistant human aml stem cells home to and engraft within the bone-marrow endosteal region', *Nature biotechnology* **25**(11), 1315.

Jacobs, S., Ausema, A., Zwart, E., Weersing, E., Kingma, M. J., El Menshawi, Y. A., de Haan, G., Bystrykh, L. V. and Belderbos, M. E. (2019), 'Quantitative distribution of patient-derived leukemia clones in murine xenografts revealed by cellular barcodes', *Leukemia* pp. 1–5.

Jaiswal, S., Fontanillas, P., Flannick, J., Manning, A., Grauman, P. V., Mar, B. G., Lindsley, R. C., Mermel, C. H., Burtt, N., Chavez, A. et al. (2014), 'Age-related clonal hematopoiesis associated with adverse outcomes', *New England Journal of Medicine* **371**(26), 2488–2498.

Jakob, J. A., Bassett Jr, R. L., Ng, C. S., Curry, J. L., Joseph, R. W., Alvarado, G. C., Rohlfs, M. L., Richard, J., Gershenwald, J. E., Kim, K. B. et al. (2012), 'Nras mutation status is an independent prognostic factor in metastatic melanoma', *Cancer* **118**(16), 4014–4023.

Jan, M. and Majeti, R. (2013), 'Clonal evolution of acute leukemia genomes', *Oncogene* **32**(2), 135.

Jan, M., Snyder, T. M., Corces-Zimmerman, M. R., Vyas, P., Weissman, I. L., Quake, S. R. and Majeti, R. (2012), 'Clonal evolution of preleukemic hematopoietic stem cells precedes human acute myeloid leukemia', *Science translational medicine* **4**(149), 149ra118–149ra118.

Jeong, E. G., Kim, M. S., Nam, H. K., Min, C. K., Lee, S., Chung, Y. J., Yoo, N. J. and Lee, S. H. (2008), 'Somatic mutations of jak1 and jak3 in acute leukemias and solid cancers', *Clinical cancer research* **14**(12), 3716–3721.

Jiang, Y., Wang, R., Urrutia, E., Anastopoulos, I. N., Nathanson, K. L. and Zhang, N. R. (2018), 'Codex2: full-spectrum copy number variation detection by high-throughput dna sequencing', *Genome biology* **19**(1), 202.

Jones, P., Taylor, S. and Wilson, V. (1983), Inhibition of dna methylation by 5-azacytidine, *in* 'Modified nucleosides and cancer', Springer, pp. 202–211.

Jongen-Lavrencic, M., Sun, S. M., Dijkstra, M. K., Valk, P. J. and Löwenberg, B. (2008), 'Microrna expression profiling in relation to the genetic heterogeneity of acute myeloid leukemia', *Blood, The Journal of the American Society of Hematology* **111**(10), 5078–5085.

Kamel-Reid, S., Letarte, M., Sirard, C., Doedens, M., Grunberger, T., Fulop, G., Freedman, M. H., Phillips, R. A. and Dick, J. E. (1989), 'A model of human acute lymphoblastic leukemia in immune-deficient scid mice', *Science* **246**(4937), 1597–1600.

Kantarjian, H. M., Thomas, X. G., Dmoszynska, A., Wierzbowska, A., Mazur, G., Mayer, J., Gau, J.-P., Chou, W.-C., Buckstein, R., Cermak, J. et al. (2012), 'Multicenter, randomized, open-label, phase iii trial of decitabine versus patient choice, with physician advice, of either supportive care or low-dose cytarabine for the treatment of older patients with newly diagnosed acute myeloid leukemia', *Journal of clinical oncology* **30**(21), 2670.

Kawai, M., Komiyama, H., Hosoya, M., Okubo, H., Fujii, T., Yokoyama, N., Sato, C., Ueyama, T., Okuzawa, A., Goto, M. et al. (2016), 'Impact of chromosome 17q deletion in the primary lesion of colorectal cancer on liver metastasis', *Oncology letters* **12**(6), 4773–4778.

Kikuchi, J., Kuroda, Y., Koyama, D. and Furukawa, Y. (2018), 'Cell adhesion-induced phosphorylation and inactivation of ezh2 confer drug resistance to acute myeloid leukemia cells', *International journal of hematology* **107**(3), 383–385.

Kim, K. H. and Roberts, C. W. (2016), 'Targeting ezh2 in cancer', *Nature medicine* **22**(2), 128.

Klco, J. M., Spencer, D. H., Miller, C. A., Griffith, M., Lamprecht, T. L., O'Laughlin, M., Fronick, C., Magrini, V., Demeter, R. T., Fulton, R. S. et al. (2014), 'Functional heterogeneity of genetically defined subclones in acute myeloid leukemia', *Cancer cell* **25**(3), 379–392.

Koboldt, D. C., Zhang, Q., Larson, D. E., Shen, D., McLellan, M. D., Lin, L., Miller, C. A., Mardis, E. R., Ding, L. and Wilson, R. K. (2012), 'Varscan 2: somatic mutation and copy number alteration discovery in cancer by exome sequencing', *Genome research* **22**(3), 568–576.

Konig, H. and Levis, M. (2015), 'Targeting flt3 to treat leukemia', *Expert opinion on therapeutic targets* **19**(1), 37–54.

Kreso, A. and Dick, J. E. (2014), 'Evolution of the cancer stem cell model', *Cell stem cell* **14**(3), 275–291.

Kreso, A., O'Brien, C. A., Van Galen, P., Gan, O. I., Notta, F., Brown, A. M., Ng, K., Ma, J., Wienholds, E., Dunant, C. et al. (2013), 'Variable clonal repopulation dynamics influence chemotherapy response in colorectal cancer', *Science* **339**(6119), 543–548.

Krivtsov, A. V., Figueroa, M. E., Sinha, A. U., Stubbs, M. C., Feng, Z., Valk, P. J., Delwel, R., Döhner, K., Bullinger, L., Kung, A. L. et al. (2013), 'Cell of origin determines clinically relevant subtypes of mll-rearranged aml', *Leukemia* **27**(4), 852.

Krönke, J., Bullinger, L., Teleanu, V., Tschürtz, F., Gaidzik, V. I., Kühn, M. W., Rücker, F. G., Holzmann, K., Paschka, P., Kapp-Schwörer, S. et al. (2013), 'Clonal evolution in relapsed npm1-mutated acute myeloid leukemia', *Blood, The Journal of the American Society of Hematology* **122**(1), 100–108.

Labuhn, M., Perkins, K., Matzk, S., Varghese, L., Garnett, C., Papaemmanuil, E., Metzner, M., Kennedy, A., Amstislavskiy, V., Risch, T. et al. (2019), 'Mechanisms of progression of myeloid preleukemia to transformed myeloid leukemia in children with down syndrome', *Cancer cell* **36**(2), 123–138.

Landau, D. A., Clement, K., Ziller, M. J., Boyle, P., Fan, J., Gu, H., Stevenson, K., Sougnez, C., Wang, L., Li, S. et al. (2014), 'Locally disordered methylation forms the basis of intratumor methylome variation in chronic lymphocytic leukemia', *Cancer cell* **26**(6), 813–825.

Lapidot, T., Sirard, C., Vormoor, J., Murdoch, B., Hoang, T., Caceres-Cortes, J., Minden, M., Paterson, B., Caligiuri, M. A. and Dick, J. E. (1994), 'A cell initiating human acute myeloid leukaemia after transplantation into scid mice', *nature* **367**(6464), 645.

Lavallée, V.-P., Lemieux, S., Boucher, G., Gendron, P., Boivin, I., Armstrong, R. N., Sauvageau, G. and Hébert, J. (2016), 'Rna-sequencing analysis of core binding factor aml identifies recurrent zbtb7a mutations and defines runx1-cbfa2t3 fusion signature', *Blood, The Journal of the American Society of Hematology* **127**(20), 2498–2501.

Lawrence, M., Huber, W., Pages, H., Aboyoun, P., Carlson, M., Gentleman, R., Morgan, M. T. and Carey, V. J. (2013), 'Software for computing and annotating genomic ranges', *PLoS computational biology* **9**(8).

Lechman, E. R., Gentner, B., Ng, S. W., Schoof, E. M., van Galen, P., Kennedy, J. A., Nucera, S., Ciceri, F., Kaufmann, K. B., Takayama, N. et al. (2016), 'mir-126 regulates distinct self-renewal outcomes in normal and malignant hematopoietic stem cells', *Cancer cell* **29**(2), 214–228.

Lee, E. M., Bachmann, P. S. and Lock, R. B. (2007), 'Xenograft models for the preclinical evaluation of new therapies in acute leukemia', *Leukemia & lymphoma* **48**(4), 659–668.

Lek, M., Karczewski, K. J., Minikel, E. V., Samocha, K. E., Banks, E., Fennell, T., O'Donnell-Luria, A. H., Ware, J. S., Hill, A. J., Cummings, B. B. et al. (2016), 'Analysis of protein-coding genetic variation in 60,706 humans', *Nature* **536**(7616), 285–291.

Levy, S. F., Blundell, J. R., Venkataram, S., Petrov, D. A., Fisher, D. S. and Sherlock, G. (2015), 'Quantitative evolutionary dynamics using high-resolution lineage tracking', *Nature* **519**(7542), 181.

Li, H. (2013), 'Aligning sequence reads, clone sequences and assembly contigs with bwa-mem', *arXiv preprint arXiv:1303.3997* .

Li, H. and Durbin, R. (2009a), 'Fast and accurate short read alignment with burrows–wheeler transform', *bioinformatics* **25**(14), 1754–1760.

Li, H., Handsaker, B., Wysoker, A., Fennell, T., Ruan, J., Homer, N., Marth, G., Abecasis, G. and Durbin, R. (2009b), 'The sequence alignment/map format and samtools', *Bioinformatics* **25**(16), 2078–2079.

Li, Q., Bohin, N., Wen, T., Ng, V., Magee, J., Chen, S.-C., Shannon, K. and Morrison, S. J. (2013a), 'Oncogenic nras has bimodal effects on stem cells that sustainably increase competitiveness', *Nature* **504**(7478), 143–147.

Li, S., Garrett-Bakelman, F. E., Chung, S. S., Sanders, M. A., Hricik, T., Rapaport, F., Patel, J., Dillon, R., Vijay, P., Brown, A. L. et al. (2016a), 'Distinct evolution and dynamics of epigenetic and genetic heterogeneity in acute myeloid leukemia', *Nature medicine* **22**(7), 792.

Li, S., Garrett-Bakelman, F., Perl, A. E., Luger, S. M., Zhang, C., To, B. L., Lewis, I. D., Brown, A. L., D'Andrea, R. J., Ross, M. E. et al. (2014), 'Dynamic evolution of clonal epialleles revealed by methclone', *Genome biology* **15**(9), 472.

Li, S., Mason, C. E. and Melnick, A. (2016b), 'Genetic and epigenetic heterogeneity in acute myeloid leukemia', *Current opinion in genetics & development* **36**, 100–106.

Liem, N. L., Papa, R. A., Milross, C. G., Schmid, M. A., Tajbakhsh, M., Choi, S., Ramirez, C. D., Rice, A. M., Haber, M., Norris, M. D. et al. (2004), 'Characterization of childhood acute lymphoblastic leukemia xenograft models for the preclinical evaluation of new therapies', *Blood* **103**(10), 3905–3914.

Liu, W.-H., Mrozek-Gorska, P., Herold, T., Schwarzkopf, L., Pich, D., Völse, K., Wirth, A.-K., Melo-Narváez, M. C., Carlet, M., Hammerschmidt, W. et al. (2019a), 'Inducible transgene expression in pdx models in vivo identifies klf4 as therapeutic target for b-all', *bioRxiv* p. 737726.

Liu, Y., Mi, Y., Mueller, T., Kreibich, S., Williams, E. G., Van Drogen, A., Borel, C., Frank, M., Germain, P.-L., Bludau, I. et al. (2019b), 'Multi-omic measurements of heterogeneity in hela cells across laboratories', *Nature biotechnology* **37**(3), 314.

Lu, R., Neff, N. F., Quake, S. R. and Weissman, I. L. (2011), 'Tracking single hematopoietic stem cells in vivo using high-throughput sequencing in conjunction with viral genetic barcoding', *Nature biotechnology* **29**(10), 928.

Luczak, M., Kaźmierczak, M., Handschuh, L., Lewandowski, K., Komarnicki, M. and Figlerowicz, M. (2012), 'Comparative proteome analysis of acute myeloid leukemia with and without maturation', *Journal of proteomics* **75**(18), 5734–5748.

Lund, K., Adams, P. and Copland, M. (2014), 'Ezh2 in normal and malignant hematopoiesis', *Leukemia* **28**(1), 44–49.

Lyons, A. B. (2000), 'Analysing cell division in vivo and in vitro using flow cytometric measurement of cfse dye dilution', *Journal of immunological methods* **243**(1-2), 147–154.

Maetzig, T., Morgan, M. and Schambach, A. (2018), 'Fluorescent genetic barcoding for cellular multiplex analyses', *Experimental hematology* .

Maetzig, T., Ruschmann, J., Lai, C. K., Ngom, M., Imren, S., Rosten, P., Norddahl, G. L., von Krosigk, N., Milde, L. S., May, C. et al. (2017), 'A lentiviral fluorescent genetic barcoding system for flow cytometry-based multiplex tracking', *Molecular Therapy* **25**(3), 606–620.

Manola, K. N. (2009), 'Cytogenetics of pediatric acute myeloid leukemia', *European journal of haematology* **83**(5), 391–405.

Martincorena, I., Raine, K. M., Gerstung, M., Dawson, K. J., Haase, K., Van Loo, P., Davies, H., Stratton, M. R. and Campbell, P. J. (2018), 'Universal patterns of selection in cancer and somatic tissues', *Cell* **173**(7), 1823.

Marusyk, A., Almendro, V. and Polyak, K. (2012), 'Intra-tumour heterogeneity: a looking glass for cancer?', *Nature Reviews Cancer* **12**(5), 323–334.

Marusyk, A., Janiszewska, M. and Polyak, K. (2020), 'Intratumor heterogeneity: The rosetta stone of therapy resistance', *Cancer Cell* **37**(4), 471–484.

McCubrey, J. A., Steelman, L. S., Franklin, R. A., Abrams, S. L., Chappell, W. H., Wong, E. W., Lehmann, B., Terrian, D. M., Basecke, J., Stivala, F. et al. (2007), 'Targeting the raf/mek/erk, pi3k/akt and p53 pathways in hematopoietic drug resistance', *Advances in enzyme regulation* **47**, 64.

McMahon, C. M., Ferng, T., Canaani, J., Wang, E. S., Morrissette, J. J., Eastburn, D. J., Pellegrino, M., Durruthy-Durruthy, R., Watt, C. D., Asthana, S. et al. (2019), 'Clonal selection with ras pathway activation mediates secondary clinical resistance to selective flt3 inhibition in acute myeloid leukemia', *Cancer discovery* **9**(8), 1050–1063.

Melnick, A. M. (2010), 'Epigenetics in aml', *Best practice & research Clinical haematology* **23**(4), 463–468.

Metzeler, K. H., Herold, T., Rothenberg-Thurley, M., Amler, S., Sauerland, M. C., Görlich, D., Schneider, S., Konstandin, N. P., Dufour, A., Bräundl, K. et al. (2016), 'Spectrum and prognostic relevance of driver gene mutations in acute myeloid leukemia', *Blood* **128**(5), 686–698.

Minamoto, T., Mai, M. and Ronai, Z. (2000), 'K-ras mutation: early detection in molecular diagnosis and risk assessment of colorectal, pancreas, and lung cancers–a review.', *Cancer Detection and prevention* **24**(1), 1–12.

Morgan, M., Pages, H., Obenchain, V. and Hayden, N. (2019), 'Rsamtools: Binary alignment (bam), fasta, variant call (bcf), and tabix file import'.
URL: *http://bioconductor.org/packages/Rsamtools*

Morin, R. D., Johnson, N. A., Severson, T. M., Mungall, A. J., An, J., Goya, R., Paul, J. E., Boyle, M., Woolcock, B. W., Kuchenbauer, F. et al. (2010), 'Somatic mutations altering ezh2 (tyr641) in follicular and diffuse large b-cell lymphomas of germinal-center origin', *Nature genetics* **42**(2), 181.

Müller-Tidow, C., Tschanter, P., Röllig, C., Thiede, C., Koschmieder, A., Stelljes, M., Koschmieder, S., Dugas, M., Gerss, J., Butterfaß-Bahloul, T. et al. (2016), 'Azacitidine in combination with intensive induction chemotherapy in older patients with acute myeloid leukemia: The aml-aza trial of the study alliance leukemia', *Leukemia* **30**(3), 555–561.

Mullighan, C. G., Phillips, L. A., Su, X., Ma, J., Miller, C. B., Shurtleff, S. A. and Downing, J. R. (2008), 'Genomic analysis of the clonal origins of relapsed acute lymphoblastic leukemia', *Science* **322**(5906), 1377–1380.

Murphy, K. and Weaver, C. (2016), *Janeway's immunobiology*, Garland Science.

National Cancer Institute (2020), 'Adult acute myeloid leukemia treatment (pdq) – health professional version'.
URL: *https://www.cancer.gov/types/leukemia/hp/adult-aml-treatment-pdq*

Nowell, P. C. (1976), 'The clonal evolution of tumor cell populations', *Science* **194**(4260), 23–28.

Ojamies, P., Kontro, M., Edgren, H., Ellonen, P., Lagström, S., Almusa, H., Miettinen, T., Eldfors, S., Tamborero, D., Wennerberg, K. et al. (2017), 'Monitoring therapy responses at the leukemic subclone level by ultra-deep amplicon resequencing in acute myeloid leukemia', *Leukemia* **31**(5), 1048–1058.

Oki, Y. and Issa, J.-P. J. (2009), Epigenetic mechanisms in aml–a target for therapy, *in* 'Acute Myelogenous Leukemia', Springer, pp. 19–40.

Ostrander, E. L., Kramer, A. C., Mallaney, C., Celik, H., Koh, W. K., Fairchild, J., Haussler, E., Zhang, C. R. and Challen, G. A. (2020), 'Divergent effects of dnmt3a and tet2 mutations on hematopoietic progenitor cell fitness', *Stem cell reports* .

Othus, M., Wood, B. L., Stirewalt, D. L., Estey, E. H., Petersdorf, S. H., Appelbaum, F. R., Erba, H. P. and Walter, R. B. (2016), 'Effect of measurable ('minimal') residual disease (mrd) information on prediction of relapse and survival in adult acute myeloid leukemia', *Leukemia* **30**(10), 2080.

Pan, C., Kumar, C., Bohl, S., Klingmueller, U. and Mann, M. (2009), 'Comparative proteomic phenotyping of cell lines and primary cells to assess preservation of cell type-specific functions', *Molecular & Cellular Proteomics* **8**(3), 443–450.

Papaemmanuil, E., Gerstung, M., Bullinger, L., Gaidzik, V. I., Paschka, P., Roberts, N. D., Potter, N. E., Heuser, M., Thol, F., Bolli, N. et al. (2016), 'Genomic classification and prognosis in acute myeloid leukemia', *New England Journal of Medicine* **374**(23), 2209–2221.

Papageorgiou, S. G., Kontos, C. K., Kotsianidis, I., Karousi, P., Symeonidis, A., Galanopoulos, A., Bouchla, A., Hatzimichael, E., Repousis, P., Zikos, P. et al. (2020), 'Effectiveness of 5-azacytidine in older patients with high-risk myelodysplastic syndromes and oligoblastic acute myeloid leukemia: A retrospective analysis of the hellenic (greek) mds study group', *Journal of Geriatric Oncology* **11**(1), 121–124.

Paradis, E. and Schliep, K. (2019), 'ape 5.0: an environment for modern phylogenetics and evolutionary analyses in r', *Bioinformatics* **35**(3), 526–528.

Parekh, S., Ziegenhain, C., Vieth, B., Enard, W. and Hellmann, I. (2018), 'zumis-a fast and flexible pipeline to process rna sequencing data with umis', *Gigascience* **7**(6), giy059.

Patel, A. P., Tirosh, I., Trombetta, J. J., Shalek, A. K., Gillespie, S. M., Wakimoto, H., Cahill, D. P., Nahed, B. V., Curry, W. T., Martuza, R. L. et al. (2014), 'Single-cell rna-seq highlights intratumoral heterogeneity in primary glioblastoma', *Science* **344**(6190), 1396–1401.

Peeters, M., Douillard, J.-Y., Van Cutsem, E., Siena, S., Zhang, K., Williams, R. and Wiezorek, J. (2013), 'Mutant kras codon 12 and 13 alleles in patients with metastatic colorectal cancer: assessment as prognostic and predictive biomarkers of response to panitumumab', *J Clin Oncol* **31**(6), 759–765.

Pellegrino, M., Sciambi, A., Treusch, S., Durruthy-Durruthy, R., Gokhale, K., Jacob, J., Chen, T. X., Geis, J. A., Oldham, W., Matthews, J. et al. (2018), 'High-throughput single-cell dna sequencing of acute myeloid leukemia tumors with droplet microfluidics', *Genome research* **28**(9), 1345–1352.

Petti, A. A., Williams, S. R., Miller, C. A., Fiddes, I. T., Srivatsan, S. N., Chen, D. Y., Fronick, C. C., Fulton, R. S., Church, D. M. and Ley, T. J. (2019), 'A general approach for detecting expressed mutations in aml cells using single cell rna-sequencing', *Nature communications* **10**(1), 1–16.

Pollyea, D. A. and Jordan, C. T. (2017), 'Therapeutic targeting of acute myeloid leukemia stem cells', *Blood* **129**(12), 1627–1635.

Poplin, R., Ruano-Rubio, V., DePristo, M. A., Fennell, T. J., Carneiro, M. O., Van der Auwera, G. A., Kling, D. E., Gauthier, L. D., Levy-Moonshine, A., Roazen, D. et al. (2018), 'Scaling accurate genetic variant discovery to tens of thousands of samples', *BioRxiv* p. 201178.

Quah, B. J. and Parish, C. R. (2010), 'The use of carboxyfluorescein diacetate succinimidyl ester (cfse) to monitor lymphocyte proliferation', *JoVE (Journal of Visualized Experiments)* (44), e2259.

Rabinovich, B. A., Ye, Y., Etto, T., Chen, J. Q., Levitsky, H. I., Overwijk, W. W., Cooper, L. J., Gelovani, J. and Hwu, P. (2008), 'Visualizing fewer than 10 mouse t cells with an enhanced firefly luciferase in immunocompetent mouse models of cancer', *Proceedings of the National Academy of Sciences* **105**(38), 14342–14346.

Radford, D. M., Fair, K. L., Phillips, N. J., Ritter, J. H., Steinbrueck, T., Holt, M. S. and Donis-Keller, H. (1995), 'Allelotyping of ductal carcinoma in situ of the breast: deletion of loci on 8p, 13q, 16q, 17p and 17q', *Cancer research* **55**(15), 3399–3405.

Radujkovic, A., Dietrich, S., Bochtler, T., Krämer, A., Schöning, T., Ho, A. D., Dreger, P. and Luft, T. (2014), 'Azacitidine and low-dose cytarabine in palliative patients with acute myeloid leukemia and high bone marrow blast counts–a retrospective single-center experience', *European journal of haematology* **93**(2), 112–117.

Ravandi, F., Jorgensen, J., Borthakur, G., Jabbour, E., Kadia, T., Pierce, S., Brandt, M., Wang, S., Konoplev, S., Wang, X. et al. (2017), 'Persistence of minimal residual disease assessed by multiparameter flow cytometry is highly prognostic in younger patients with acute myeloid leukemia', *Cancer* **123**(3), 426–435.

Ravandi, F., Walter, R. B. and Freeman, S. D. (2018), 'Evaluating measurable residual disease in acute myeloid leukemia', *Blood advances* **2**(11), 1356–1366.

Redell, M. S., Ruiz, M. J., Gerbing, R. B., Alonzo, T. A., Lange, B. J., Tweardy, D. J. and Meshinchi, S. (2013), 'Facs analysis of stat3/5 signaling reveals sensitivity to g-csf and il-6 as a significant prognostic factor in pediatric aml: a children's oncology group report', *Blood, The Journal of the American Society of Hematology* **121**(7), 1083–1093.

Renaud, G., Stenzel, U., Maricic, T., Wiebe, V. and Kelso, J. (2015), 'deml: robust demultiplexing of illumina sequences using a likelihood-based approach', *Bioinformatics* **31**(5), 770–772.

Renneville, A., Roumier, C., Biggio, V., Nibourel, O., Boissel, N., Fenaux, P. and Preudhomme, C. (2008), 'Cooperating gene mutations in acute myeloid leukemia: a review of the literature', *Leukemia* **22**(5), 915.

Reya, T., Morrison, S. J., Clarke, M. F. and Weissman, I. L. (2001), 'Stem cells, cancer, and cancer stem cells', *nature* **414**(6859), 105.

Richter-Pechańska, P., Kunz, J. B., Bornhauser, B., von Knebel Doeberitz, C., Rausch, T., Erarslan-Uysal, B., Assenov, Y., Frismantas, V., Marovca, B., Waszak, S. M. et al. (2018), 'Pdx models recapitulate the genetic and epigenetic landscape of pediatric t-cell leukemia', *EMBO molecular medicine* **10**(12).

Roh, V., Abramowski, P., Hiou-Feige, A., Cornils, K., Rivals, J.-P., Zougman, A., Aranyossy, T., Thielecke, L., Truan, Z., Mermod, M. et al. (2018), 'Cellular barcoding identifies clonal substitution as a hallmark of local recurrence in a surgical model of head and neck squamous cell carcinoma', *Cell reports* **25**(8), 2208–2222.

Rothenberg-Thurley, M., Amler, S., Goerlich, D., Köhnke, T., Konstandin, N. P., Schneider, S., Sauerland, M. C., Herold, T., Hubmann, M., Ksienzyk, B. et al. (2018), 'Persistence of pre-leukemic clones during first remission and risk of relapse in acute myeloid leukemia', *Leukemia* **32**(7), 1598–1608.

Sachs, K., Sarver, A. L., Noble-Orcutt, K. E., LaRue, R. S., Antony, M. L., Chang, D., Lee, Y., Navis, C. M., Hillesheim, A. L., Nykaza, I. R. et al. (2020), 'Single-cell gene expression analyses reveal distinct self-renewing and proliferating subsets in the leukemia stem cell compartment in acute myeloid leukemia', *Cancer Research* **80**(3), 458–470.

Sachs, Z., LaRue, R. S., Nguyen, H. T., Sachs, K., Noble, K. E., Mohd Hassan, N. A., Diaz-Flores, E., Rathe, S. K., Sarver, A. L., Bendall, S. C. et al. (2014), 'Nras g12v oncogene facilitates self-renewal in a murine model of acute myelogenous leukemia', *Blood, The Journal of the American Society of Hematology* **124**(22), 3274–3283.

Saito, H., Inazawa, J., Saito, S., Kasumi, F., Koi, S., Sagae, S., Kudo, R., Saito, J., Noda, K. and Nakamura, Y. (1993), 'Detailed deletion mapping of chromosome 17q in ovarian and breast cancers: 2-cm region on 17q21. 3 often and commonly deleted in tumors', *Cancer research* **53**(14), 3382–3385.

Saito, Y., Uchida, N., Tanaka, S., Suzuki, N., Tomizawa-Murasawa, M., Sone, A., Najima, Y., Takagi, S., Aoki, Y., Wake, A. et al. (2010), 'Induction of cell cycle entry eliminates human leukemia stem cells in a mouse model of aml', *Nature biotechnology* **28**(3), 275.

Sandén, C., Lilljebjörn, H., Pietras, C. O., Henningsson, R., Saba, K. H., Landberg, N., Thorsson, H., von Palffy, S., Peña-Martinez, P., Högberg, C. et al. (2020), 'Clonal competition within complex evolutionary hierarchies shapes aml over time', *Nature Communications* **11**(1), 1–10.

Sashida, G., Harada, H., Matsui, H., Oshima, M., Yui, M., Harada, Y., Tanaka, S., Mochizuki-Kashio, M., Wang, C., Saraya, A. et al. (2014), 'Ezh2 loss promotes development of myelodysplastic syndrome but attenuates its predisposition to leukaemic transformation', *Nature communications* **5**(1), 1–14.

Sashida, G. and Iwama, A. (2017), 'Multifaceted role of the polycomb-group gene ezh2 in hematological malignancies', *International journal of hematology* **105**(1), 23–30.

Schepers, K., Swart, E., van Heijst, J. W., Gerlach, C., Castrucci, M., Sie, D., Heimerikx, M., Velds, A., Kerkhoven, R. M., Arens, R. et al. (2008), 'Dissecting t cell lineage relationships by cellular barcoding', *Journal of Experimental Medicine* **205**(10), 2309–2318.

Schlenk, R. F., Döhner, K., Krauter, J., Fröhling, S., Corbacioglu, A., Bullinger, L., Habdank, M., Späth, D., Morgan, M., Benner, A. et al. (2008), 'Mutations and treatment outcome in cytogenetically normal acute myeloid leukemia', *New England Journal of Medicine* **358**(18), 1909–1918.

Schoofs, T. and Müller-Tidow, C. (2011), 'Dna methylation as a pathogenic event and as a therapeutic target in aml', *Cancer treatment reviews* **37**, S13–S18.

Selim, A. G. and Moore, A. S. (2018), 'Molecular minimal residual disease monitoring in acute myeloid leukemia: challenges and future directions', *The Journal of Molecular Diagnostics* **20**(4), 389–397.

Shaffer, B. C., Gillet, J.-P., Patel, C., Baer, M. R., Bates, S. E. and Gottesman, M. M. (2012), 'Drug resistance: still a daunting challenge to the successful treatment of aml', *Drug Resistance Updates* **15**(1-2), 62–69.

Sharma, S. V., Lee, D. Y., Li, B., Quinlan, M. P., Takahashi, F., Maheswaran, S., McDermott, U., Azizian, N., Zou, L., Fischbach, M. A. et al. (2010), 'A chromatin-mediated reversible drug-tolerant state in cancer cell subpopulations', *Cell* **141**(1), 69–80.

Shiba, N., Yoshida, K., Shiraishi, Y., Okuno, Y., Yamato, G., Hara, Y., Nagata, Y., Chiba, K., Tanaka, H., Terui, K. et al. (2016), 'Whole-exome sequencing reveals the spectrum of gene mutations and the clonal evolution patterns in paediatric acute myeloid leukaemia', *British journal of haematology* **175**(3), 476–489.

Shih, A. H., Abdel-Wahab, O., Patel, J. P. and Levine, R. L. (2012), 'The role of mutations in epigenetic regulators in myeloid malignancies', *Nature reviews Cancer* **12**(9), 599–612.

Shlush, L. I. (2018), 'Age-related clonal hematopoiesis', *Blood, The Journal of the American Society of Hematology* **131**(5), 496–504.

Shlush, L. I., Mitchell, A., Heisler, L., Abelson, S., Ng, S. W., Trotman-Grant, A., Medeiros, J. J., Rao-Bhatia, A., Jaciw-Zurakowsky, I., Marke, R. et al. (2017), 'Tracing the origins of relapse in acute myeloid leukaemia to stem cells', *Nature* **547**(7661), 104.

Shlush, L. I., Zandi, S., Mitchell, A., Chen, W. C., Brandwein, J. M., Gupta, V., Kennedy, J. A., Schimmer, A. D., Schuh, A. C., Yee, K. W. et al. (2014), 'Identification of pre-leukaemic haematopoietic stem cells in acute leukaemia', *Nature* **506**(7488), 328.

Shultz, L. D., Lyons, B. L., Burzenski, L. M., Gott, B., Chen, X., Chaleff, S., Kotb, M., Gillies, S. D., King, M., Mangada, J. et al. (2005), 'Human lymphoid and myeloid cell development in nod/ltsz-scid il2rγnull mice engrafted with mobilized human hemopoietic stem cells', *The Journal of Immunology* **174**(10), 6477–6489.

Shultz, L. D., Schweitzer, P. A., Christianson, S. W., Gott, B., Schweitzer, I. B., Tennent, B., McKenna, S., Mobraaten, L., Rajan, T. and Greiner, D. L. (1995), 'Multiple defects in innate and adaptive immunologic function in nod/ltsz-scid mice.', *The Journal of Immunology* **154**(1), 180–191.

Siegel, R. L., Miller, K. D. and Jemal, A. (2020), 'Cancer statistics, 2020', *CA: A Cancer Journal for Clinicians* **70**(1), 7–30.

Skoda, R. C. and Schwaller, J. (2019), 'Dual roles of ezh2 in acute myeloid leukemia'.

Ståhlberg, A., Krzyzanowski, P. M., Egyud, M., Filges, S., Stein, L. and Godfrey, T. E. (2017), 'Simple multiplexed pcr-based barcoding of dna for ultrasensitive mutation detection by next-generation sequencing', *nature protocols* **12**(4), 664.

Stief, S. M., Hanneforth, A.-L., Weser, S., Mattes, R., Carlet, M., Liu, W.-H., Bartoschek, M. D., Moreno, H. D., Oettle, M., Kempf, J. et al. (2019), 'Loss of kdm6a confers drug resistance in acute myeloid leukemia', *Leukemia* p. 1.

Stone, R. M., Mandrekar, S. J., Sanford, B. L., Laumann, K., Geyer, S., Bloomfield, C. D., Thiede, C., Prior, T. W., Döhner, K., Marcucci, G. et al. (2017), 'Midostaurin plus chemotherapy for acute myeloid leukemia with a flt3 mutation', *New England Journal of Medicine* **377**(5), 454–464.

Stone, R. M., Manley, P. W., Larson, R. A. and Capdeville, R. (2018), 'Midostaurin: its odyssey from discovery to approval for treating acute myeloid leukemia and advanced systemic mastocytosis', *Blood advances* **2**(4), 444–453.

Stresemann, C. and Lyko, F. (2008), 'Modes of action of the dna methyltransferase inhibitors azacytidine and decitabine', *International journal of cancer* **123**(1), 8–13.

Tabe, Y. and Konopleva, M. (2015), 'Role of microenvironment in resistance to therapy in aml', *Current hematologic malignancy reports* **10**(2), 96–103.

Tartaglia, M., Martinelli, S., Iavarone, I., Cazzaniga, G., Spinelli, M., Giarin, E., Petrangeli, V., Carta, C., Masetti, R., Aricò, M. et al. (2005), 'Somatic ptpn11 mutations in childhood acute myeloid leukaemia', *British journal of haematology* **129**(3), 333–339.

Terwijn, M., Zeijlemaker, W., Kelder, A., Rutten, A. P., Snel, A. N., Scholten, W. J., Pabst, T., Verhoef, G., Löwenberg, B., Zweegman, S. et al. (2014), 'Leukemic stem cell frequency: a strong biomarker for clinical outcome in acute myeloid leukemia', *PloS one* **9**(9).

Terziyska, N., Alves, C. C., Groiss, V., Schneider, K., Farkasova, K., Ogris, M., Wagner, E., Ehrhardt, H., Brentjens, R. J., Zur Stadt, U. et al. (2012), 'In vivo imaging enables high resolution preclinical trials on patients' leukemia cells growing in mice', *PLoS One* **7**(12), e52798.

The Cancer Genome Atlas Research Network (2013), 'Genomic and epigenomic landscapes of adult de novo acute myeloid leukemia', *New England Journal of Medicine* **368**(22), 2059–2074.

Thomas, D. and Majeti, R. (2017), 'Biology and relevance of human acute myeloid leukemia stem cells', *Blood* **129**(12), 1577–1585.

Thomas, X., Dmoszynska, A., Wierzbowska, A., Kuliczkowski, K., Mayer, J., Shelekhova, T., Gau, J., Chou, W., Buckstein, R., Cermak, J. et al. (2011), 'Results from a randomized phase iii trial of decitabine versus supportive care or low-dose cytarabine for the treatment of older patients with newly diagnosed aml.', *Journal of Clinical Oncology* **29**(15_suppl), 6504–6504.

Tiacci, E., Grossmann, V., Martelli, M. P., Kohlmann, A., Haferlach, T. and Falini, B. (2012), 'The corepressors bcor and bcorl1: two novel players in acute myeloid leukemia', *Haematologica* **97**(1), 3.

Townsend, E. C., Murakami, M. A., Christodoulou, A., Christie, A. L., Köster, J., DeSouza, T. A., Morgan, E. A., Kallgren, S. P., Liu, H., Wu, S.-C. et al. (2016), 'The public repository of xenografts enables discovery and randomized phase ii-like trials in mice', *Cancer cell* **29**(4), 574–586.

Turajlic, S., Sottoriva, A., Graham, T. and Swanton, C. (2019), 'Resolving genetic heterogeneity in cancer', *Nature Reviews Genetics* **20**(7), 404–416.

Urrutia, E., Chen, H., Zhou, Z., Zhang, N. R. and Jiang, Y. (2018), 'Integrative pipeline for profiling dna copy number and inferring tumor phylogeny', *Bioinformatics* **34**(12), 2126–2128.

Van den Heuvel-Eibrink, M., Wiemer, E., Prins, A., Meijerink, J., Vossebeld, P., van der Holt, B., Pieters, R. and Sonneveld, P. (2002), 'Increased expression of the breast cancer resistance protein (bcrp) in relapsed or refractory acute myeloid leukemia (aml)', *Leukemia* **16**(5), 833–839.

Van der Auwera, G. A., Carneiro, M. O., Hartl, C., Poplin, R., Del Angel, G., Levy-Moonshine, A., Jordan, T., Shakir, K., Roazen, D., Thibault, J. et al. (2013), 'From fastq data to high-confidence variant calls: the genome analysis toolkit best practices pipeline', *Current protocols in bioinformatics* **43**(1), 11–10.

van der Heijden, M., Miedema, D. M., Waclaw, B., Veenstra, V. L., Lecca, M. C., Nijman, L. E., van Dijk, E., van Neerven, S. M., Lodestijn, S. C., Lenos, K. J. et al. (2019), 'Spatiotemporal regulation of clonogenicity in colorectal cancer xenografts', *Proceedings of the National Academy of Sciences* **116**(13), 6140–6145.

van Galen, P., Hovestadt, V., Wadsworth II, M. H., Hughes, T. K., Griffin, G. K., Battaglia, S., Verga, J. A., Stephansky, J., Pastika, T. J., Story, J. L. et al. (2019), 'Single-cell rna-seq reveals aml hierarchies relevant to disease progression and immunity', *Cell* **176**(6), 1265–1281.

Van Limbergen, H., Poppe, B., Michaux, L., Herens, C., Brown, J., Noens, L., Berneman, Z., De Bock, R., De Paepe, A. and Speleman, F. (2002), 'Identification of cytogenetic subclasses and recurring chromosomal aberrations in aml and mds with complex karyotypes using m-fish', *Genes, Chromosomes and Cancer* **33**(1), 60–72.

Verovskaya, E., Broekhuis, M. J., Zwart, E., Weersing, E., Ritsema, M., Bosman, L. J., van Poele, T., de Haan, G. and Bystrykh, L. V. (2014), 'Asymmetry in skeletal distribution of mouse hematopoietic stem cell clones and their equilibration by mobilizing cytokines', *Journal of Experimental Medicine* **211**(3), 487–497.

Vetrie, D., Helgason, G. V. and Copland, M. (2020), 'The leukaemia stem cell: similarities, differences and clinical prospects in cml and aml', *Nature Reviews Cancer* pp. 1–16.

Vick, B., Rothenberg, M., Sandhöfer, N., Carlet, M., Finkenzeller, C., Krupka, C., Grunert, M., Trumpp, A., Corbacioglu, S., Ebinger, M. et al. (2015), 'An advanced preclinical mouse model for acute myeloid leukemia using patients' cells of various genetic subgroups and in vivo bioluminescence imaging', *PloS one* **10**(3), e0120925.

Virani, S., Colacino, J. A., Kim, J. H. and Rozek, L. S. (2012), 'Cancer epigenetics: a brief review', *ILAR journal* **53**(3-4), 359–369.

Waanders, E., Gu, Z., Dobson, S. M., Antić, Ž., Crawford, J. C., Ma, X., Edmonson, M. N., Payne-Turner, D., van de Vorst, M., Jongmans, M. C. et al. (2020), 'Mutational landscape and patterns of clonal evolution in relapsed pediatric acute lymphoblastic leukemia', *Blood Cancer Discovery* .

Wang, Q., Dong, S., Yao, H., Wen, L., Qiu, H., Qin, L., Ma, L. and Chen, S. (2014), 'Etv6 mutation in a cohort of 970 patients with hematologic malignancies', *Haematologica* **99**(10), e176.

Wang, Q.-s., Wang, Y., Lv, H.-y., Han, Q.-w., Fan, H., Guo, B., Wang, L.-l. and Han, W.-d. (2015), 'Treatment of cd33-directed chimeric antigen receptor-modified t cells in one patient with relapsed and refractory acute myeloid leukemia', *Molecular Therapy* **23**(1), 184–191.

Wang, X., Dai, H., Wang, Q., Wang, Q., Xu, Y., Wang, Y., Sun, A., Ruan, J., Chen, S. and Wu, D. (2013), 'Ezh2 mutations are related to low blast percentage in bone marrow and-7/del (7q) in de novo acute myeloid leukemia', *PLoS One* **8**(4).

Wang, Y., Waters, J., Leung, M. L., Unruh, A., Roh, W., Shi, X., Chen, K., Scheet, P., Vattathil, S., Liang, H. et al. (2014a), 'Clonal evolution in breast cancer revealed by single nucleus genome sequencing', *Nature* **512**(7513), 155.

Watson, C. J., Papula, A., Poon, G. Y., Wong, W. H., Young, A. L., Druley, T. E., Fisher, D. S. and Blundell, J. R. (2020), 'The evolutionary dynamics and fitness landscape of clonal hematopoiesis', *Science* **367**(6485), 1449–1454.

Wattel, E., Preudhomme, C., Hecquet, B., Vanrumbeke, M., Quesnel, B., Dervite, I., Morel, P. and Fenaux, P. (1994), 'p53 mutations are associated with resistance to chemotherapy and short survival in hematologic malignancies', *Blood* **84**(9), 3148–3157.

Weber, K., Thomaschewski, M., Benten, D. and Fehse, B. (2012), 'Rgb marking with lentiviral vectors for multicolor clonal cell tracking', *Nature protocols* **7**(5), 839.

Weber, K., Thomaschewski, M., Warlich, M., Volz, T., Cornils, K., Niebuhr, B., Täger, M., Lütgehetmann, M., Pollok, J.-M., Stocking, C. et al. (2011), 'Rgb marking facilitates multicolor clonal cell tracking', *Nature medicine* **17**(4), 504.

Wei, A., Strickland, S. A., Hou, J.-Z., Fiedler, W., Lin, T. L., Walter, R. B., Enjeti, A. K., Hong, W.-J., Chyla, B., Popovic, R. et al. (2018), 'Venetoclax with low-dose cytarabine induces rapid, deep, and durable responses in previously untreated older adults with aml ineligible for intensive chemotherapy'.

Welch, J. S., Ley, T. J., Link, D. C., Miller, C. A., Larson, D. E., Koboldt, D. C., Wartman, L. D., Lamprecht, T. L., Liu, F., Xia, J. et al. (2012), 'The origin and evolution of mutations in acute myeloid leukemia', *Cell* **150**(2), 264–278.

Wickham, H. (2016), *ggplot2: elegant graphics for data analysis*, Springer.

Wickham, H., Averick, M., Bryan, J., Chang, W., McGowan, L., François, R., Grolemund, G., Hayes, A., Henry, L., Hester, J. et al. (2019), 'Welcome to the tidyverse', *Journal of Open Source Software* **4**(43), 1686.

Wu, C., Li, B., Lu, R., Koelle, S. J., Yang, Y., Jares, A., Krouse, A. E., Metzger, M., Liang, F., Loré, K. et al. (2014), 'Clonal tracking of rhesus macaque hematopoiesis highlights a distinct lineage origin for natural killer cells', *Cell Stem Cell* **14**(4), 486–499.

Xiang, Z., Zhao, Y., Mitaksov, V., Fremont, D. H., Kasai, Y., Molitoris, A., Ries, R. E., Miner, T. L., McLellan, M. D., DiPersio, J. F. et al. (2008), 'Identification of somatic jak1 mutations in patients with acute myeloid leukemia', *Blood, The Journal of the American Society of Hematology* **111**(9), 4809–4812.

Xiao, Y., Zou, P., Wang, J., Song, H., Zou, J. and Liu, L. (2012), 'Lower phosphorylation of p38 mapk blocks the oxidative stress-induced senescence in myeloid leukemic cd34+ cd38- cells', *Journal of Huazhong University of Science and Technology [Medical Sciences]* **32**(3), 328–333.

Xie, M., Lu, C., Wang, J., McLellan, M. D., Johnson, K. J., Wendl, M. C., McMichael, J. F., Schmidt, H. K., Yellapantula, V., Miller, C. A. et al. (2014), 'Age-related mutations associated with clonal hematopoietic expansion and malignancies', *Nature medicine* **20**(12), 1472.

Yagi, T., Morimoto, A., Eguchi, M., Hibi, S., Sako, M., Ishii, E., Mizutani, S., Imashuku, S., Ohki, M. and Ichikawa, H. (2003), 'Identification of a gene expression signature associated with pediatric aml prognosis', *Blood* **102**(5), 1849–1856.

Yang, X., Qian, J., Sun, A., Lin, J., Xiao, G., Yin, J., Chen, S. and Wu, D. (2013), 'Ras mutation analysis in a large cohort of chinese patients with acute myeloid leukemia', *Clinical biochemistry* **46**(7-8), 579–583.

Ye, K., Schulz, M. H., Long, Q., Apweiler, R. and Ning, Z. (2009), 'Pindel: a pattern growth approach to detect break points of large deletions and medium sized insertions from paired-end short reads', *Bioinformatics* **25**(21), 2865–2871.

Ye, Z.-W., Zhang, J., Townsend, D. M. and Tew, K. D. (2015), 'Oxidative stress, redox regulation and diseases of cellular differentiation', *Biochimica et Biophysica Acta (BBA)-General Subjects* **1850**(8), 1607–1621.

Yilmaz, M., Wang, F., Loghavi, S., Bueso-Ramos, C., Gumbs, C., Little, L., Song, X., Zhang, J., Kadia, T., Borthakur, G. et al. (2019), 'Late relapse in acute myeloid leukemia (aml): clonal evolution or therapy-related leukemia?', *Blood cancer journal* **9**(2), 7.

Yu, G. and He, Q.-Y. (2016), 'Reactomepa: an r/bioconductor package for reactome pathway analysis and visualization', *Molecular BioSystems* **12**(2), 477–479.

Zhao, L., Liu, Z., Levy, S. F. and Wu, S. (2018), 'Bartender: a fast and accurate clustering algorithm to count barcode reads', *Bioinformatics* **34**(5), 739–747.

Zhou, F.-L., Zhang, W.-G., Wei, Y.-C., Meng, S., Bai, G.-G., Wang, B.-Y., Yang, H.-Y., Tian, W., Meng, X., Zhang, H. et al. (2010), 'Involvement of oxidative stress in the relapse of acute myeloid leukemia', *Journal of Biological Chemistry* **285**(20), 15010–15015.

Ziegenhain, C., Vieth, B., Parekh, S., Reinius, B., Guillaumet-Adkins, A., Smets, M., Leonhardt, H., Heyn, H., Hellmann, I. and Enard, W. (2017), 'Comparative analysis of single-cell rna sequencing methods', *Molecular cell* **65**(4), 631–643.

Zong, H., Sen, S., Zhang, G., Mu, C., Albayati, Z. F., Gorenstein, D. G., Liu, X., Ferrari, M., Crooks, P. A., Roboz, G. J. et al. (2016), 'In vivo targeting of leukemia stem cells by directing parthenolide-loaded nanoparticles to the bone marrow niche', *Leukemia* **30**(7), 1582.

Zorita, E., Cusco, P. and Filion, G. J. (2015), 'Starcode: sequence clustering based on all-pairs search', *Bioinformatics* **31**(12), 1913–1919.

A. Appendix

A.1. Limiting Dilution Transplantation Assays (LDTAs)

A.1.1. Bulk PDX AML Samples

Table A.1. LDTAs of various PDX AML samples (related to figure 4.1), part 1.

Sample	# of cells injected[$]	# of mice injected / engrafted	LIC frequency (Mean ± 95% CI)
AML-388	72,000	1 / 1	1/3,665 (1/939 - 1/14,300)
	24,000	1 / 1	
	21,870	1 / 1	
	7,290	1 / 1	
	2,430	2 / 1	
	710	1 / 0	
	270	2 / 0	
	90	1 / 0	
	30	2 / 0	
AML-415	121,500	1 / 1	1/1,577 (1/416 - 1/1,577)
	40,500	1 / 1	
	13,500	2 / 2	
	4,500	2 / 2	
	1,500	2 / 1	

[$] cells from PDX AML samples were transplanted into recipient mice in limiting dilutions at numbers indicated; bioluminescence *in vivo* imaging (BLI), blood measurement, or flow cytometric analysis of bone marrow was performed to determine engraftment after up to 37 weeks post transplantation; LIC frequency was calculated using the ELDA software (Hu and Smyth, 2009); mean ± 95% CI is depicted.
LIC = leukaemia initiating cell frequency.

Table A.2. LDTAs of various PDX AML samples (related to figure 4.1), part 2.

Sample	# of cells injected[$]	# of mice injected / engrafted	LIC frequency (Mean ± 95% CI)
AML-491	10,000	3 / 3	1/1,799 (1/945 - 1/3,426)
	5,400	2 / 2	
	2,000	2 / 1	
	1,800	2 / 0	
	1,200	6 / 6	
	1,000	2 / 1	
	600	5 / 0	
	200	3 / 0	
	100	4 / 0	
AML-573	121,500	1 / 1	1/7,853 (1/2,082 - 1/29,619)
	40,500	1 / 1	
	13,500	1 / 1	
	4,500	2 / 1	
	1,500	2 / 0	
	500	3 / 0	
AML-579	72,900	1 / 1	1/351 (1/77.6 - 1/1,590)
	24,300	2 / 2	
	7,100	1 / 1	
	2,700	2 / 2	
	900	1 / 1	
	300	2 / 1	

[$] cells from PDX AML samples were transplanted into recipient mice in limiting dilutions at numbers indicated; BLI, blood measurement, or flow cytometric analysis of bone marrow was performed to determine engraftment after up to 37 weeks post transplantation; LIC frequency was calculated using the ELDA software (Hu and Smyth, 2009); mean ± 95% CI is depicted.
LIC = leukaemia initiating cell frequency.

Table A.3. LDTAs of various PDX AML samples (related to figure 4.1), part 3.

Sample	# of cells injected[$]	# of mice injected / engrafted	LIC frequency (Mean ± 95% CI)
AML-661	8,100	1 / 1	1/546 (1/230 - 1/1,403)
	2,700	1 / 1	
	900	3 / 1	
	300	3 / 1	
	100	4 / 2	
	33	4 / 2	
	11	3 / 0	

[$] cells from PDX AML samples were transplanted into recipient mice in limiting dilutions at numbers indicated; BLI, blood measurement, or flow cytometric analysis of bone marrow was performed to determine engraftment after up to 37 weeks post transplantation; LIC frequency was calculated using the ELDA software (Hu and Smyth, 2009); mean ± 95% CI is depicted.
LIC = leukaemia initiating cell frequency.

A.1.2. Generation of PDX AML Single Cell Clones

Table A.4. Generation of PDX AML SCCs (related to figure 4.4).

Sample	# of cells injected[$]	# of mice injected / engrafted	LIC frequency (Mean ± 95% CI)
AML-491	33,000	3 / 1	1/5,810 (1/3,328 – 1/10,143)
	32,000	1 / 1	
	21,400	1 / 1	
	16,500	1 / 1	
	11,000	9 / 8	
	3,300	9 / 8	
	1,100	9 / 6	
AML-661	10,000	1 / 1	1/525 (1/237 – 1/1,161)
	3,000	5 / 4	
	1,000	5 / 5	
	300	4 / 2	
	100	4 / 4	

[$] cells from bulk PDX AML-491 or AML-661 were transplanted into recipient mice in limiting dilutions at numbers indicated; blood measurement was performed to determine engraftment after up to 38 weeks post transplantation; LIC frequency was calculated using the ELDA software (Hu and Smyth, 2009); mean ± 95% CI is depicted.
LIC = leukaemia initiating cell frequency.

A.1.3. LDTAs of one KRAS^{G12A} and one NRAS^{Q61K} PDX AML SCC.

Table A.5. LDTAs of one one KRAS^{G12A} and one NRAS^{Q61K} PDX AML SCC (related to figure 4.10).

Sample	# of cells injected[$]	# of mice injected / engrafted	LIC frequency (Mean ± 95% CI)
PDX AML SCC 3 (*KRAS^{mut}*)	1,000,000	1 / 1	1/21,878 (1/6,263 - 1/76,426)
	100,000	2 / 2	
	10,000	3 / 1	
	5,000	3 / 0	
	2,500	2 / 1	
	1,250	2 / 0	
PDX AML SCC 7 (*NRAS^{mut}*)	1,000,000	1 / 1	1/1,725 (1/625 - 1/4,567)
	100,000	2 / 2	
	10,000	3 / 3	
	5,000	3 / 3	
	2,500	2 / 2	
	1,250	2 / 0	

[$] cells from bulk PDX AML-491 or AML-661 were transplanted into recipient mice in limiting dilutions at numbers indicated; BLI was performed to determine engraftment after up to 9 weeks post transplantation; LIC frequency and statistical significance (Chi-square test) was calculated using the ELDA software (Hu and Smyth, 2009); mean ± 95% CI is depicted; p = 0.0009.
LIC = leukaemia initiating cell frequency.

A.2. Genetic and Transcriptomic Characterisation of PDX AML Single Cell Clones

A.2.1. Exome Sequencing of PDX AML Single Cell Clones

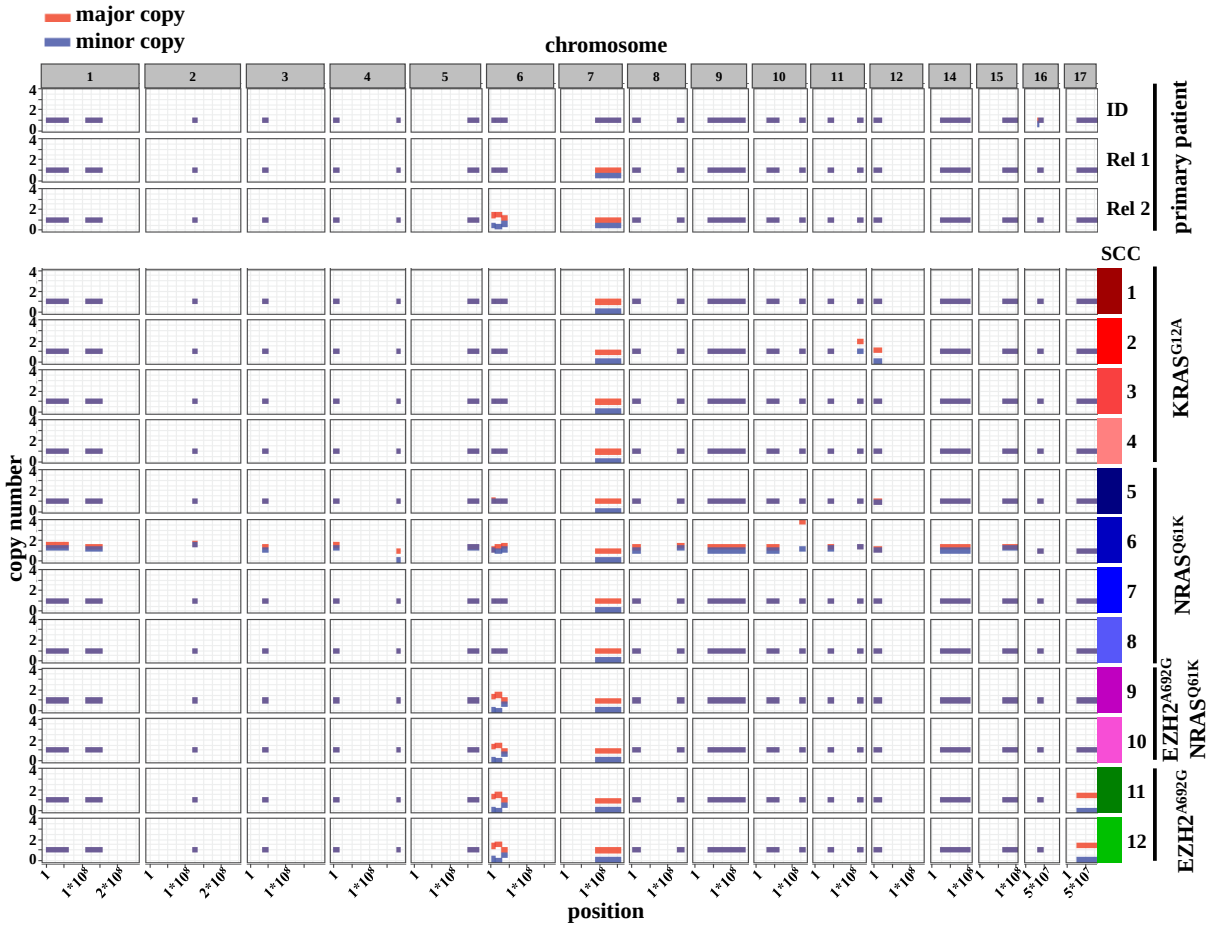

Figure A.1. Copy number variant (CNV) analyses of exome sequencing of primary patient's material and PDX AML SCCs. gDNA was isolated from every PDX AML SCC and exome libraries preped for 100 bp paired-end sequencing (sample preparation by LAFUGA, Ludwig-Maximilians-Universität München). Data was demultiplexed and analysed by Ilse Valtierra, Ludwig-Maximilians-Universität München, using existing whole exome sequencing data from primary patient's material (initial diagnosis (ID), relapse 1 (Rel 1) and relapse 2 (Rel 2) as well as complete remission samples) as control. Copy number variants (CNVs) were analysed using ID and complete remission samples as control.
ID = initial diagnosis; Rel 1 = relapse 1; Rel 2 = relapse 2.

A.2.2. Transcriptome Sequencing of PDX AML Single Cell Clones

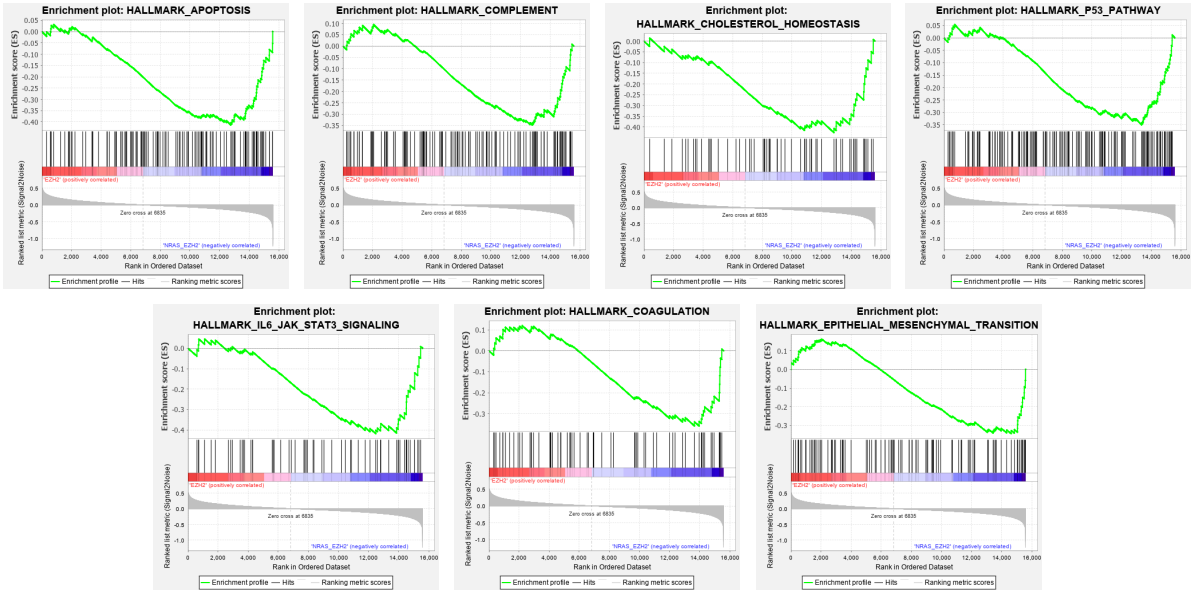

Figure A.2. Gene set enrichment analysis comparing *EZH2*^{A692G} PDX AML SCCs to *EZH2*^{A692G} *NRAS*^{Q61K} SCCs. Comparision of PDX AML SCC 11 and SCC 12 (both *EZH2*^{A692G}) to SCC 9 and SCC 10 (both *EZH2*^{A692G} *NRAS*^{Q61K}).

A.3. Statistical Significance

A.3.1. Competitive *In Vivo* Growth of PDX AML Single Cell Clones

Table A.6. Statistical significance of competitive *in vivo* growth of eleven PDX AML SCCs, part 1 (related to figure 4.12).

Comparison	Significance[#]		
	d17	d37	d78
SCC 1 vs SCC 6	****	***	**
SCC 1 vs SCC 11	****	****	****
SCC 1 vs SCC 12	****	****	***
SCC 2 vs SCC 6	****	**	**
SCC 2 vs SCC 11	****	****	****
SCC 2 vs SCC 12	****	****	**
SCC 3 vs SCC 6	****	***	**
SCC 3 vs SCC 11	****	****	****
SCC 3 vs SCC 12	****	****	***
SCC 4 vs SCC 6	****	**	**
SCC 4 vs SCC 11	****	****	****
SCC 4 vs SCC 12	****	****	***
SCC 5 vs SCC 6	****	***	**
SCC 5 vs SCC 11	****	****	****
SCC 5 vs SCC 12	****	****	***
SCC 6 vs SCC 7	****	***	**
SCC 6 vs SCC 8	****	*	ns
SCC 6 vs SCC 9	****	**	ns
SCC 6 vs SCC 11	ns	****	****
SCC 6 vs SCC 12	****	****	ns
SCC 7 vs SCC 11	****	****	****
SCC 7 vs SCC 12	****	****	***
SCC 8 vs SCC 11	****	****	****
SCC 8 vs SCC 12	****	****	*

[#] Statistical signficance was tested with two-way ANOVA with Tukey correction. If comparision is not listed, it was not significant at all time points.
* = $p < 0.05$; ** = $p < 0.01$; *** = $p < 0.001$; **** = $p < 0.0001$; ns = not significant.

Table A.7. Statistical significance of competitive *in vivo* growth of eleven PDX AML SCCs, part 2 (related to figure 4.12).

Comparison	Significance[#]		
	d17	d37	d78
SCC 9 vs SCC 11	****	****	****
SCC 9 vs SCC 12	****	****	ns
SCC 11 vs SCC 12	****	ns	****

[#] Statistical signficance was tested with two-way ANOVA with Tukey correction. If comparision is not listed, it was not significant at all time points.
* = $p < 0.05$; ** = $p < 0.01$; *** = $p < 0.001$; **** = $p < 0.0001$; ns = not significant.

Table A.8. Statistical significance of competitive *in vivo* growth of four PDX AML SCCs (related to figure 4.12).

Comparison	Significance[#]	
	d32	d59
SCC 9 vs SCC 10	ns	*
SCC 9 vs SCC 11	****	****
SCC 9 vs SCC 12	****	ns
SCC 10 vs SCC 11	****	****
SCC 10 vs SCC 12	****	ns
SCC 11 vs SCC 12	ns	****

[#] Statistical signficance was tested with two-way ANOVA with Tukey correction. If comparision is not listed, it was not significant at all time points.
* = $p < 0.05$; **** = $p < 0.0001$; ns = not significant.

A.3.2. Competitive *In Vivo* Chemotherapy of PDX AML Single Cell Clones

Table A.9. Statistical significance of competitive *in vivo* therapy of eleven PDX AML SCCs with Ara-C (related to figure 4.16).

Comparison	Significance[#]
SCC 1 vs SCC 2	**
SCC 1 vs SCC 3	*
SCC 1 vs SCC 5	**
SCC 1 vs SCC 6	**
SCC 1 vs SCC 7	**
SCC 1 vs SCC 8	**
SCC 1 vs SCC 9	**
SCC 2 vs SCC 11	**
SCC 3 vs SCC 11	*
SCC 5 vs SCC 11	**
SCC 6 vs SCC 11	**
SCC 7 vs SCC 11	**
SCC 8 vs SCC 11	**
SCC 9 vs SCC 11	**

[#] Statistical signficance was tested with one-way ANOVA with Tukey correction. If comparision is not listed, it was not significant.
* = $p < 0.05$; ** = $p < 0.01$.

Table A.10. Statistical significance of competitive *in vivo* therapy of four PDX AML SCCs with Ara-C (related to figure 4.17).

Comparison	Significance[#]
SCC 9 vs SCC 11	*
SCC 9 vs SCC 12	**
SCC 10 vs SCC 11	*
SCC 10 vs SCC 12	**

[#] Statistical signficance was tested with one-way ANOVA with Tukey correction. If comparision is not listed, it was not significant.
* = $p < 0.05$; ** = $p < 0.01$.

Acknowledgements

Zuerst möchte ich mich bei Prof. Dr. Irmela Jeremias bedanken für die Möglichkeit dieses interessante Projekt zu bearbeiten und die Richtung des Projekts so stark mitlenken zu können, die intensive Betreuung, die anregenden Diskussionen, sowie das tolle Team, das sie in ihrer Abteilung zusammen gestellt hat. Ich habe unsere Zusammenarbeit als sehr produktiv empfunden.

Besonders bedanke ich mich bei Prof. Dr. Wolfgang Enard für die Betreuung meiner Doktorarbeit, die wissenschaftlichen Diskussionen und die motivierende Begeisterung, die einfach ansteckt.

Vielen Dank auch an alle Mitglieder meines Thesis Advisory Comittees, Prof. Dr. Irmela Jeremias, Prof. Dr. Wolfgang Enard, Prof. Dr. Ursula Zimber-Strobl und Dr. Binje Vick dafür, dass sie sich immer wieder in mein Projekt eingedacht haben und hilfreiche Ideen und Input gegeben haben.

Mein rießiger Dank gilt auch Dr. Binje Vick, meiner PostDoc-Betreuerin. Ich konnte nicht nur super wissenschaftlich mit dir diskutieren und gemeinsam Denken, du hattest auch immer ein offenes Ohr für mich, hast mich immer unterstützt und warst für mich da. Ich hätte es einfach nicht besser treffen können mit dir als PostDoc-Betreuerin!

Außerdem möchte ich auch die ganze Abteilung Apoptose in Hämatopoietischen Stammzellen danken für die gute Zusammenarbeit, die freundliche Atmosphäre, die interessanten Diskussionen und Anregungen zu meinem Projekt. Vielen Dank an Prof. Dr. Tobias Herold und Dr. Vindi Jurinovic für die Hilfe bei den Auswertungen und die motivierenden und netten Meetings. Ich bedanke mich besonders bei den Technischen Assistentinnen und dem Technischen Assistent für die tatkräfige Unterstützung in meinem Projekt - ohne euch wäre vieles so nicht möglich gewesen - und die netten und lustigen Gespräche. Ein großes Dankeschön auch an meine Mit-Doktoranden für die entspannte, angenehme und oftmals lustige Stimmung in unserem Büro, die amüsanten Nachmittage und Abenden sowie die warmherzigen und aufbauenden Gespräche.

Darüber hinaus möchte ich mich bei allen Kooperationspartnern für die gute Zusammenarbeit und die produktiven Diskussionen bedanken, insbesondere Daniel Richter, Ilse Valtierra, Johannes Bagnoli und Dr. Ines Hellmann.

Danke auch an alle Mitarbeiter der Tierhaltung für die Versorgung meiner Mäuse.

Zuletzt möchte ich mich herzlich bei meiner Familie, meinem Freund und meinen Freunden für die Unterstützung, Empathie und Motivation bedanken. Vielen Dank, dass ihr immer für mich da seid!